

A Dissertation

entitled

A superelastic variable stiffness knee actuator for a knee-ankle-foot orthosis

by

Feng Tian

Submitted to the Graduate Faculty as partial fulfillment of the requirements for the

Doctor of Philosophy Degree in Mechanical Engineering

Dr. Mohamed Samir Hefzy, Committee Chair

Dr. Mohammad Elahinia, Committee Member

Dr. Charles Armstrong, Committee Member

Dr. Kenton Kaufman, Committee Member

Dr. Lesley Berhan, Committee Member

Dr. Patricia R. Komuniecki, Dean
College of Graduate Studies

The University of Toledo

December 2015

Copyright 2015, Feng Tian

This document is copyrighted material. Under copyright law, no parts of this document may be reproduced without the expressed permission of the author.

An Abstract of

A Superelastic Variable Stiffness Knee Actuator for a Knee-Ankle-Foot Orthosis

by

Feng Tian

Submitted to the Graduate Faculty as partial fulfillment of the requirements for the
Doctor of Philosophy Degree in Mechanical Engineering

The University of Toledo

December 2015

Quadriceps weakness is primarily caused by neurological and muscular diseases. Individuals with such deficiency have limited ability to initiate knee extension or to control knee flexion. Knee-ankle-foot orthoses (KAFOs) are commonly prescribed to assist in abnormal ambulation caused by weak quadriceps. The purpose of this research is to develop a knee actuating system for knee-ankle-foot orthoses, which mimics normal knee joint behavior. The novel device is called the UT dynamic KAFO. This device is based on the superelastic property of Nitinol, an alloy of Nickel and Titanium.

As the first step, a literature review for the biomechanics of human walking was performed. This was necessary to study kinematic and kinetic characteristics of a normal knee joint over the entire walking cycle. In this context, the knee kinematic and kinetic characteristics caused by weak quadriceps are discussed and compared to that of the normal knee joint. This understanding is essential in determining the requirements for the novel knee actuating system.

The existing KAFOs were comprehensively studied. Three types of KAFOs have been reported in the literature: passive, stance control (SCKAFOs), and dynamic. Various

knee-ankle-foot orthoses are discussed, including their designs, functionality, applications, and limitations. Passive KAFOs are the most used conventional type that provides strong support for the knee joint. Stance control KAFOs lock the knee during the stance phase and allow free knee rotations during the swing phase. Dynamic KAFOs control the knee joint throughout the entire walking gait cycle. In addition to the characteristics of existing KAFOs, the fundamental properties and applications of Nitinol, both shape memory and superelastic alloys, were studied.

The conceptual design of the dynamic knee actuator with superelastic Nitinol was proposed and numerical simulations were conducted to verify the concept and to determine proper geometries for the actuator. Based on this, the dynamic knee module was modeled and analyzed and the optimal structures were obtained. The resulting knee module has three working modes: free, locked, and dynamic. A control system was developed to operate among the three modes. A prototype was first fabricated using additive manufacturing and then improved to the final device. The final prototype was added to a conventional KAFO.

The resulting UT dynamic KAFO was evaluated in motion analysis tests on a healthy subject. The subject had no history of lower extremity pathology. Joint kinematics, kinetics, and electromyography data of both lower limbs was collected and calculated to compare the walking patterns in normal walking and walking with the UT dynamic KAFO. When compared with a locked knee KAFO, the results indicate that the dynamic KAFO is able to improve gait. Thus, we have concluded that the UT dynamic KAFO is able to assist gait in a manner that approximates a normal gait pattern.

I dedicate this document to my beloved parents Yunwen Tian and Haiyan Lin.

Acknowledgements

First of all, I would like to thank God for being with me throughout my Ph.D. study. He is my strength, my wisdom, my encouragement, guiding me over all the difficulties so that I could complete this research.

Second, I would like to thank my two advisors: Dr. Mohamed Samir Hefzy and Dr. Mohammad Elahinia, for supporting my study and research continuously. They have a great influence on me, both personally and professionally, which helps me a lot during my study in the University of Toledo and will also bring benefits in my future life. I also want to thank my committee members Dr. Charles Armstrong, Dr. Kenton Kaufman, Dr. Manish Kumar, and Dr. Lesley Berhan for sparing time from their busy schedules and giving me valuable advice for the study. Mr. Paul Trestan, Dr. Kaufman, and Dr. Armstrong provided me lots of help and important feedbacks in the KAFO survey.

Besides, I would like to express my appreciation towards Dr. Vijay Goel and his research team for their generous help in training and calibrating my Nitinol samples, Mr. John Jaegly and his team for helping me with the design and fabricating the knee module, Mr. Michael Stevens and Mr. Terence Smith from Marshall Kloebe for providing KAFO technical support, and my lab mates for their time and kind help over my study.

Finally, I would like to thank my friends and family, without whom it is impossible for me to complete this study. It is their love that supports me all the way. They are the people whom I love the most in this world.

Table of Contents

Abstract.....	iii
Acknowledgements.....	vi
Table of Contents	vii
List of Tables.....	xii
List of Figures.....	xiv
List of Abbreviations.....	xxv
List of Symbols.....	xxvii
1 Introduction.....	1
1.1 Biomechanics of Human Walking	2
1.2 Kinematic and Kinetic Characteristics of a Normal Knee Joint	4
1.3 Abnormal Walking Gaits Caused by Weak Quadriceps.....	7
1.4 Shape Memory Alloys.....	9
1.4.1 Shape Memory Effect	11
1.4.2 Superelastic Effect	12
1.4.3 Applications of Nitinol in Lower Limb Braces.....	14
1.5 Summary	22
2 Knee-Ankle-Foot Orthosis.....	23
2.1 Passive KAFOs	23
2.1.1 Drop Lock KAFO	24

2.1.2	Posterior Offset KAFO	25
2.1.3	Polycentric Joint KAFO.....	26
2.1.4	Bail Lock KAFO.....	27
2.1.5	Ratchet Lock KAFO	28
2.1.6	Dial Lock KAFO.....	29
2.2	Stance Control KAFOs	30
2.2.1	Otto Bock Free Walk/ Becker Orthopedic UTX.....	30
2.2.2	Fillauer® Swing KAFO.....	31
2.2.3	Becker 9001 E-Knee Orthosis	33
2.2.4	Horton Stance Control Orthosis.....	34
2.2.5	Belt-Clamping Joint SCKAFO	36
2.2.6	Hydraulic Stance Control KAFO.....	39
2.2.7	The Sensor Walk®	41
2.2.8	Quasi-Passive Compliant Stance Control KAFO	42
2.2.9	A Motor Powered Knee-Ankle-Foot Orthosis	45
2.3	Dynamic KAFOs	47
2.3.1	Spring Actuated Dynamic KAFO	47
2.3.2	Pneumatically Powered KAFO.....	50
2.3.3	The C-brace®.....	52
2.4	Problems and Limitations of Current KAFOs	54
2.5	Summary	62
3	Development of the Dynamic Knee Actuator	63
3.1	Conceptual Design of the Dynamic Knee Actuator.....	64

3.1.1	Determine the Proper Material and Loading Condition	64
3.1.2	Conceptual Design of the Dynamic Knee Actuator	65
3.2	Design of the Nitinol Knee Actuator	67
3.2.1	A 3D Constitutive Model for Nitinol	67
3.2.2	Calibrating the Properties of the Superelastic Nitinol	67
3.2.2.1	Calibration Setup and Procedure	67
3.2.2.2	Calibration Results.....	70
3.2.3	Numerical Simulation Results of the Nitinol Rods.....	73
3.2.4	Training the Nitinol Rods.....	78
3.2.4.1	Training Setup and Procedure.....	79
3.2.4.2	Training Results	81
3.3	Design of the Torsional Springs in the Knee Actuator.....	83
3.4	Summary	87
4	Development of the Dynamic Knee Module	88
4.1	Design of the Dynamic Knee Module	88
4.2	FEM Analyses of the Dynamic Knee Module	94
4.2.1	The External Frame of the Dynamic Knee Module.....	95
4.2.2	The Actuating Fixtures of the Dynamic Knee Module.....	98
4.2.3	The Support Disks and the Internal Frame of the Dynamic Knee Module	101
4.2.4	The Engagement Mechanisms of the Dynamic Knee Module	104
4.3	Design of the Control System	105
4.4	Prototypes of the Dynamic Knee Module.....	108

4.5	Summary	112
5	Results.....	113
5.1	Hypothesis of the Motion Analysis Tests.....	113
5.2	Experimental Setup and Procedure of the Motion Analysis Tests	114
5.3	Experimental Results of the Motion Analysis Tests	119
5.3.1	Spatiotemporal Parameters	119
5.3.2	Kinematic Characteristics	130
5.3.3	Kinetic Characteristics	140
5.4	Summary	144
6	Discussion.....	145
6.1	Discussion of the Spatiotemporal Results.....	145
6.2	Discussion of the Kinematic Results	148
6.3	Discussion of the Kinetic Results	151
6.4	Summary	152
7	KAFO Industry Overview.....	153
7.1	KAFO Market in the US	153
7.2	Ecosystem for the KAFO Market	157
7.2.1	The Process of Prescribing KAFOs for Patients.....	158
7.2.2	The Process of Licensing New KAFOs in Manufacturers.....	160
7.2.3	The Process of Marketing New KAFOs	163
7.3	Business Model for the UT Dynamic KAFO	164
7.4	Directions for Future Research in the KAFO Area.....	169
7.5	Summary	170

8	Conclusions and Future Work.....	171
	References.....	173

List of Tables

Table 2-1. The Summarization of Various Passive KAFOs. The Table Is Adopted from Reference [16].	57
Table 2-2. The Summarization of Various Stance Control KAFOs. The Table Is Adopted from Reference [16].	59
Table 2-3. The Summarization of Various Dynamic KAFOs. The Table Is Adopted from Reference [16].	61
Table 3-1. The Calibration Conditions of the NiTi#1 Superelastic Rod Sample.	68
Table 3-2. The Dimensions and Training Parameters of the Two NiTi#1 Superelastic Rods.	78
Table 4-1. Description of All Parts in the Dynamic Knee Joint Module.	92
Table 4-2. Material Properties Used to Simulate the Parts of the Dynamic Knee Module.	95
Table 5-1. Average Step Length with One Standard Deviation in the Three Testing Conditions. The Right and Left Sides Represent the Orthotic and Sound Legs, Respectively.	120
Table 5-2. Average Stride Length with One Standard Deviation in the Three Testing Conditions. The Right and Left Sides Represent the Orthotic and Sound Legs, Respectively.	122
Table 5-3. Average Cadence with One Standard Deviation in the Three Testing	

Conditions. The Right and Left Sides Represent the Orthotic and Sound Legs, Respectively.	124
Table 5-4. Stance Phase Percentage with One Standard Deviation in the Three Testing Conditions. The Right and Left Represent the Orthotic and Sound Legs, Respectively.	126
Table 5-5. Average of Double Limb Support with One Standard Deviation in the Three Testing Conditions. The Right and Left Sides Represent the Orthotic and Sound Legs, Respectively.	128
Table 5-6. Single Limb Support with One Standard Deviation in the Three Testing Conditions. The Right and Left Represent the Orthotic and Sound Legs, Respectively.	129
Table 5-7. Maximum Knee Flexion Angle during the Stance Phase in the Three Testing Conditions. The Right and Left Represent the Orthotic and Sound Legs, Respectively.	132
Table 5-8. Maximum Knee Flexion Angle during the Swing Phase in the Three Testing Conditions. The Right and Left Represent the Orthotic and Sound Legs, Respectively.	133
Table 6-1. Average Spatiotemporal Parameters with One Standard Deviation for the Three Testing Conditions. The Right and Left Sides Represent the Orthotic and Sound Legs, Respectively.	147
Table 7-1. The Costs and Insurance Coverages of the Three KAFO Types.	155

List of Figures

Figure 1-1. A Complete Walking Gait Cycle. This figure Is Adopted and Modified from Reference [6].....	2
Figure 1-2. Flexion Angle Change of a Normal Knee Joint During the Entire Walking Gait Cycle. The figure Is Adopted from Reference [16].	4
Figure 1-3. Knee Joint Internal Moment Normalized by Body Weight During the Entire Walking Gait Cycle. The figure Is Adopted from Reference [16].	5
Figure 1-4. The Stiffness Profile for a Normal Knee Joint: Weight-Normalized Internal Knee Moment vs. Knee Angle. Point 1: the Heel Strike; Point 2: the Foot Flat; Point 3: the Heel Off; Point 4: the End of the Initial Swing Phase; Point 5: the Next Heel Strike. The Figure Is Adopted from Reference [17].	6
Figure 1-5. Kinematics and Kinetics Characteristics of Patients with Different Levels of Quadriceps Weakness: (a) and (b) for Slight Weakness, (c) and (d) for Medium Weakness, and (e) and (f) for Severe Weakness. The Figure Is Adopted from Reference [20].	8
Figure 1-6. Comparison of the Knee Stiffness Profiles between the Individual with Severe Quadriceps Weakness and a Healthy Subject. All Data for the Weak Quadriceps Graph Is Extracted from Figures 1-5(e) and (f).	9
Figure 1-7. Three Different Crystalline Structures of Nitinol Alloys and the Relationship between Them. The Figure Is Adopted from Reference [28].	10
Figure 1-8. Forward and Reverse Phase Transformation Processes of Nitinol Alloys. The	

Figure Is Adopted and Modified from Reference [29].	11
Figure 1-9. Phase Diagram of Nitinol with Shape Memory Effects. The Figure Is Adopted and Modified from Reference [30].	12
Figure 1-10. Phase Diagram of Nitinol with Superelastic Effect. The Figure Is Adopted and Modified from Reference [31].	14
Figure 1-11. A Robotic Lower Leg with the Flexible Orthosis Actuated by Nitinol with Shape Memory Effect: (a) the Knee Actuators and (b) the Ankle Actuators. The Figure Is Adopted from Reference [32].	15
Figure 1-12. The Active Ankle-Foot Orthosis Actuated by Nitinol Wires with Shape Memory Effect. The Figure Is Adopted from Reference [34].	17
Figure 1-13. The Active Ankle-Foot Orthosis Actuated by Nitinol Wires with Superelastic Effect. The Figure Is Adopted from Reference [37].	17
Figure 1-14. An Active AFO Uses a Superelastic Actuator under Combined Axial-Torsional Loads. (a) The Superelastic Ankle Actuator. (b) An Overall View of the AAFO. The Figure Is Adopted from Reference [40].	19
Figure 1-15. The Active AFO with an Adjustable Ankle Hinge Made with Superelastic Alloy. The Figure Is Adopted from Reference [39].	19
Figure 1-16. The Ankle Rehabilitation Device with an Ankle Actuator on the Shank Segment Uses Shape Memory Nitinol Wires. The Figure Is Adopted from Reference [42].	21
Figure 1-17. (a) Lower Leg Orthoses Actuated by Superelastic Nitinol Actuators. (b) Parts of a Hinge Joint. (c) The Assembly of the Hinge Joint with Superelastic Nitinol Actuators. The Figure Is Adopted from Reference [41].	21

Figure 2-1. The Knee Joint Mechanism of a Drop Lock KAFO: (a) the Knee Joint Is Locked during Walking; (b) the Knee Joint Is Free for Bending. This Figure Is Adopted from Reference [44].	24
Figure 2-2. The Knee Joint Mechanism of a Posterior Offset Joint KAFO. The Figure Is Adopted from Reference [45].	25
Figure 2-3. The Knee Joint Mechanism of a Polycentric Joint KAFO. The Figure Is Adopted from Reference [45].	26
Figure 2-4. (a) A Bail Lock KAFO; (b) the Knee Joint Mechanism of a Bail Lock KAFO. The figure Is Adopted from Reference [45].	27
Figure 2-5. (a) The Side View of a Ratchet Lock Knee Joint; (b) the Ratchet Locking Mechanism; (c) the Knee Flexion Range of the Ratchet Lock Knee Joint. The Figure Is Adopted and Modified from Reference [48].	28
Figure 2-6. A Dial Lock KAFO. The Figure Is Adopted and Modified from Reference [49].	29
Figure 2-7. Otto Bock Free Walk/Becker Orthopedic UTX: (a) Spring-Loaded Pawl Locks the Knee Joint during the Stance Phase; (b) Ankle Dorsiflexion Pulls Down the Cable and Releases the Joint in the Late Stance Phase. The Figure Is Adopted from Reference [55].	31
Figure 2-8. Gravity-Activated Fillauer Swing Phase Lock: (a) the Weighted Pawl Falls into the Locking Position to Resist Flexion during the Stance Phase; (b) the Pawl Falls out of the Locking Position to Allow Free Motion during the Swing Phase. The Figure Is Adopted from Reference [55].	32
Figure 2-9. The Electromagnetic Knee Joint Mechanism of the Becker Orthopedic 9001	

E-Knee Brace. The Figure Is Adopted from Reference [55].	34
Figure 2-10. (a) The Horton Stance Control KAFO; (b) the Knee Joint Mechanism of the Horton SCKAFO. The Figures Are Adopted from Reference [55].	35
Figure 2-11. The Friction-Based Belt Clamping SCKAFO: (a) the Lateral View; (b) the Front View. The Figures Are Adopted from Reference [58].	38
Figure 2-12. The Knee Joint Mechanism of the Belt Clamping Knee-Ankle-Foot Orthosis. The Figure Is Adopted from Reference [58].	39
Figure 2-13. The Knee Joint Mechanism of the Hydraulically Powered Stance Control KAFO: (a) When the Gear Is Engaged during the Stance Phase; (b) When the Gear Is Disengaged during the Swing Phase. The Figures Are Adopted and Modified from Reference [63].	40
Figure 2-14. (a) The Sensor Walk® Stance Control KAFO. The Figure Is Adopted from Reference [64]; (b) the One-Way Wrap-Spring Clutch Mechanism of the Sensor Walk®. The Figure Is Adopted from Reference [68].	42
Figure 2-15. (a) The Quasi-Passive Compliant Stance Control KAFO; (b) the Knee Joint Mechanism of the Quasi-Passive SCKAFO. Top: Engagement of the Support Spring and the Return Spring during the Stance Phase. Bottom: Disengagement of the Support Spring during the Swing Phase. The Figures Are Adopted and Modified from Reference [70].	44
Figure 2-16. (a) The Motor Powered Stance Control KAFO. The Figure Is Adopted and Modified from Reference [71]; (b) the Knee Joint Mechanism of the Motor Powered Stance Control KAFO. The Figure Is Adopted and Modified from Reference [73].	46
Figure 2-17. The Spring Actuated Dynamic KAFO. The Figure Is Adopted and Modified	

from Reference [19, 74].	49
Figure 2-18. Function of the Knee Joint Mechanism of the Dynamic KAFO during the Entire Gait Cycle: (a) Start of Shock Absorption; (b) Weight Bearing; (c) Start of Swing Phase; (d) Knee Flexion in the Swing Phase. The Figure Is Adopted from Reference [19].	49
Figure 2-19. The Pneumatically Powered Knee-Ankle-Foot Orthosis. The Figure Is Adopted and Modified from Reference [75].	52
Figure 2-20. The C-brace® from OttoBock, Which Is Actuated by a Hydraulically Powered Mechanism. The Figure Is Adopted and Modified from Reference [77].	54
Figure 3-1. The Experimental Setup for Calibrating the NiTi#1 Superelastic Rod Sample.	69
Figure 3-2. The Experimental Setup for Sample Calibration: the NiTi#1 Superelastic Sample is Mounted on the Grippers.	69
Figure 3-3. Calibrated Phase Diagram for the NiTi#1 Superelastic Rod Sample.	70
Figure 3-4. Comparison of the Torque vs. Angle of Rotation of the NiTi#1 Superelastic Rod Sample between the Experimental and Simulation Results. The Calibration Temperature Is 24°C.	71
Figure 3-5. Comparison of the Torque vs. Angle of Rotation of the NiTi#1 Superelastic Rod Sample between the Experimental and Simulation Results. The Calibration Temperature Is 35°C.	72
Figure 3-6. Comparison of the Torque vs. Angle of Rotation of the NiTi#1 Superelastic Rod Sample between the Experimental and Simulation Results. The Calibration Temperature Is 45°C.	72

Figure 3-7. Adiabatic Simulation Result for the Superelastic Nitinol Rod Used in the Stance Actuating Part: Torque vs. Angle of Rotation.	75
Figure 3-8. Adiabatic Simulation Result for the Superelastic Nitinol Rod Used in the Swing Actuating Part: Torque vs. Angle of Rotation.....	75
Figure 3-9. The Stiffness Profile of the Dynamic Knee Actuator and that of a Normal Knee Joint. Pink Dash Curve: Normal Knee Stiffness Profile. Blue Curve: Stance Actuator Response. Red Curve: Swing Actuator Response. The Figure Is Adopted from Reference [89].....	76
Figure 3-10. Adiabatic Simulation Result for the Superelastic Nitinol Rod Used in the Stance Actuating Part: Shear Stress vs. Shear Strain.....	77
Figure 3-11. Adiabatic Simulation Result for the Superelastic Nitinol Rod Used in the Swing Actuating Part: Shear Stress vs. Shear Strain.	77
Figure 3-12. The MTS 858 Mini Bionix® II Biomaterials Testing System.	80
Figure 3-13. The NiTi#1 Superelastic Rod Is Installed on the MTS 858 Testing Machine.	80
Figure 3-14. The Two NiTi#1 Superelastic Rods Assembled with the Alloy Fixtures....	81
Figure 3-15. The Training Process of the Superelastic Nitinol Rod Used in the Stance Actuating Part. The 1 st and the 10 th Cycles Are Highlighted.....	82
Figure 3-16. The Training Process of the Superelastic Nitinol Rod Used in the Swing Actuating Part. The 1 st and the 10 th Cycles Are Highlighted.....	82
Figure 3-17. The Testing Setup Used to Calibrate the Shear Modulus of the Two Rubber Tubes.	84
Figure 3-18. The Neoprene Spring Rubber Tube and the 60A Polyurethane Tube Used in	

the Calibration Tests.....	84
Figure 4-1. The Conceptual Design of the Dynamic Knee Module: 1) the Internal Frame of the Knee Module That Is Connected to the Shank Segment; 2) the External Frame of the Knee Module That Is Connected to the Thigh Segment; 3) the Stance Actuating Part That Combines a Stiff Superelastic Nitinol Rod and a Stiff Torsional Spring In Parallel; 4) the Swing Actuating Part That Combines a Soft Superelastic Nitinol Rod and a Soft Torsional Spring in Parallel; 5) Two Push-Pull Solenoids. This Figure Is Adopted from Reference [16].....	90
Figure 4-2. The Dynamic Knee Module Assembly. (A) Swing Side of the External Frame of the Knee Module; (B) Stance Side of the External Frame of the Knee Module; (C) Swing Side of the Internal Frame of the Knee Module; (D) Stance Side of the Internal Frame of the Knee Module; (E) Swing Actuating Part; (F) Stance Actuating Part; (G) Swing Support Disk; (H) Stance Support Disk; (I) Swing Sleeve Bearing; (J) Stance Sleeve Bearing; (K) Stance Engagement Mechanism; (L) Swing Engagement Mechanism.....	91
Figure 4-3. The FEA Simulation Result of the Swing Side Part of the External Frame..	96
Figure 4-4. The FEA Simulation Result of the Swing Side Part of the External Frame..	97
Figure 4-5. The FEA Simulation Result of the Stance Side Part of the External Frame.	97
Figure 4-6. The FEA Simulation Result of the Stance Side Part of the External Frame.	98
Figure 4-7. The FEA Simulation Result of the Stance Fixture That Connects the Stance Superelastic Rod to the Dynamic Knee Module.....	99
Figure 4-8. The FEA Simulation Result of the Stance Fixture That Connects the Stance Superelastic Rod to the Dynamic Knee Module.....	99

Figure 4-9. The FEA Simulation Result of the Swing Fixture that Connects the Swing Superelastic Rod to the Dynamic Knee Module.....	100
Figure 4-10. The FEA Simulation Result of the Swing Fixture That Connects the Swing Superelastic Rod to the Dynamic Knee Module.....	100
Figure 4-11. The FEA Simulation Result of the Stance Side Assembly Combining the Stance Support Disk and the Stance Internal Frame.....	102
Figure 4-12. The FEA Simulation Result of the Stance Side Assembly Combining the Stance Support Disk and the Stance Internal Frame.....	102
Figure 4-13. The FEA Simulation Result of the Swing Side Assembly Combining the Swing Support Disk and the Swing Internal Frame.....	103
Figure 4-14. The FEA Simulation Result of the Swing Side Assembly Combining the Swing Support Disk and the Swing Internal Frame.....	103
Figure 4-15. The FEA Simulation Result of the Slider in the Stance Engagement Mechanism.....	104
Figure 4-16. The FEA Simulation Result of the Slider in the Swing Engagement Mechanism.....	105
Figure 4-17. The Connection of the Arduino UNO Board and Control Circuit.	107
Figure 4-18. The Preliminary Prototype of the Dynamic Knee Module.	108
Figure 4-19. The Connection between the Dynamic Knee Module and the Microcontroller.	109
Figure 4-20. The Stance and Swing Actuating Parts with Fixtures at Both Ends.	110
Figure 4-21. The Parts of the Dynamic Knee Joint Module.	110
Figure 4-22. The Final Prototype of the Dynamic Knee Joint Module.	111

Figure 4-23. The UT Dynamic KAFO Prototype with the Knee Module, the Control System, the Foot Switch, and the 12VDC Battery.....	111
Figure 5-1. The Marker Setup and EMG Sensors When Walking without the KAFO...	116
Figure 5-2. The Marker Setup and EMG Sensors When Walking without the KAFO...	116
Figure 5-3. The Marker Setup and EMG Sensors When Testing with the UT Dynamic KAFO.....	117
Figure 5-4. The Marker Setup and EMG Sensors When Testing with the UT Dynamic KAFO.....	117
Figure 5-5. Average Step Length with One Standard Deviation in the Three Testing Conditions. The Right and Left Sides Represent the Orthotic and Sound Legs, Respectively.	121
Figure 5-6. Average Stride Length with One Standard Deviation in the Three Testing Conditions. The Right and Left Sides Represent the Orthotic and Sound Legs, Respectively.	123
Figure 5-7. Average Cadence with One Standard Deviation in the Three Testing Conditions. The Right and Left Sides Represent the Orthotic and Sound Legs, Respectively.	125
Figure 5-8. Average Stance Phase Percentage with One Standard Deviation in the Three Testing Conditions. The Right and Left Represent the Orthotic and Sound Legs, Respectively.	126
Figure 5-9. Average Double Limb Support with One Standard Deviation for the Orthotic Leg in the Three Testing Conditions.	128
Figure 5-10. Average Single Limb Support with One Standard Deviation in the Three	

Testing Conditions. The Right and Left Sides Represent the Orthotic and Sound Legs, Respectively. 130

Figure 5-11. Knee Angle Change over the Entire Gait Cycle with One Standard Deviation in the Three Testing Conditions. The Red and Blue Solid Lines Represent the End of Stance Phase for the Slow Walking and the Dynamic Walking, Respectively. 132

Figure 5-12. Maximum Knee Stance Flexion Angles with One Standard Deviation in the Three Testing Conditions. The Right and Left Sides Represent the Orthotic and Sound Legs, Respectively. 133

Figure 5-13. Maximum Knee Swing Flexion Angles with One Standard Deviation in the Three Testing Conditions. The Right and Left Sides Represent the Orthotic and Sound Legs, Respectively. 134

Figure 5-14. Ankle Angle Change over the Entire Gait Cycle with One Standard Deviation in the Three Testing Conditions. The Red and Blue Solid Lines Represent the End of Stance Phase for the Slow Walking and the Dynamic Walking, Respectively. .. 135

Figure 5-15. Sagittal Hip Angle Change over the Entire Gait Cycle with One Standard Deviation in the Three Walking Conditions. The Red and Blue Solid Lines Represent the End of Stance Phase for the Slow Walking and the Dynamic Walking, Respectively. .. 137

Figure 5-16. Frontal Hip Angle Change over the Entire Gait Cycle with One Standard Deviation in the Three Testing Conditions. The Red and Blue Solid Lines Represent the End of Stance Phase for the Slow Walking and the Dynamic Walking, Respectively. .. 138

Figure 5-17. Pelvic Obliquity over the Entire Gait Cycle with One Standard Deviation in the Three Walking Conditions. The Red and Blue Solid Lines Represent the End of Stance Phase for the Slow Walking and the Dynamic Walking, Respectively. 140

Figure 5-18. Knee Moment over the Entire Gait Cycle with One Standard Deviation in the Three Walking Conditions. The Red and Blue Solid Lines Represent the End of Stance Phase for the Slow Walking and the Dynamic Walking, Respectively. 142

Figure 5-19. Comparison of the Knee Stiffness Profiles (Weight-Normalized Knee Moment vs. Knee Angle Change) in the Slow Walking and the Locked Mode. 143

Figure 5-20. Comparison of the Knee Stiffness Profiles (Weight-Normalized Knee Moment vs. Knee Angle Change) in the Slow Walking and the Dynamic Mode..... 144

Figure 7-1. The KAFO Ecosystem Flow Chart. 158

Figure 7-2. The Business Model Canvas for the Dynamic Knee Joint Module. 168

List of Abbreviations

A	Austenite Phase
A _f	Austenite Finish Temperature
A _s	Austenite Start Temperature
AAFO	Active Ankle-Foot Orthosis
AFO	Ankle-Foot Orthosis
Al	Aluminum
AM	Additive Manufacturing
C	Celsius
CAD	Computer Aided Design
EMG	Electromyography
FEA	Finite Element Analysis
FSR	Force Sensitive Resistor
GPa	Giga Pascals
GRF	Ground Reaction Force
K	Kelvin
KAFO	Knee-Ankle-Foot Orthosis
M	Martensite Phase
m	Meter
M ^{dt}	Detwinned Martensite Phase
M _f	Martensite Finish Temperature
M _s	Martensite Start Temperature
M ^t	Twinned Martensite Phase
mm	Millimeter
MPa	Mega Pascals
N	Newton
Pa	Pascal
PTFE	Polytetrafluoroethylene (Teflon)

SCKAFOStance Control Knee-Ankle-Foot Orthosis
SESuperelastic Effect
SEASuperelastic Alloy
SMAShape Memory Alloy
SMEShape Memory Effect

3SPScan, Spin, and Selectively Photocure

List of Symbols

C_A	Stress influence coefficient of austenite
C_M	Stress influence coefficient of martensite
D_i	Inside diameter
D_o	Outside diameter
E_A	Austenite modulus of elasticity
E_M	Martensite modulus of elasticity
G	Shear modulus
J	The polar moment of inertia of the cross sectional area
L	Gauge length
T	Torque
ε	Material transformation strain
θ	Angle of rotation
σ_f	Transformation finish stress from twinned martensite to detwinned martensite
σ_s	Transformation start stress from twinned martensite to detwinned martensite
τ	Shear stress

Chapter 1

Introduction

The purpose of this research is to develop a dynamic knee actuating system for knee-ankle-foot orthoses (KAFOs) with superelastic Nitinol, which reproduces normal knee joint behavior. This actuating system can be mounted on a conventional KAFO. The resulting device is named the UT dynamic KAFO. Four main study areas play important roles in developing the knee actuating system. Biomechanics of human walking is the first area. It is necessary to study the kinematic and kinetic characteristics of a normal knee joint over the entire walking cycle. This helps to determine the requirements of the knee actuator to reproduce the normal knee motions by compensating for the muscle deficiencies. The next area focuses on the knee kinematic and kinetic characteristics of individuals with weak quadriceps. The third aspect is on Nitinol. The material properties and responses are studied as the foundation of developing the knee actuating system using this alloy. At last, contemporary KAFOs are discussed in details, including their designs, functionality, applications, and limitations. This chapter introduces the first three of these main research aspects. The current knee-ankle-foot orthoses will be described later in chapter 2.

1.1 Biomechanics of Human Walking

Human walking shows two main portions: stance and swing phases, which take about 60% and 40% of the entire walking gait cycle, respectively [1-5]. The stance phase can be subdivided into loading response (0-10% of gait cycle), mid-stance (10-30% of gait cycle), terminal stance (30-50% of gait cycle), and pre-swing (50-60% of gait cycle), while the swing phase consists of early swing (60-75% of gait cycle), mid-swing (75-90% of gait cycle), and terminal swing (90-100% of gait cycle). The stance phase represents the period when the foot contacts the ground. At the moment of foot off, the swing phase starts and lasts when the foot is in the air. The next cycle initiates when the foot strikes the ground again. A complete walking gait cycle is shown in figure 1-1.

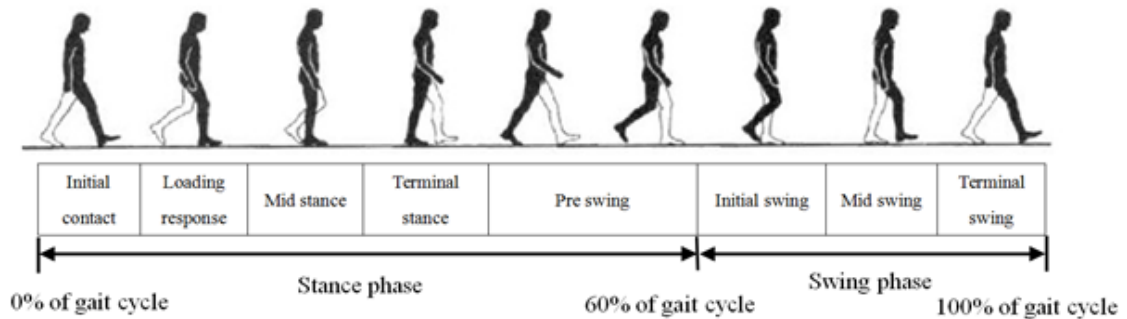


Figure 1-1. A Complete Walking Gait Cycle. This figure Is Adopted and Modified from Reference [6].

All the sub-phases in the walking gait cycle are presented as follows [7-14]:

Initial contact (0% of the gait cycle): this moment prepares the foot for the following shock absorption period via reaching a proper landing position.

Loading response (0-10% of the gait cycle): this is one of the two double limb

support periods during the stance phase and starts from the heel strike and ends at the foot flat. Heel rocker occurs during this time, which is one of the three rockers (heel rocker, ankle rocker, and forefoot rocker) in walking. The objective of this period is to transfer body weight onto the stance leg and maintain forward tendency of the body.

Mid-stance (10-30% of gait cycle): in this sub-phase the walking gait cycle enters the single limb support period. The stance leg alone supports the whole body weight and the contralateral leg is in its swing phase. Ankle rocker happens during this time.

Terminal stance (30-50% of the gait cycle): this phase starts from the heel off and ends at the heel strike of the contralateral leg, which accelerates the stance limb advancement. The third rocker, forefoot rocker, occurs during this period.

Pre-swing (50-60% of the gait cycle): this period is defined between the heel strike of the contralateral leg and the toe off of the stance leg. It is the second double limb support period. The body weight is gradually unloaded from the stance limb to the contralateral side, allowing toes of the supporting leg to leave the ground. The forefoot rocker continues during the pre-swing phase.

Early swing (60-75% of the gait cycle): early swing is the beginning of the swing phase. It initiates at the toe off and ends when the knee reaches a maximum flexion of about 60 degrees. During this period, the leg moves forward with the ankle dorsiflexed in order to clear the foot off the ground.

Mid-swing (75-90% of the gait cycle): mid-swing represents the phase between the moment of the maximum knee flexion in the swing and the moment when the tibia reaches a vertical position related to the ground. The swing leg keeps moving forward as a pendulum due to inertia forces.

Terminal swing (90-100% of the gait cycle): during the terminal swing, the tibia keeps advancing from the vertical position. The movement of the tibia is decelerated as the knee extends for the next foot contacting.

1.2 Kinematic and Kinetic Characteristics of a Normal Knee Joint

Knee angle and moment data throughout the entire normal walking gait cycle are reported in the literature [15] and shown in figures 1-2 and 1-3, respectively. Figure 1-2 indicates that the knee angle is around zero at the heel strike, to enable full extension of the leg, and then goes to about 15 degrees of flexion during the loading response. At the heel off, the knee joint extends to about 5 degrees. Then, at the end of the early swing phase, the knee tends to flex until around 60 degrees, which is the maximum flexion angle in the swing phase. During the terminal swing, the knee joint extends back to zero, preparing for the next gait cycle.

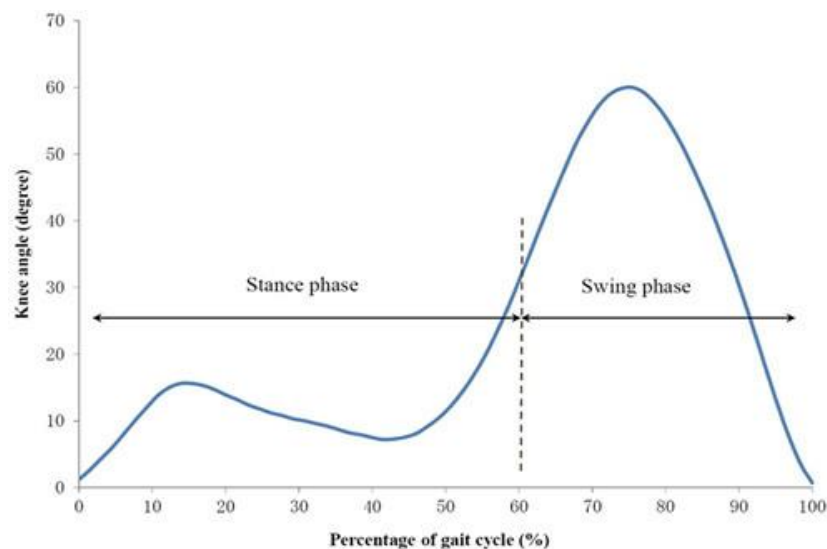


Figure 1-2. Flexion Angle Change of a Normal Knee Joint During the Entire Walking Gait Cycle. The figure is adopted from Reference [16].

Figure 1-3 shows the knee moment pattern over a normal walking gait cycle. First, extension moments are generated to control the knee flexion motion during the loading response. Then, flexion moments are followed to damp the extension movements during the mid-stance phase. Later in the terminal stance and pre-swing phases, the knee flexion motion is resisted by creating extension moments. Finally, knee flexion moments decelerate the forward movement of the leg, preparing for the next cycle.

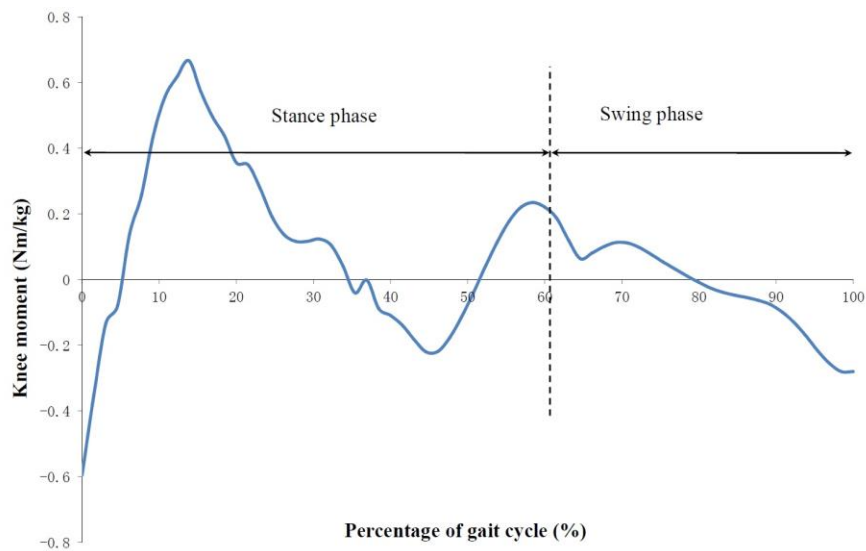


Figure 1-3. Knee Joint Internal Moment Normalized by Body Weight During the Entire Walking Gait Cycle. The figure is adopted from Reference [16].

By combining the data of the knee angle and moments listed above, normal knee joint stiffness can be calculated, as shown in the result in figure 1-4. The stiffness indicates the rate of change of the joint moment over the joint rotating angle. Individuals who cannot generate proper stiffness (resistance) in different gait periods have abnormal walking gait. The normal knee stiffness in figure 1-4 exhibits two distinct patterns for the stance and swing phases. Points 1 (heel strike), 2 (foot flat), and 3 (heel off) form the

knee stiffness curve during the loading response and the mid-stance phases. Similarly, points 3, 4 (the end of the initial swing), and 5 (full extension at next heel strike) compose the stiffness curve during the late stance, the pre-swing, and the swing phases. As shown in the figure, the knee stiffness profile during the loading response and the mid-stance phases has a higher slope and smaller hysteresis area. While in the rest of the gait cycle, the stiffness shows a lower slope and larger hysteresis. Therefore, an ideal knee actuator should offer two different stiffness patterns in order to fit the different requirements during the walking cycle. Fundamental design parameters can be obtained from figure 1-4. For a 60 kg patient, for example, the actuating elements should produce 40 Nm torque with 15 degrees of rotation and 10 Nm torque with 60 degrees of rotation, respectively.

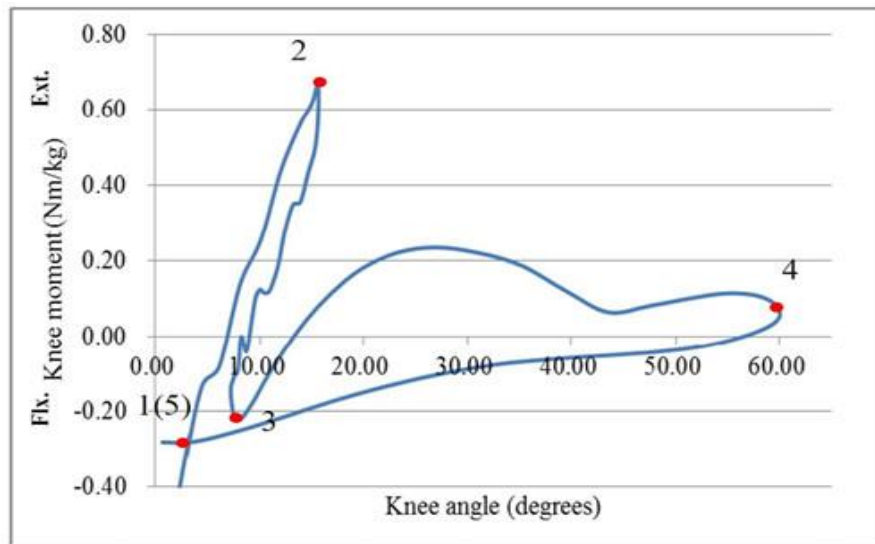


Figure 1-4. The Stiffness Profile for a Normal Knee Joint: Weight-Normalized Internal Knee Moment vs. Knee Angle. Point 1: the Heel Strike; Point 2: the Foot Flat; Point 3: the Heel Off; Point 4: the End of the Initial Swing Phase; Point 5: the Next Heel Strike. The Figure Is Adopted from Reference [17].

1.3 Abnormal Walking Gaits Caused by Weak Quadriceps

Quadriceps weakness is primarily caused by neurological and muscular diseases, such as post-polio, spinal cord injury (SCI), multiple sclerosis (MS), trauma, poliomyelitis, brain injury, inclusion body myositis (IBM), muscular dystrophy, and leg paralysis and paresis [18, 19]. Individuals with such neuromuscular disorders have limited ability to initiate knee extension or to control knee flexion. Walking with weak quadriceps is usually associated with some hyperextension compensations over the stance phase to avoid using the weak muscles [20]. This leads to a labored and unsafe gait, causing low walking speeds and limiting walking distances. Studying abnormal walking patterns caused by quadriceps weakness provides a better understanding of such dysfunction. Unfortunately, there is very limited information available for this topic.

Figure 1-5 shows the knee kinematic and kinetic characteristics of three patients who suffered from different levels of quadriceps weakness [20]. Figures 1-5(a) and (b) show slight weakness, figures 1-5(c) and (d) show medium weakness, and figures 1-5(e) and (f) show serious weakness. Figures 1-5(a) and (b) indicate that if patients have mild quadriceps weakness, their knee kinematic and kinetic profiles are very similar to those of healthy subjects. These patients can still perform knee extension to some extent during the whole walking gait cycle. In such cases, the deficit extension moments should be assisted by a KAFO. However, as the quadriceps strength decreases, the patients prefer to keep their legs in a hyperextended position during the stance phase. Such walking habits make it impossible to measure their residual muscle strength and determine the required compensation moments. Usually, for patients with severe quadriceps weakness a locked knee KAFO that fixes their legs in the full extension and can provide sufficient stability

during walking and standing is prescribed. The knee angle and moment data of the individual with severe quadriceps weakness have been extracted from figures 1-5(e) and (f) by Plot Digitizer 2.0 and the corresponding knee stiffness profile (the blue graph) is calculated and compared with the normal one (the red graph) in figure 1-6. Like the normal stiffness, the stiffness profile associated with weak quadriceps also has two sections. The stance section on the left side shows similar pattern to that of normal walking but in the opposite direction. And the swing section on the right side is close to the normal pattern. This indicates that quadriceps weakness induces knee hyperextension during the stance phase, causing high flexion moments to balance such motion.

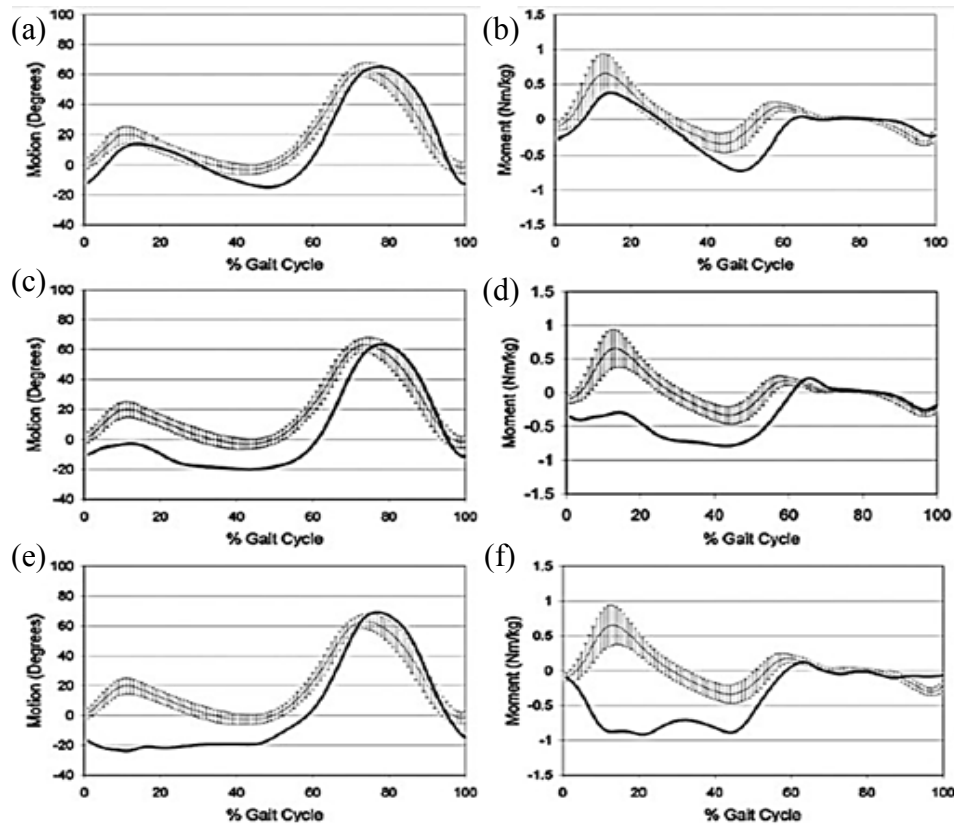


Figure 1-5. Kinematics and Kinetics Characteristics of Patients with Different Levels of Quadriceps Weakness: (a) and (b) for Slight Weakness, (c) and (d) for Medium Weakness, and (e) and (f) for Severe Weakness. The Figure Is Adopted from Reference [20].

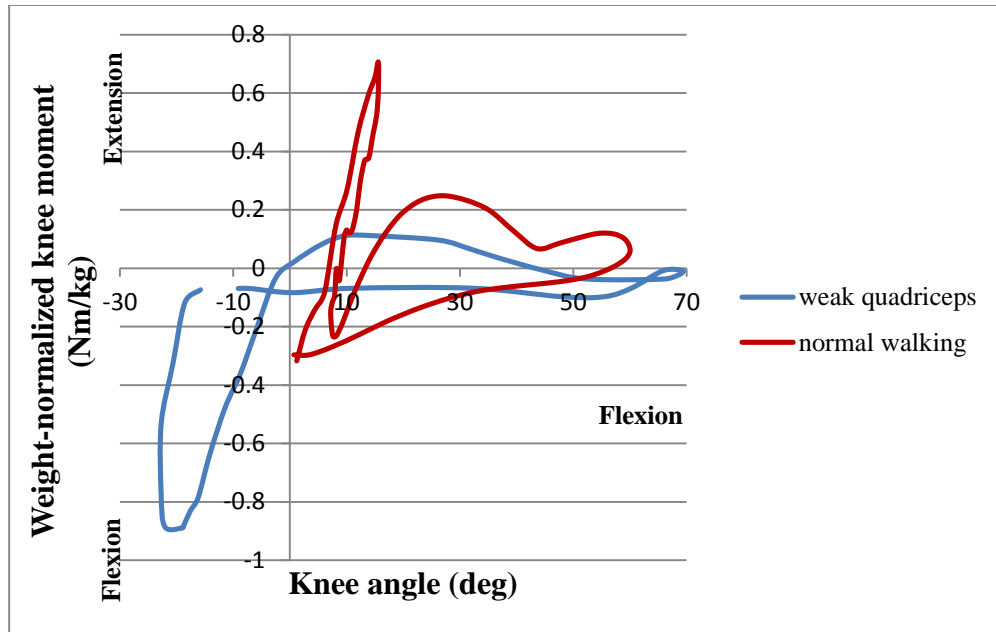


Figure 1-6. Comparison of the Knee Stiffness Profiles between the Individual with Severe Quadriceps Weakness and a Healthy Subject. All Data for the Weak Quadriceps Graph Is Extracted from Figures 1-5(e) and (f).

1.4 Shape Memory Alloys

Shape memory alloys, when used for actuation, offer biocompatibility, reduced weight, and small volume [21-26]. Nitinol is the most popular type of shape memory alloy and has been used to develop the dynamic knee actuating system in this research. Such an actuating system is expected to be lightweight and have a small size, making its wide acceptance possible in daily life. The ability of shape recovery in Nitinol is due to a phase transformation between the parent phase (austenite) and the martensitic phase in a reversible way under a variation of temperature and/or a load [27]. In general, Nitinol can transfer among three different phases: austenite phase (A), twinned martensite phase

(M^t), and detwinned martensite phase (M^{dt}). Each phase has its own crystal structure and material property, as shown in figure 1-7. The austenite phase also called parent phase, means that the material is in the high-temperature condition. The twinned and detwinned martensite phases occur in the low-temperature condition. Different from the other two phases, the detwinned martensite phase can only be induced by high loads. The transformation from the austenite to the martensite phases is called the forward transformation while the reverse transformation means the material changes back to the austenite phase. Martensitic start temperature M_s , martensitic finish temperature M_f , austenitic start temperature A_s , and austenitic finish temperature A_f are the four characteristic parameters associated with the phase transformation, as shown in figure 1-8. Nitinol has two distinct properties: shape memory effect and superelastic effect.

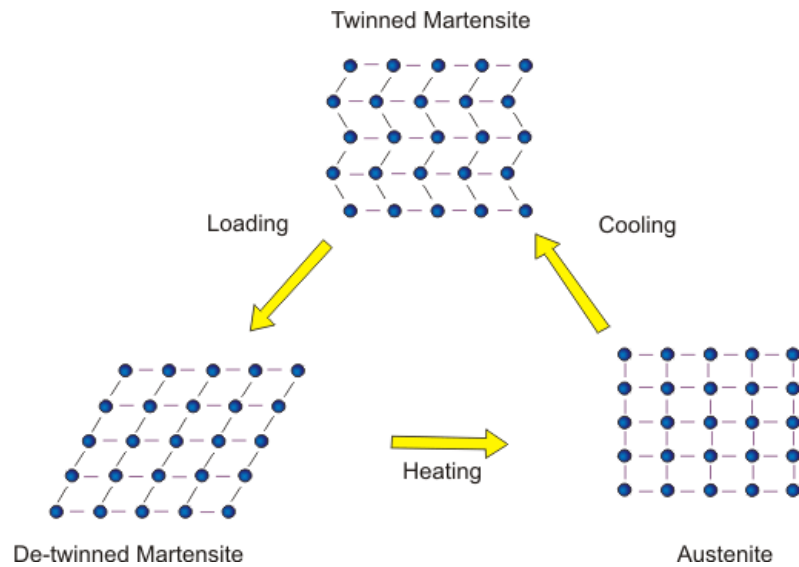


Figure 1-7. Three Different Crystalline Structures of Nitinol Alloys and the Relationship between Them. The Figure Is Adopted from Reference [28].

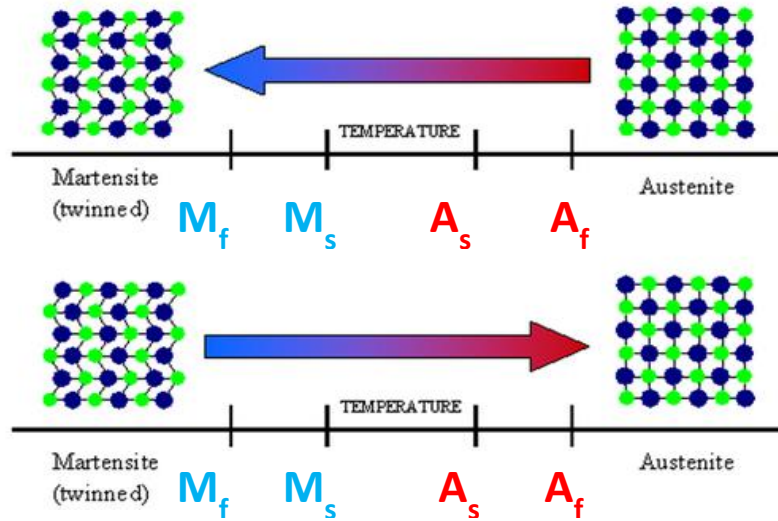


Figure 1-8. Forward and Reverse Phase Transformation Processes of Nitinol Alloys. The Figure Is Adopted and Modified from Reference [29].

1.4.1 Shape Memory Effect

The shape memory effect is the material behavior in response to the changing temperatures. Figure 1-9 illustrates the shape memory effect (SME) in a phase diagram: stress vs. strain vs. temperature. The starting temperature and stress is quite low and the material initiates from its twinned martensitic phase (point 2). The material is then loaded and transforms into the detwinned martensite phase as soon as the stress generated in the material exceeds the detwinned start stress level (σ_s). The detwinning process completes when the material stress reaches the detwinned finish stress level (σ_f). Continuously loading the material makes it deform elastically in the detwinned martensite phase, which is shown in the figure as point 3. The material recoils the elastic deformation and remains in the detwinned martensite when the external load is removed (point 4). Large residual strain (about 8%) can be observed at this time. When the material is heated up to the

austenite finish temperature (A_f), it will transform back to the austenite phase (point 1), eliminating all the shape changes. Finally, the material stabilizes in the twinned martensite phase (point 2) after cooling down to the original temperature and no shape change can be observed in this period.

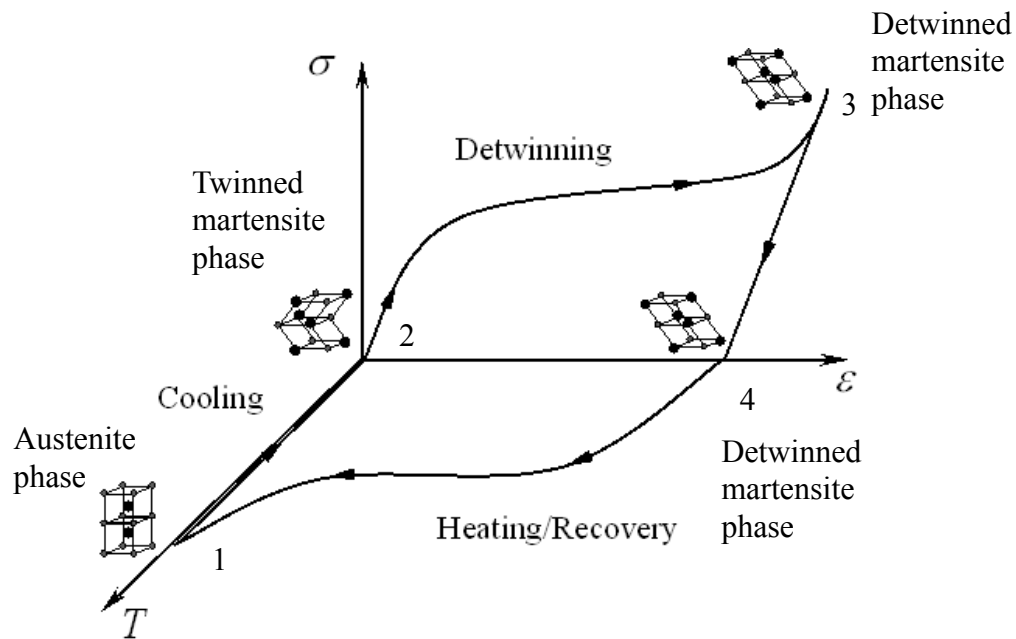


Figure 1-9. Phase Diagram of Nitinol with Shape Memory Effects. The Figure Is Adopted and Modified from Reference [30].

1.4.2 Superelastic Effect

The superelastic effect can be triggered when applying a sufficiently high mechanical load to the material. In the beginning, the material is in the austenite phase. The external load leads to a stress-induced transformation and creates a much higher recoverable strain (about 8%) than conventional materials. This strain can be eliminated

by simply unloading the material. The stress vs. strain curve in figure 1-10 shows the superelastic effect.

When a mechanical load is applied, the material first undergoes elastic deformation. The curve identified by the original point and point A represents for this period. At a certain load (force or moment), the material stress reaches σ_{Ms} (the initiation of forward transformation, point A), transforming the material from the austenite into the detwinned martensite phases. The transformation process ends at the stress level σ_{Mf} (the completion of forward transformation, point B) where the material is in the fully detwinned martensite phase. Further loading causes elastic deformation of the material in the detwinned martensite phase. During unloading, the Nitinol returns back to the austenite phase from σ_{As} (the initiation of reverse transformation, point C) and this process completes at σ_{Af} (the completion of reverse transformation, point D). Finally, the material recovers back to its starting shape. Nitinol with superelastic effect can match a wide range of applications where large deformations are required during loading and unloading.

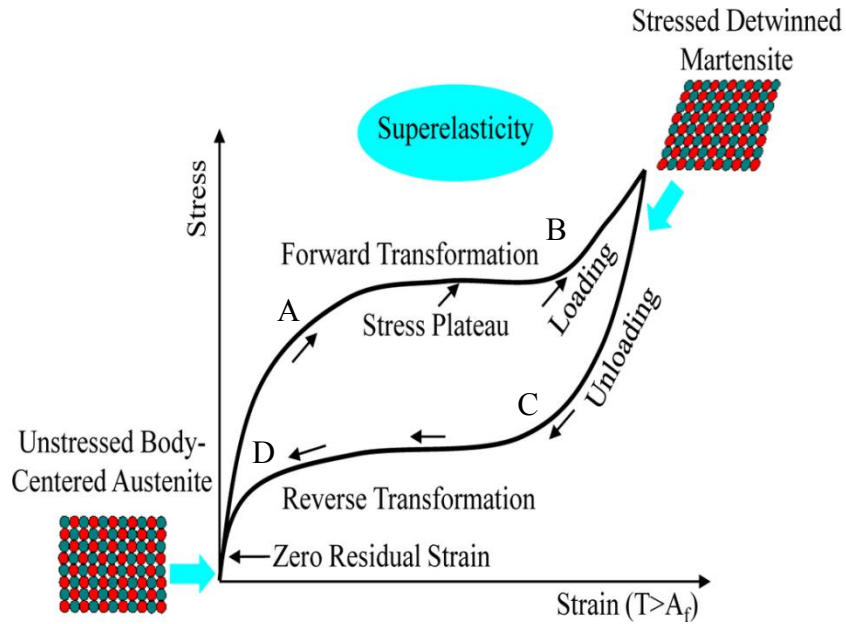


Figure 1-10. Phase Diagram of Nitinol with Superelastic Effect. The Figure Is Adopted and Modified from Reference [31].

1.4.3 Applications of Nitinol in Lower Limb Braces

Stirling, et al. [32] have developed a flexible lower leg orthosis with shape memory effect (SME) Nitinol actuators, covering both the knee and ankle joints. Shape memory alloys are formed into wire actuators in this design to trigger joint movements. There are nine actuators integrated into the device. Each actuator consists of four SME wires in parallel in order to generate enough force. The wires are shortened by passing a current through them so that the joint motions can be changed. At the knee level, there are four actuators on the posterior surface of the knee joint to assist knee flexion and one actuator on the anterior surface to assist knee extension, as seen in figure 1-11.a. Engaging the wire actuator on the anterior surface helps to extend the knee joint while engaging those on the opposite surface flexes the knee. The same concept is used at the

ankle level. Also there are four actuators but all in different directions: one set on the frontal surface to assist ankle dorsiflexion, one set on the dorsal surface to assist ankle plantar flexion, and two sets on the medial and lateral surfaces to perform pronation and supination, respectively, as shown in figure 1-11.b. The heating and cooling process of the shape memory wires makes the response time of this orthosis too slow to be used in real walking motions. It can only be used as a rehabilitation device for joint function recovery.

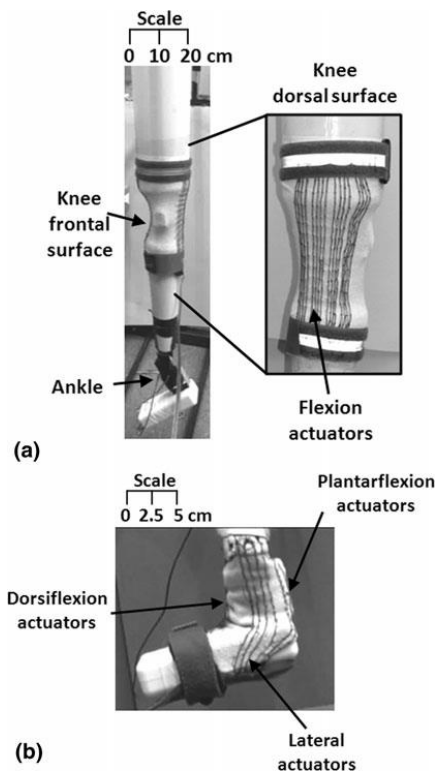


Figure 1-11. A Robotic Lower Leg with the Flexible Orthosis Actuated by Nitinol with Shape Memory Effect: (a) the Knee Actuators and (b) the Ankle Actuators. The Figure Is Adopted from Reference [32].

Deshpande et al. [33-35] have developed an active ankle-foot orthosis (AAFO), using shape memory Nitinol to reproduce the normal ankle stiffness profile. In this study, an innovative actuation system is proposed by embedding SMA wires on a conventional ankle-foot orthosis (AFO). The AAFO aims at assisting the dorsiflexion motion for those who are able to plantarflex their ankle normally but lack dorsiflexion. In order to reproduce the healthy ankle stiffness pattern, different combinations of shape memory alloys (SMA) and superelastic alloys (SEA) have been simulated and tested. A solution of arranging two shape memory wires in parallel has been proved to have the potential of mimicking the normal ankle behavior. This active AFO design is illustrated in figure 1-12. However, a complex control system needs to be associated with the brace, and the slow response time caused by heating/cooling diminishes its practical applicability. Based on the previous research, Deberg, et al. [36-38] developed an active ankle actuator with superelastic Nitinol. The device is shown in figure 1-13. This actuator provides a much quicker response and makes it possible to use the brace for functional ambulation. Ankle plantarflexion tends to stretch the superelastic wires, which resists hyper plantarflexion motions and stores the energy to assist dorsiflexion. Motion analysis tests have been performed and the results indicate that this AAFO is able to improve abnormal gait in a patient with a condition causing drop foot.

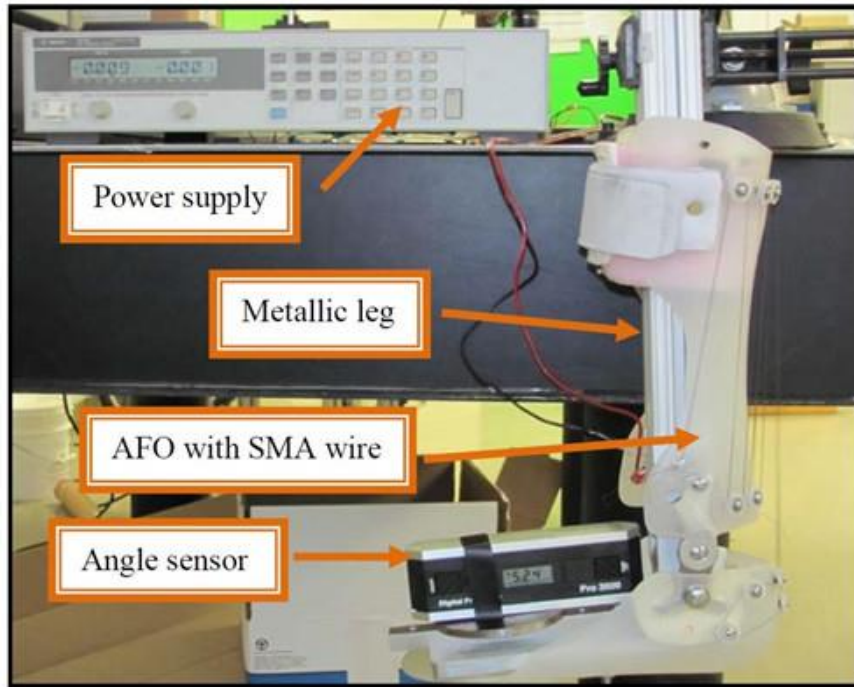


Figure 1-12. The Active Ankle-Foot Orthosis Actuated by Nitinol Wires with Shape Memory Effect. The Figure Is Adopted from Reference [34].



Figure 1-13. The Active Ankle-Foot Orthosis Actuated by Nitinol Wires with Superelastic Effect. The Figure Is Adopted from Reference [37].

Gorzin et al. [39, 40] have proposed a conceptual AAFO using a superelastic rod actuator with a design based on the multi-axial behavior of the material. This superelastic rod is located parallel to the ankle axis and is loaded under torsion on one end via ankle rotation and under compression on the other end via a linear solenoid, as illustrated in figure 1-14. Such axial loading makes it possible to adjust the torsional stiffness of the superelastic rod over the entire gait cycle and to match various stiffness profiles of different walking speeds. The working process of the actuator is described as follows. First, the superelastic actuator acts during the loading response to avoid foot slapping without any axial load, providing the smallest torsional stiffness in this period. Then, the linear solenoid engages during the mid-stance phase, increasing the actuator stiffness for energy absorbing in the terminal stance. Third, by reducing the axial load in the pre-swing phase, the user is able to perform the push off by overcoming less resistance and continue storing torsional energy in the superelastic actuator. Finally, both the axial and torsional loads are removed from the superelastic rod. The stored energy is released to lift the foot up to the neutral position over the swing phase. Also, Gorzin et al. [39] have published another AAFO concept with a superelastic actuator loaded under bending moments, as shown in figure 1-15. The ankle mechanism includes a superelastic hinge, an adjustable joint, a linear actuator, a slider, and a carriage guide. In this design, the linear actuator determines the location of the slider and adjusts the length of the hinge according to different stiffness requirements at the ankle. Plantarflexion motions deform the superelastic hinge element and generate bending energy in the hinge, which will be released to assist ankle dorsiflexion after the foot leaves the ground.

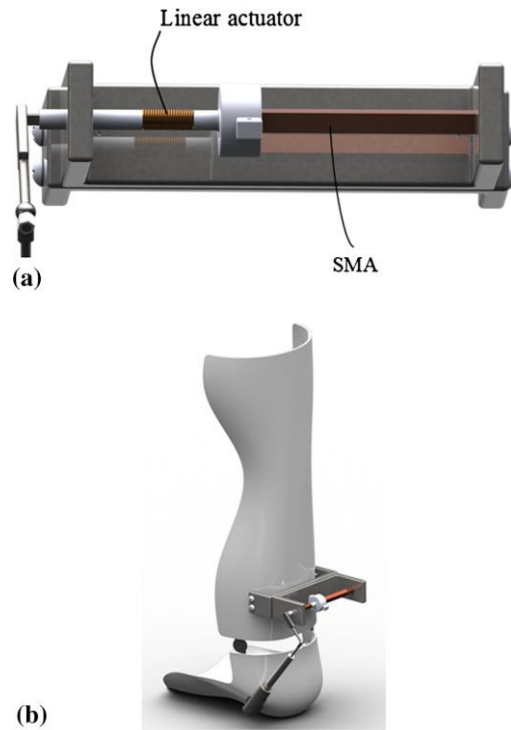


Figure 1-14. An Active AFO Uses a Superelastic Actuator under Combined Axial-Torsional Loads. (a) The Superelastic Ankle Actuator. (b) An Overall View of the AAFO. The Figure Is Adopted from Reference [40].

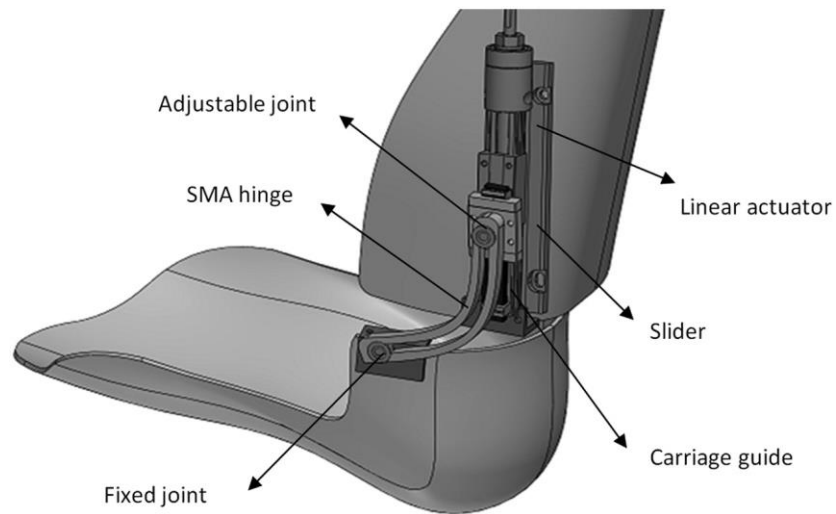


Figure 1-15. The Active AFO with an Adjustable Ankle Hinge Made with Superelastic Alloy. The Figure Is Adopted from Reference [39].

Pittaccio et al. [41] developed a rehabilitation device called Toe-Up for individuals suffered from paresis at their ankle joints. The device is shown in figure 1-16, which is composed of a shank brace, a foot brace, and an ankle actuator. The ankle actuator includes two pseudoelastic bias springs and some shape memory Nitinol wires. There are four sets of shape memory wires arranged in the actuator in order to provide enough pulling force at the ankle. This device provides cyclic ankle motions between two specific positions. In the beginning, the two springs stretches the shape memory wires, keeping the ankle in a plantarflexion position. By engaging the shape memory actuator, the wires are shortened to initiate dorsiflexion motions until the designed position. Then, the two springs recoil the ankle back to its original place for the next cycle as the actuator is disengaged. Superelastic Nitinol also has been made into spring actuators with specific shapes. The AFO device shown in figure 1-17 is developed to maintain the ankle at a fixed position in order to relieve muscle contractures and spasticity around the joint. Two springs made of superelastic NiTi are involved in this hinge, being shaped as a capital letter omega. This particular shape allows the material to be loaded uniformly along its entire length, avoiding stress concentration and producing nonlinear recovery forces along elongation. The recovery forces will be high when the springs are far from their original shape and will be gentler when the joint is close to its designed angle.

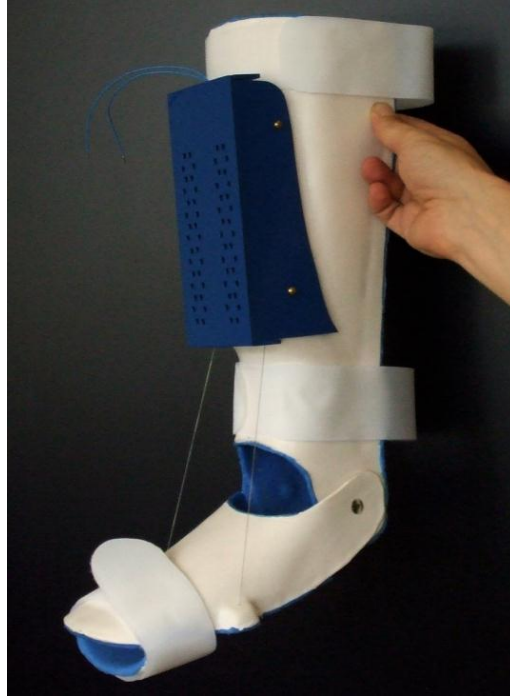


Figure 1-16. The Ankle Rehabilitation Device with an Ankle Actuator on the Shank Segment Uses Shape Memory Nitinol Wires. The Figure Is Adopted from Reference [42].

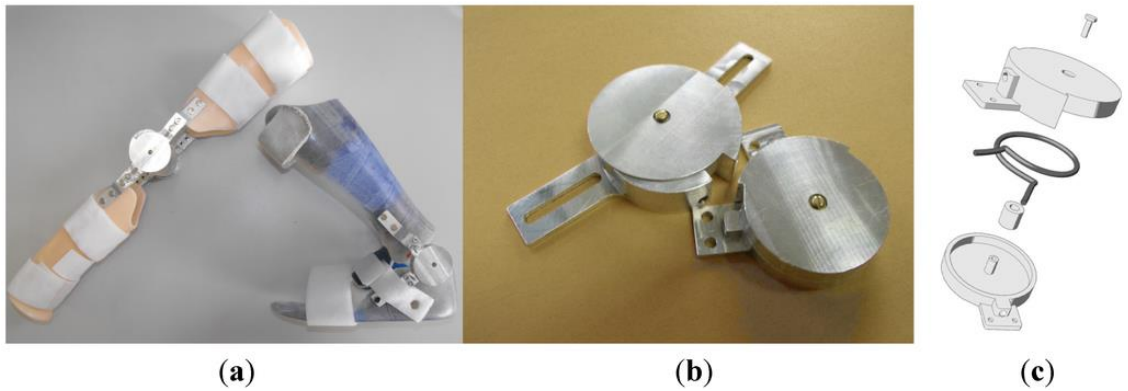


Figure 1-17. (a) Lower Leg Orthoses Actuated by Superelastic Nitinol Actuators. (b) Parts of a Hinge Joint. (c) The Assembly of the Hinge Joint with Superelastic Nitinol Actuators. The Figure Is Adopted from Reference [41].

1.5 Summary

The purpose of this research is to develop a dynamic knee actuating system for a knee-ankle-foot orthosis which can be prescribed for individuals with weak quadriceps, thus producing normalized knee motions in walking. Biomechanics of human walking, normal knee behavior, and abnormal gait caused by quadriceps weakness are important aspects that need to be studied before designing the knee actuating system. The proposed system will be actuated by Nitinol, which is the most popular type of shape memory materials currently in use. Nitinol has a unique ability to recover its original shape, and also provides the potential for creating actuators that are light weight and small in volume. This makes Nitinol an attractive option for this research. Applications of Nitinol have already been found in some rehabilitation devices.

Chapter 2

Knee-Ankle-Foot Orthoses

Knee-ankle-foot orthoses (KAFOs) are designed to assist abnormal ambulation, providing compensation motions for joints and muscles of the lower leg. There are three types of KAFOs in the market: passive KAFOs, stance control KAFOs (SCKAFOs), and dynamic KAFOs. The conventional passive KAFOs use simple mechanisms to either lock the knee joint or set it free over the entire gait cycle. SCKAFOs block knee motions in the stance and release the knee in the swing. Dynamic KAFOs control the knee joint during both the stance and swing phases to mimic normal knee performance. This chapter includes a detailed description of various KAFOs and summarizes their problems and limitations.

2.1 Passive KAFOs

Some passive KAFOs fix the knee joint in the full extension position all the time. Such devices provide enough support but cause stiff walking patterns. Others allow free knee motions inversely, producing limited stability [43]. Passive KAFOs are the most conventional type and are often prescribed for individuals with severe quadriceps

weakness, broken bones, unilateral leg paralysis/paresis, and other similar diseases. This section discusses some typical passive KAFOs in the market.

2.1.1 Drop Lock KAFO

A drop lock KAFO uses a straight-set knee joint and a sleeve lock [44-46] that slides up and down to achieve locking/ unlocking. The joint can be locked automatically via reaching full extension at the knee and unlocked by manually removing the sleeve [45]. Figure 2-1.a shows that the drop lock keeps the knee joint in the straight position during walking. And figure 2-1.b shows that the knee joint is released for sitting. For patients with severe muscle weakness, KAFOs with a drop-lock are typically prescribed in order to get enough stability.

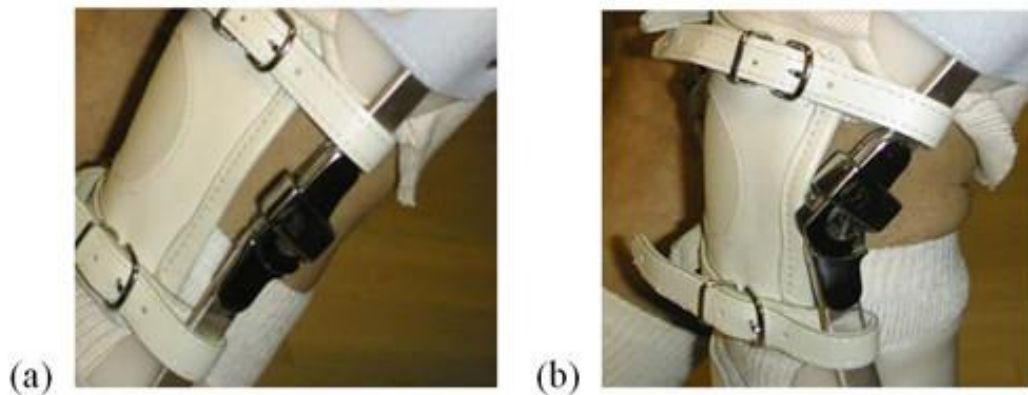


Figure 2-1. The Knee Joint Mechanism of a Drop Lock KAFO: (a) the Knee Joint Is Locked during Walking; (b) the Knee Joint Is Free for Bending. This Figure Is Adopted from Reference [44].

2.1.2 Posterior Offset KAFO

The posterior offset KAFO is designed to enable the maintenance of knee stability without locking the joint. In this design, the knee mechanism is located posteriorly to the anatomic knee joint, as shown in figure 2-2, thus positioning the user's body weight anteriorly [45, 46]. During the stance phase, the extension position can be kept steadily as long as the ground reaction force (GRF) vector passes over the hinge axis. During the swing phase, the knee joint is allowed to rotate freely. Keeping balance with the posterior offset KAFO requires some compensation motions, such as slightly leaning the upper body forward [45]. These devices provide limited stability and in some cases drop locks are used to strengthen the support. Offset joint KAFOs work efficiently for those without knee or hip flexion contracture.



Figure 2-2. The Knee Joint Mechanism of a Posterior Offset Joint KAFO. The Figure Is Adopted from Reference [45].

2.1.3 Polycentric Joint KAFO

Theoretically, the polycentric joint KAFO [45, 47], as shown in figure 2-3, is designed to reproduce natural knee movements because an anatomical knee joint has both translational and rotatory motions instead of only rotating around a single axis. Like the posterior offset joint KAFO, this device achieves extension stability during the stance phase because the GRF is anterior to the instantaneous knee center of rotation (COR). Again the knee joint is free to rotate during the swing phase. However, a polycentric joint is more complex than a hinge joint. Hence, it is not used very often, especially in SCKAFOs and dynamic KAFOs. There is only one application of the polycentric knee joint in dynamic KAFOs, which will be discussed later.



Figure 2-3. The Knee Joint Mechanism of a Polycentric Joint KAFO. The Figure Is Adopted from Reference [45].

2.1.4 Bail Lock KAFO

A bail lock KAFO, as shown in figure 2-4, uses a spring-loaded bail mechanism to lock and release the knee joint. The spring is pre-loaded to lock the knee at the fully extended position [45, 46]. Lifting up the bail can compress the spring and remove the lock from its original locking position. The bail lock connects both the medial and lateral joints so that they can be locked and unlocked simultaneously. This design is convenient for those who use KAFOs bilaterally or have some degree of functional disability in their hands. However, the bail protrudes posteriorly when the knee is flexed, causing cosmetic problems.

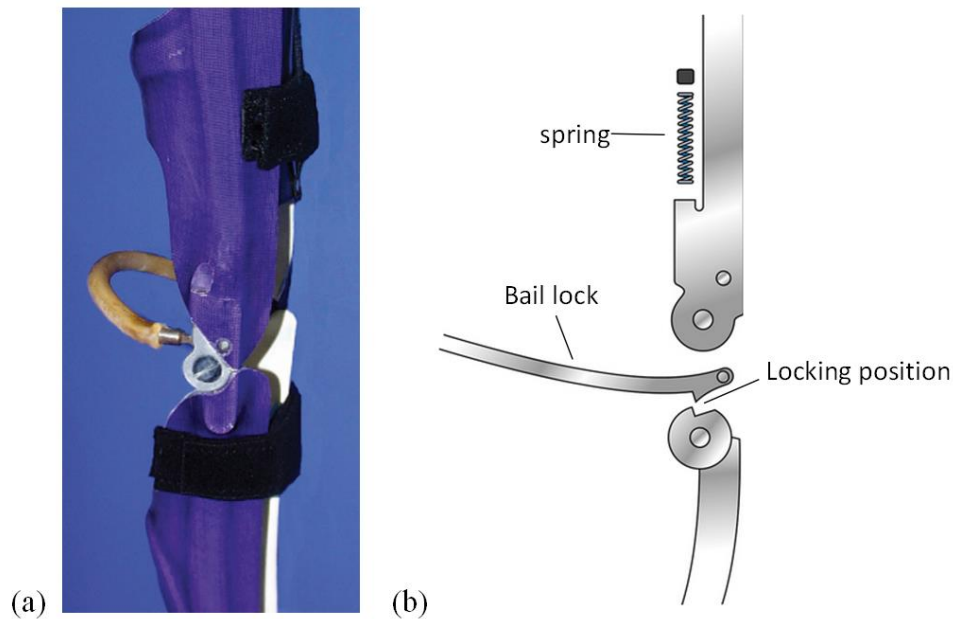


Figure 2-4. (a) A Bail Lock KAFO; (b) the Knee Joint Mechanism of a Bail Lock KAFO.

The figure Is Adopted from Reference [45].

2.1.5 Ratchet Lock KAFO

The ratchet lock knee mechanism consists of a ratcheting disk and a side release lever, as shown in figure 2-5 [45, 48]. Flexion motion of the knee joint is always blocked when the ratchet is engaged, but meanwhile the extension motion is free due to the unidirectional ratchet mechanism. Pressing down the release lever can disengage the ratchet, making the knee joint act as a straight-set joint. The ratchet mechanism permits the knee joint to be locked at various flexion angles during the whole gait cycle. This device is suitable for individuals with knee flexion contracture deficiencies. Choosing right ratchets allows reaching proper operating increments in the device.

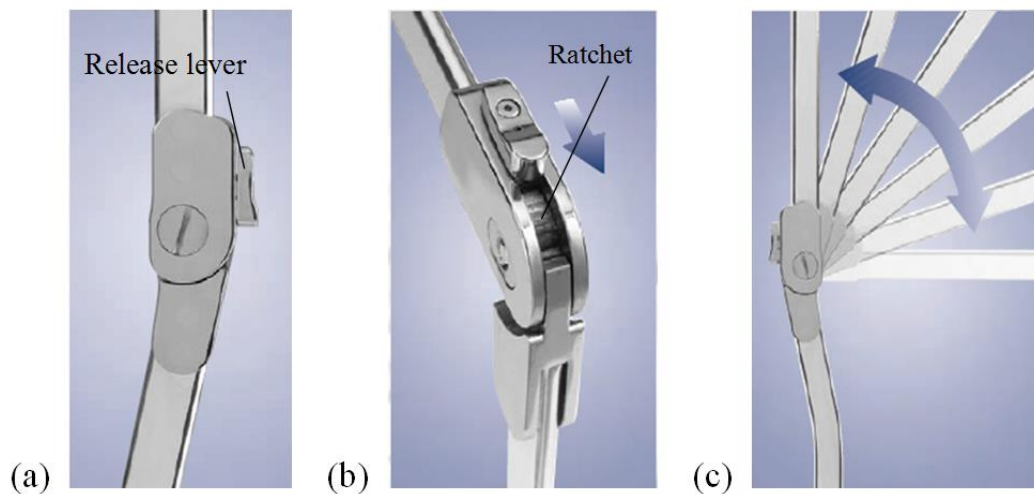


Figure 2-5. (a) The Side View of a Ratchet Lock Knee Joint; (b) the Ratchet Locking Mechanism; (c) the Knee Flexion Range of the Ratchet Lock Knee Joint. The Figure Is Adopted and Modified from Reference [48].

2.1.6 Dial Lock KAFO

There is a serrated disk and a dial lock included in the knee joint mechanism of a dial lock KAFO. The serrated disk makes it possible to lock the knee joint at various flexion angles. The device is able to fit different flexion contractures by increasing or decreasing the locking angles [45, 46, 49]. Compared with the ratchet lock KAFO, the serrated disk can accommodate specific disability requirements more precisely since it has more increments than the ratchets. The knee joint is engaged automatically by doing extension motions and can be disengaged manually by pulling up the dial. This design is good for patients who have knee flexion contractures and undergo recovery gradually. A dial lock KAFO is shown in figure 2-6.

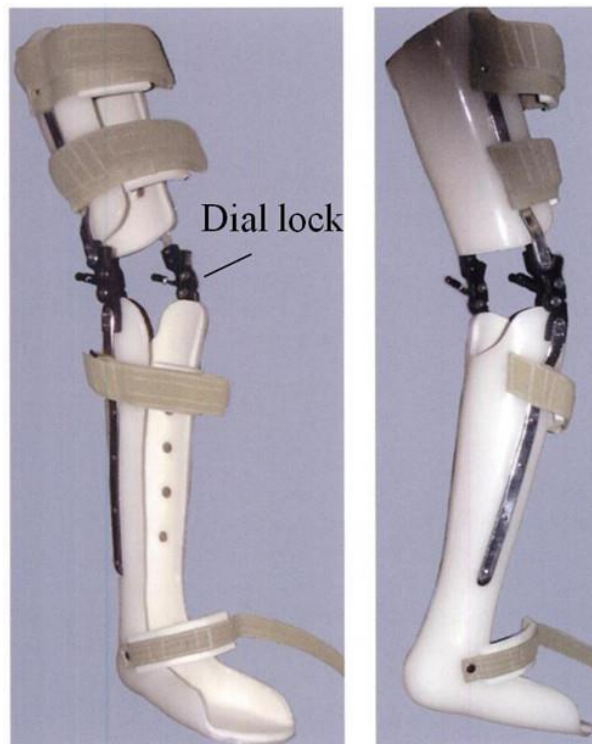


Figure 2-6. A Dial Lock KAFO. The Figure Is Adopted and Modified from Reference [49].

2.2 Stance Control KAFOs

A stance control KAFO (SCKAFO) prohibits knee movements in the stance while allowing free rotation at the knee in the swing [50-52]. SCKAFOs generate smoother gait compared to the passive KAFOs. Also, gait compensation motions and energy consumption are reduced due to the flexible knee during the swing phase [53, 54]. This section describes some popular SCKAFOs.

2.2.1 Otto Bock Free Walk/ Becker Orthopedic UTX

Otto Bock HealthCare's Free Walk and Becker Orthopedic's UTX [55] use similar knee mechanisms which include a spring-loaded pawl lock and a control cable. The control cable connects the pawl lock to the foot part of the KAFO. When the knee joint is at full extension, the pawl lock automatically fits into the locking space. Then, the joint rotation is blocked during the stance phase to guarantee stability, as shown in figure 2-7.a. When the ankle dorsiflexes to about 10 degrees, the control cable is pulled down to remove the pawl out of the locking position, setting the knee free during the swing phase. Figure 2-7.b shows the free motion of the knee joint during the swing phase.

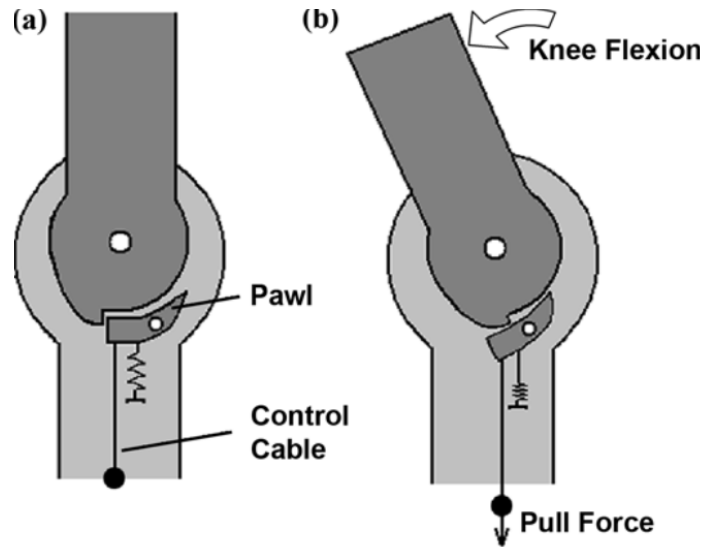


Figure 2-7. Otto Bock Free Walk/Becker Orthopedic UTX: (a) Spring-Loaded Pawl Locks the Knee Joint during the Stance Phase; (b) Ankle Dorsiflexion Pulls Down the Cable and Releases the Joint in the Late Stance Phase. The Figure Is Adopted from Reference [55].

2.2.2 Fillauer® Swing KAFO

A weighted pawl actuated by gravity is used in the knee joint mechanism of the Fillauer® swing KAFO [55], as shown in figure 2-8. During the stance phase, the weighted pawl falls into the locking position automatically as shown in figure 2-8.a, blocking the knee joint motion. This is caused by moving the thigh segment forward before the moment of heel strike. Then during the swing phase, the pawl leaves the locking position when the thigh segment moves behind the body, as shown in figure 2-8.b. This locking/ unlocking mechanism has to be adjusted in order to meet specific users' requirements. The part connected to the thigh segment is always in contact with the weighted pawl during the stance phase, thus creating a friction force that resists releasing

the lock. Users are asked to extend intentionally in late stance in order to eliminate the friction force and disengage the pawl easily. There is a switch located on this orthosis to change its knee function among three modes: free mode, lock mode, and stance control mode. In the free mode, the joint moves freely during the whole gait cycle. In the lock mode, the knee is locked all the time. In the stance control mode, the joint is locked during the stance phase and unlocked during the swing phase.

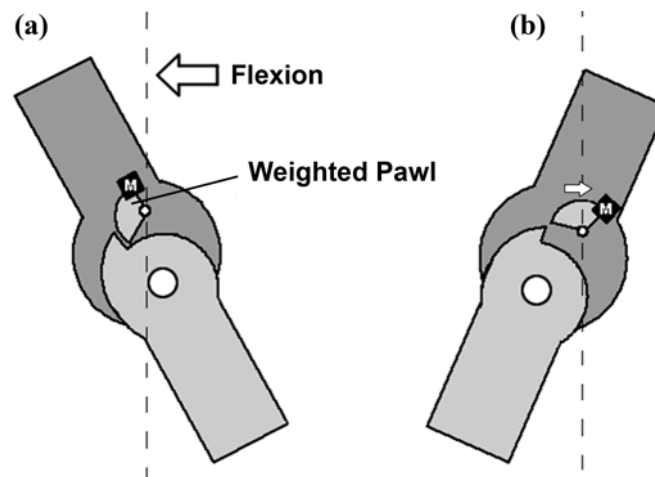


Figure 2-8. Gravity-Activated Fillauer Swing Phase Lock: (a) the Weighted Pawl Falls into the Locking Position to Resist Flexion during the Stance Phase; (b) the Pawl Falls out of the Locking Position to Allow Free Motion during the Swing Phase. The Figure Is Adopted from Reference [55].

Otto Free Walk/ Becker Orthopedic UTX and Fillauer® swing KAFO use simpler mechanisms and are much lighter than other SCKAFOs because they don't have any power supply. However, patients must intentionally extend their knee when switching in order to counteract the flexion moments, engaging and disengaging the mechanical joints. Also, individuals with the disability at ankle or hip cannot be prescribed with these orthoses.

2.2.3 Becker 9001 E-Knee Orthosis

The knee joint of the Becker 9001 E-Knee Orthosis is controlled by a one-way dog clutch, as shown in figure 2-9 [55]. There are (1) two circular ratchet plates, (2) a coil, (3) a tension spring, (4) a foot switch, and (5) a battery pack in this knee joint mechanism. At the initial contact, the coil is closed and two ratchet plates come together based on the foot switch signals, overcoming the spring force. Then the flexion is blocked and the extension is allowed during the stance phase. When the foot clears the ground, the coil will open in order to depart the two ratchet plates. This means that the knee joint can rotate during the swing phase. There are some disadvantages existed in the design. First, the flexion motion of this orthosis cannot be blocked at once due to the nature of the engagement of the ratchets. Second, the two ratchet plates and the coil make the joint heavy. Third, extension motion is also required to engage/ disengage the two ratchets. Furthermore, this system makes big noises when the ratchet plates rotate to extend after being engaged.

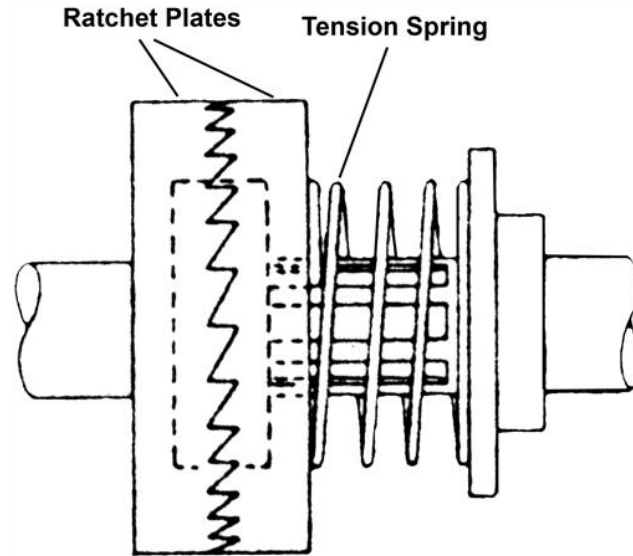


Figure 2-9. The Electromagnetic Knee Joint Mechanism of the Becker Orthopedic 9001 E-Knee Brace. The Figure Is Adopted from Reference [55].

2.2.4 Horton Stance Control Orthosis

The Horton Stance Control Orthosis [55-57] uses a cam based locking mechanism at the knee joint. The system includes: (1) a thermoplastic stirrup shell that is located under the foot part of the KAFO and can be pushed up when the foot contacts the ground, (2) an eccentric cam that is the core part in this design, (3) a friction ring that rubs with the cam to brake knee motions when bearing weight, and (4) a pushrod that rigidly connects the cam and the stirrup shell. The mechanism is shown in figures 2-10.a and 2-10.b. At the foot contact, the stirrup shell rises up together with the pushrod, causing the cam and the friction ring touch each other. As long as the foot is on the ground, the knee flexion motion is blocked and the extension motion is allowed because flexion moves the friction ring towards the cam and extension separates them apart. When the orthotic leg swings in the air, the cam will move down to disengage the locking mechanism. Similar

to the Fillauer® orthosis, the knee joint of the Horton orthosis can work under three different modes: free mode, lock mode, and stance control mode. In this SCKAFO, the knee joint can be locked at any position to match various knee flexion contractures. However, lodging pants or other stuff in the gap between the stirrup shell and the foot part causes falling problems. Also, shoes with larger size are required when using a KAFO like this. Moreover, extension motion is required to engage/ disengage the cam and the friction ring as the users switch between the stance and swing phases.

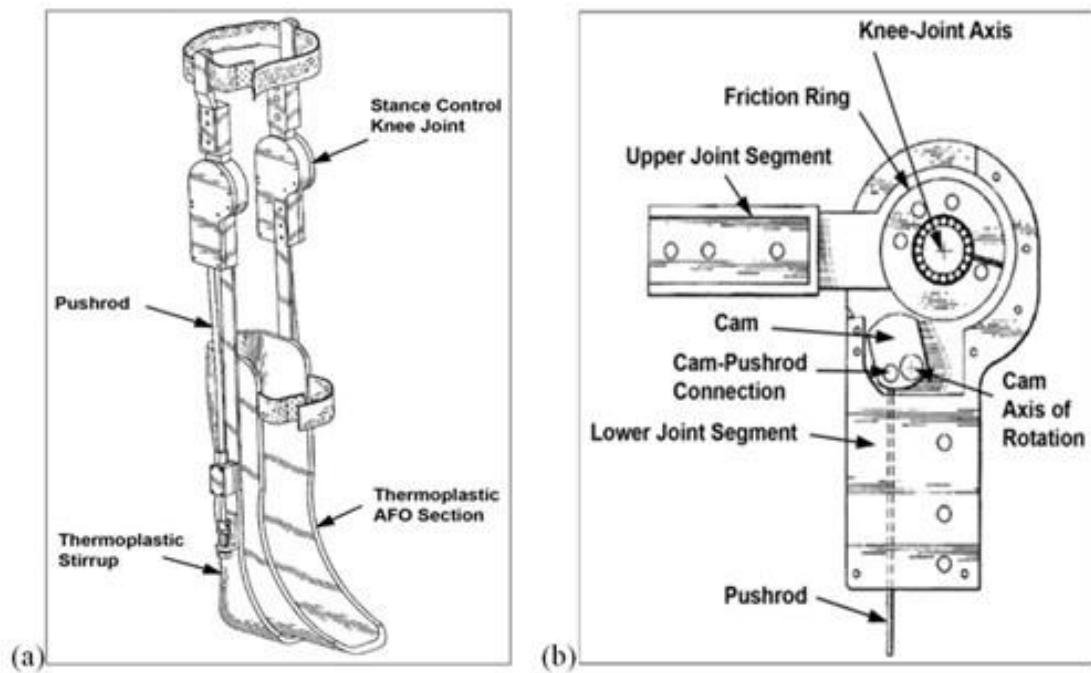


Figure 2-10. (a) The Horton Stance Control KAFO; (b) the Knee Joint Mechanism of the Horton SCKAFO. The Figures Are Adopted from Reference [55].

2.2.5 Belt-Clamping Joint SCKAFO

The belt-clamping knee mechanism in this SCKAFO [55, 58-62] is friction based, resisting knee flexion in the stance phase and releasing knee movements in the swing phase. The belt-clamping knee joint is developed as a module that can be easily installed on any passive KAFOs. The belt-clamping SCKAFO includes: (1) two knee modules on the medial and lateral sides, (2) polypropylene thigh and shank shells, (3) thigh and shank brackets, (4) a foot part, (5) three force-sensing-resistor (FSR) pressure sensors, and (6) a control system, as shown in figure 2-11. The three sensors are attached below the foot part of the orthosis. Each of the two knee modules includes (1) a belt-clamping mechanism, (2) a disc connected to the thigh brackets, and (3) two face plates connected to the shank brackets. The disc and the face plates rotate around the pin of the disc that is also the knee center. There is an extension stop pin located on the knee disc to restrict the rotation of the two face plates, avoiding the hyperextension of the knee joint. The shape of the thigh bracket and the face plates limit the flexion motion of the knee joint within 110 degrees. The belt-clamping mechanism is composed of (1) a hammer, (2) a hammer recoil spring, (3) a hammer screw, (4) a push type solenoid, (5) a belt, (6) an anvil, (7) a belt recoil spring, and (8) a spring bracket, as shown in figure 2-12. The hammer can rotate around a pin located in the center. The solenoid is always engaged to keep its plunger in the high position, fixing the hammer screw to avoid any motion of the hammer. This guarantees enough space between the anvil and the hammer, allowing free belt movements between them. The solenoid could be disengaged to drag the plunger to the down position when signals of the three FSR sensors reach a predetermined threshold at heel strike. Then the hammer tends to overcome the moment caused by the hammer

recoil spring and rotates in the clockwise direction when the knee flexes, narrowing the space between the anvil and the hammer to clamp the belt between these two parts. In this way, only slight flexion at the knee joint is allowed in stance according to the belt elasticity. On the contrary, knee extension motion makes the hammer rotate in the counterclockwise direction, loosening the clamped belt. This notes that the knee joint is free to extend during the stance phase. In the late stance phase, users have to extend their knee purposely to clear the hammer screw away from the plunger's track. Then the solenoid can be engaged and raise its plunger up again to block the hammer screw when the pressure detected by the sensors is lower than the threshold after the foot leaves the ground. Therefore, the solenoid plunger keeps the hammer away from the anvil, and the knee joint is released to be free during the swing phase.

The belt-clamping SCKAFO gives users a larger range of knee motion from 0 to 110 degrees than other devices (usually from 0 to 90 degrees). Also, this mechanism allows small angles of knee flexion in the stance phase instead of fixing the knee joint completely as others did. However, unsmooth gait occurs when users extend their knees to prepare for the switching between the two phases. Also, this device is quite heavy and large.

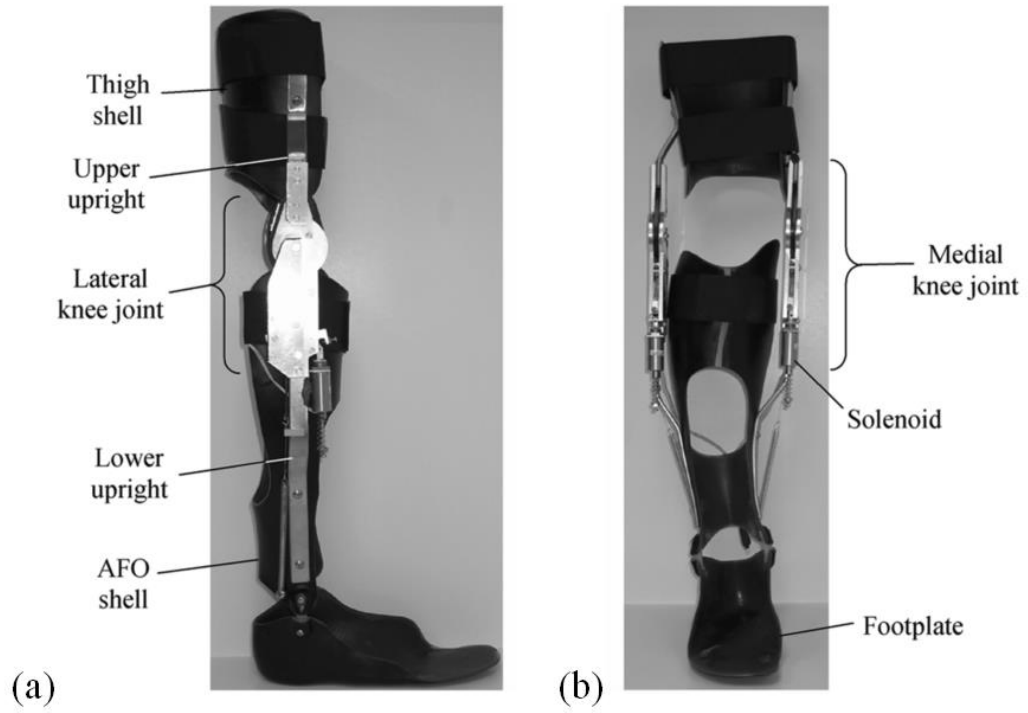


Figure 2-11. The Friction-Based Belt Clamping SCKAFO: (a) the Lateral View; (b) the Front View. The Figures Are Adopted from Reference [58].

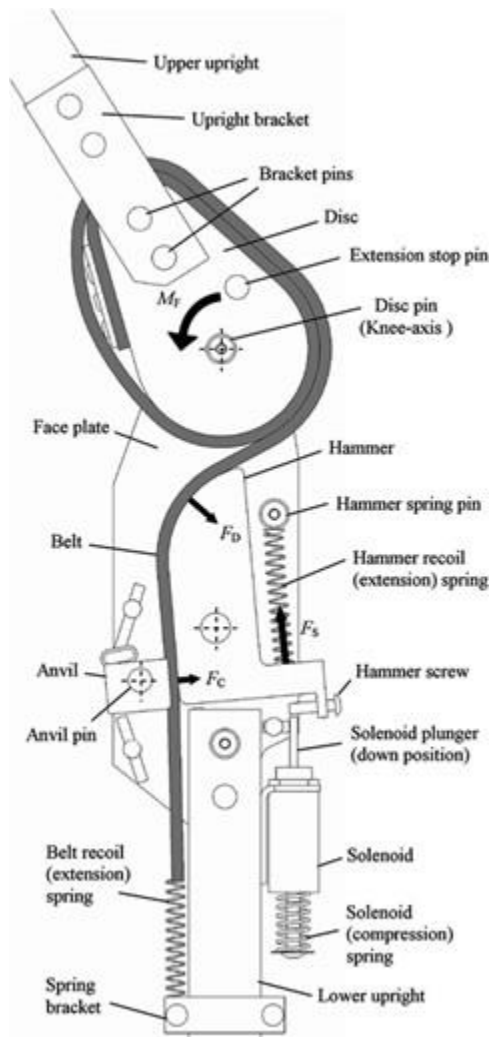


Figure 2-12. The Knee Joint Mechanism of the Belt Clamping Knee-Ankle-Foot Orthosis. The Figure Is Adopted from Reference [58].

2.2.6 Hydraulic Stance Control KAFO

A hydraulically controlled knee joint mechanism [63] has been developed for the knee-ankle-foot orthosis. This system has: (1) a fluid-filled rubber bulb, (2) a plastic pipe, (3) a cylinder, (4) a piston with a long shaft, (5) a recoiled spring, and (6) a gear-type piece with one tooth, as shown in figure 2-13. The cylinder is connected to the leg

segment of the KAFO and the gear piece is fixed on the thigh segment. The rubber bulb is filled with fluid and attached below the foot part of the KAFO. The fluid inside the bulb flows into the cylinder through the flexible plastic pipe. Patients have to extend their knee completely right before the stance phase starts, making the tooth of the gear sit in the locking position. After initial contact, the fluid enters the cylinder and rises up the shaft of the piston to a certain level, completely locking the knee joint during the stance phase, as shown in figure 2-13.a. The pressure on the bulb will be removed when the foot clears the ground and the spring will drag the piston to the lower position, removing the shaft away and allowing the gear to rotate freely during the swing phase, as shown in figure 2-13.b. Intentional extension motion is inevitable in order to engage/ disengage the gear tooth and the piston shaft. There is no extension assistance provided by this brace over the gait cycle.

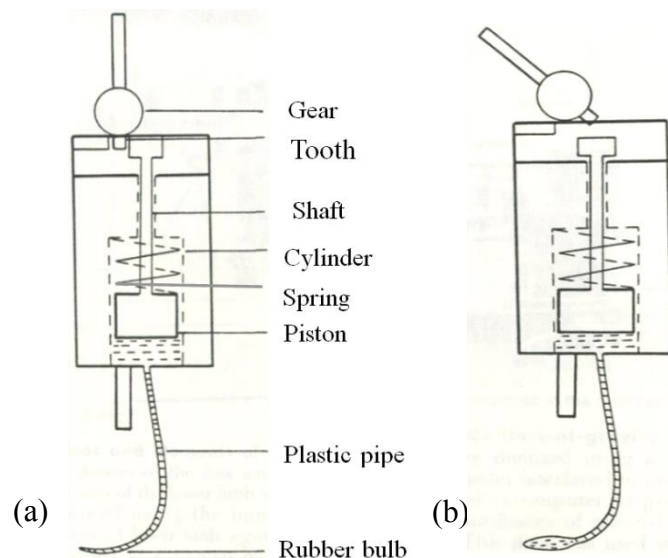


Figure 2-13. The Knee Joint Mechanism of the Hydraulically Powered Stance Control KAFO: (a) When the Gear Is Engaged during the Stance Phase; (b) When the Gear Is Disengaged during the Swing Phase. The Figures Are Adopted and Modified from Reference [63].

2.2.7 The Sensor Walk®

Otto Bock's Sensor Walk® has an electrically controlled knee joint system [64-69]. The stance control KAFO, as shown in figure 2-14.a, includes (1) a regular KAFO, (2) a wrap spring clutch knee mechanism, (3) a footswitch, (4) a control box, and (5) a battery pack. There are four pressure sensors integrated inside the footswitch. The control box consists of a linear solenoid, a knee sensor, and a microprocessor. The solenoid acts to engage and disengage the spring clutch. The knee sensor monitors joint angles and the footswitch is placed beneath the sole to detect the heel strike and the heel rise. The microprocessor is used to interpret signals from all the sensors and control the solenoid. The wrap spring clutch shown in figure 2-14.b is built with an input hub, an output hub, a shaft, and a torsional spring that wraps around both hubs. The two hubs rotate around the shaft and are located next to each other. One end of the torsional spring is fixed on the output hub and the other end called control tang is attached to the solenoid. The input hub and the output hub are connected to the thigh and shank segments of the SCKAFO, respectively.

During the stance phase, the control tang sits on the input hub so that the knee joint can be locked by applying an input flexion moment. This input moment wraps the spring tightly around the two hubs, blocking any relative movement between them. On the contrary, applying an input extension moment on the clutch helps loosen the spring. Therefore, this design prohibits knee flexion and allows knee extension during the stance phase. When the orthotic leg is in the air, the knee joint will be released for free motion since the solenoid pulls the control tang away from the input hub.

No knee extension motion is required to switch between the stance and swing phases by using the wrap-spring clutch. So it provides a more natural walking gait compared to other SCKAFOs. Also, the device can accommodate up to 15 degrees of knee flexion contracture. However, the Sensor Walk® has two main disadvantages. First, the knee joint is completely locked during the stance phase. Second, there is no extension assistance generated by the brace throughout the entire gait cycle.

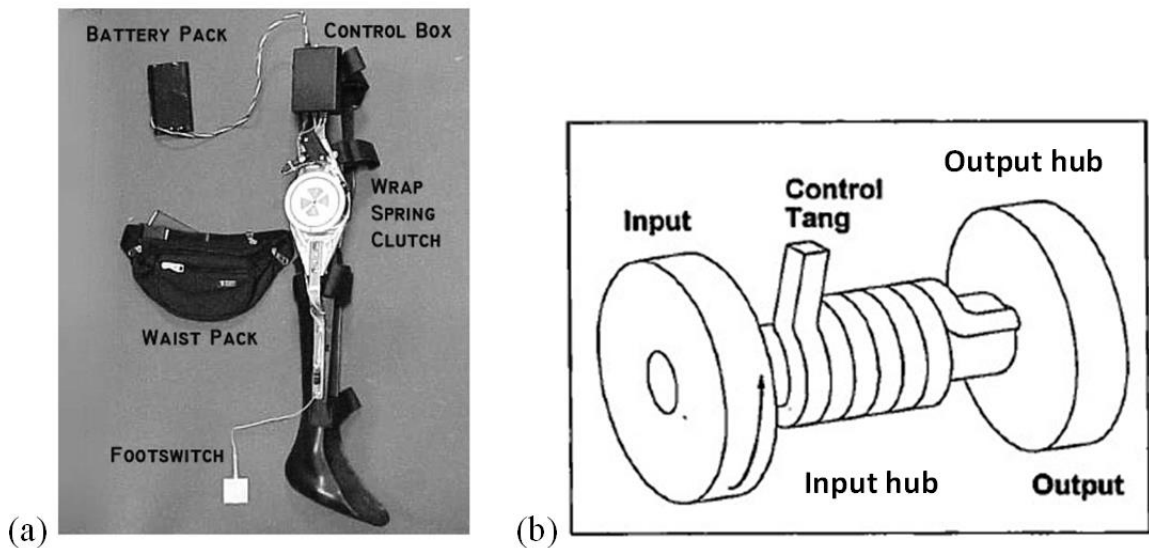


Figure 2-14. (a) The Sensor Walk® Stance Control KAFO. The Figure Is Adopted from Reference [64]; (b) the One-Way Wrap-Spring Clutch Mechanism of the Sensor Walk®. The Figure Is Adopted from Reference [68].

2.2.8 Quasi-Passive Compliant Stance Control KAFO

The quasi-passive compliant SCKAFO [70] tends to reproduce the normal knee joint stiffness profile as illustrated in figure 1-4. This device is composed of (1) a carbon

fiber KAFO, (2) a combination of a pulley and a cable, (3) four resistive sensors attached under the foot part of the orthosis, and (5) a compliant stance control knee module that can be mounted on any regular KAFOs. The pulley replaces the knee hinge of the carbon fiber KAFO and is fixed on its shank segment. One end of the control cable wraps around the pulley and the other end is welded on a shaft of the control knee module. The control module is attached to the thigh segment. The orthosis is shown in figure 2-15.a. The control module includes: (1) a pair of worm and gear, (2) a motor that drives the worm, (3) a spring-loaded push button, (4) a friction lever, (5) a bearing block, (6) a shaft, (7) a support spring, and (8) a return spring, as shown in figure 2-15.b. The support spring is rather stiff and engaged only during the stance phase while the return spring is soft and acts over the entire walking gait cycle. The two springs resist knee flexion and assist knee extension during walking by absorbing and releasing energy.

The working principle of the control module can be explained in figure 2-15.b. The foot sensor signals trigger the worm motor at the heel strike, removing the gear away from the friction lever. Meanwhile, the spring-loaded button pushes the friction lever, making the shaft and the lever interact with each other. The bearing block and friction lever are connected via a hinge, and the shaft passes through both the block and the lever. The interaction between the shaft and the lever further induces the union between the bearing block, the shaft, and the friction lever. Both the support and the return springs are engaged as the three parts bond together. They are compressed when flexing the knee joint in the loading response and recoil to assist knee extension in the late stance phase. When the foot clears the ground, the footswitch signals activate the motor and then rotate the gear toward the friction lever, pushing it away from the shaft. This breaks the

bondage between the shaft, the friction lever, and the bearing block, allowing the shaft to move freely through the other two parts. This free motion releases the support spring so that only the return spring is working during the swing phase. The return spring is too soft to cause any resistance and it is designed to recoil the knee joint back to the full extension position for the next gait cycle.

Users can achieve both knee flexion and extension motions over the walking gaits with such orthoses. However, the nonlinear knee stiffness pattern of healthy individuals is reduced into two linear lines. Similar to other SCKAFOs, knee extension motion is required to eliminate the gripping force between the friction lever, the shaft, and the bearing block so that the switching from the stance to swing phases is possible.

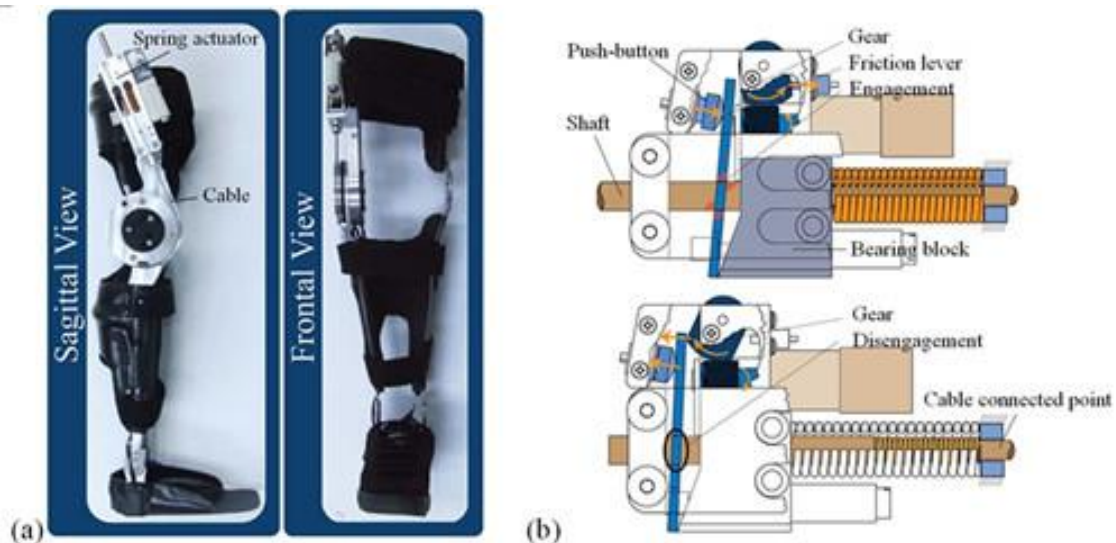


Figure 2-15. (a) The Quasi-Passive Compliant Stance Control KAFO; (b) the Knee Joint Mechanism of the Quasi-Passive SCKAFO. Top: Engagement of the Support Spring and the Return Spring during the Stance Phase. Bottom: Disengagement of the Support Spring during the Swing Phase. The Figures Are Adopted and Modified from Reference [70].

2.2.9 A Motor Powered Knee-Ankle-Foot Orthosis

All the stance control KAFOs discussed above lock the knee joint or resist knee flexion motions during the stance phase and allow free knee movements during the swing phase. However, no active moments can be generated by these devices. A motor powered knee-ankle-foot orthosis [71-73], as shown in figure 2-16, blocks the knee motion during the stance phase as other SCKAFOs but provides active knee flexion and extension moments during the swing phase. The system combines (1) a passive KAFO, (2) a motor, (3) a footswitch, (4) a planetary gearbox with a reduction ratio of 110:1, (5) a linkage mechanism, and (6) a 24V battery package. The gear box amplifies the torque generated in the motor, which is transferred to the knee joint by the linkage mechanism. Customized swing motions need to be programmed and loaded into the device in advance. The footswitch is used to detect the initial contact and the foot off of the orthotic leg. In the early stance, a high extension moment is supplied in order to eliminate the flexion moment caused by the ground reaction force (GRF). Then the full extension position is maintained over the stance phase by adjusting the extension moment value properly. During the mid-swing phase, the knee joint flexes and extends, following the preprogrammed knee motion profile. This powered orthosis has a great commercial potential since it can help paraplegic patients to achieve effective walking gaits, reducing the chance of tripping for people with ankle dorsiflexion disability. Still, it locks the knee joint during the stance phase, which seems to be a popular limitation for almost all stance control KAFOs in the market.

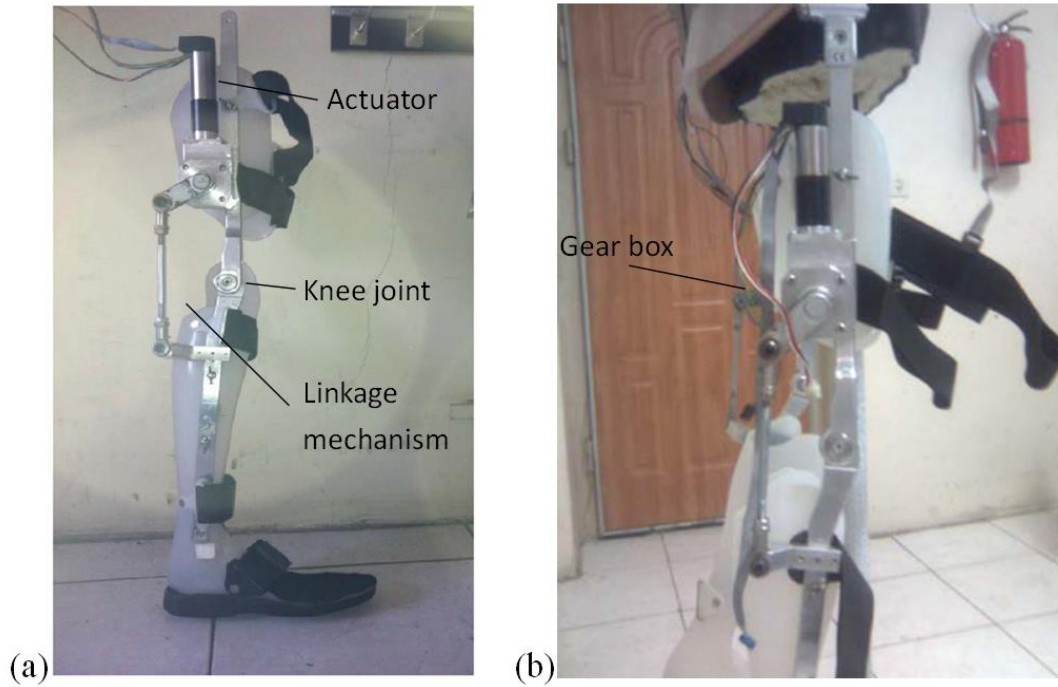


Figure 2-16. (a) The Motor Powered Stance Control KAFO. The Figure Is Adopted and Modified from Reference [71]; (b) the Knee Joint Mechanism of the Motor Powered Stance Control KAFO. The Figure Is Adopted and Modified from Reference [73].

2.3 Dynamic KAFOs

Dynamic KAFOs are designed to mimic normal walking over the entire gait cycle. So far, three dynamic KAFOs have been reported in the literature. They are actuated by a spring mechanism [19, 74], a pneumatic system [75, 76], and a hydraulic system [77-80], respectively. This section discusses these three devices.

2.3.1 Spring Actuated Dynamic KAFO

The electrically controlled dynamic KAFO [19, 74] mimics the normal knee stiffness pattern depicted in figure 1-4, which is reduced into two linear parts by the device due to two compression springs. As shown in figure 2-17, the spring actuated dynamic KAFO includes (1) a regular KAFO with a knee hinge, (2) a knee actuator, (3) an ankle actuator, and (4) a power supply. The mechanism in the ankle actuator is not discussed in this study. The knee hinge of this dynamic KAFO is a four-linkage mechanism that can create motions close to polycentric rotations of a biological knee. The knee actuator is designed to compensate for diminished or absent knee extension ability, thus replacing quadriceps function of the upper leg. In the knee actuator, there are (1) a stiff spring used in the stance phase, (2) a soft spring used in the swing phase, (3) an upper block located above the stiff spring and connected to the thigh part of the orthosis, (4) a lower block placed between the two springs and connected to the shank part of the orthosis, (5) a solenoid, (6) a microcontroller, and (7) a shaft that goes through the two blocks and is wrapped by both springs, as shown in figure 2-18. The solenoid operates

engagement/ disengagement of the stance and swing springs based on shank velocity, knee angle, and signals from a resistive pressure sensor attached under the foot part and two sensor setups on the shank part of the orthosis.

At the heel strike, the head of the solenoid extends to block the downward movement of the lower block, engaging the stiff spring only, as shown in figure 2-18.a. When the knee tends to flex, the upper block slides down along the shaft, compressing the stance spring and generating enough support during the stance phase, as shown in figure 2-18.b. Thus, knee flexion is allowed and stability is maintained as well in this period. During the late stance phase, the stiff spring recovers back to assist extension, compensating for weak quadriceps muscles. As soon as the foot clears the floor, the solenoid retracts to unlock the lower block, as shown in figure 2-18.c. Only the soft spring is activated in the swing phase due to the large stiffness difference between the two springs, as shown in figure 2-18.d. Also during the late swing phase, the soft spring recovers back to help the knee joint return to its full extension position, getting ready for the next gait cycle.

The advantage of this system is that it assists extension and allows flexion throughout the whole gait cycle. It models the normal knee stiffness pattern into two linear portions: the stance portion and the swing portion. This knee actuator mimics the functionality of the quadriceps muscles in walking but relies on healthy hamstrings to initiate knee flexion motions. The switching between the two springs must be done when the leg extends completely so that the head of the solenoid has enough space to extend or return. Also, this device is bulky and heavy and needs a complex control system. Usage of this device is limited in lab environments due to the disadvantages listed above.

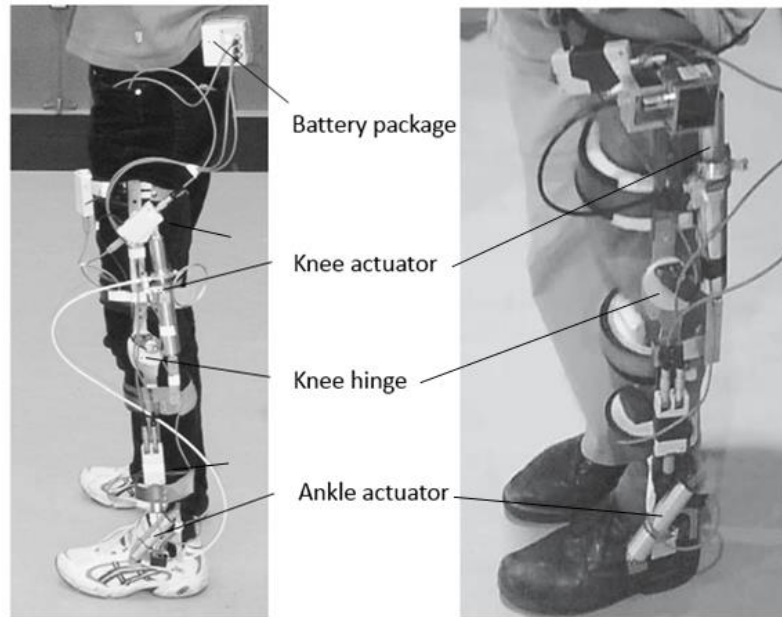


Figure 2-17. The Spring Actuated Dynamic KAFO. The Figure Is Adopted and Modified from Reference [19, 74].

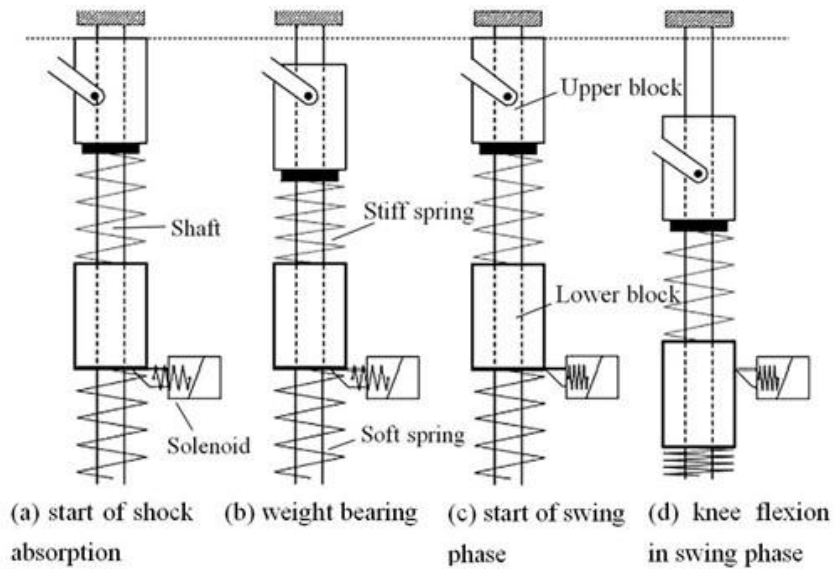


Figure 2-18. Function of the Knee Joint Mechanism of the Dynamic KAFO during the Entire Gait Cycle: (a) Start of Shock Absorption; (b) Weight Bearing; (c) Start of Swing Phase; (d) Knee Flexion in the Swing Phase. The Figure Is Adopted from Reference [19].

2.3.2 Pneumatically Powered KAFO

Sawicki and Ferris [75, 76] have developed a pneumatically powered KAFO that can provide both flexion and extension assistance. The customized device consists of (1) a polypropylene foot part, (2) a shank and a thigh part made by carbon fiber, (3) two hinge joints used as the knee and ankle joints, (4) a foot switch, (5) an external air supply, and (6) two pneumatically powered units at both the knee and ankle, as shown in figure 2-19. The two pneumatically powered units share the similar mechanism and the ankle joint is not discussed in this study. In the knee unit, there are (1) a physiologically-inspired controller, (2) four artificial pneumatic muscles, (3) eight stainless steel brackets, and (4) four proportional pressure regulators. The four artificial muscles interconnect with the external air supply via four plastic tubes. There are two brackets on each muscle, mounting the four muscles on the KAFO. Each regulator has a solenoid to deliver and a valve to deplete compressed air.

Two of the muscles are located in the anterior side of the thigh part, working as the knee extensor. The other two muscles are in the posterior side, functioning as the knee flexor. Each end of the artificial muscle has a stainless steel bracket so that one end of the muscle can be connected to the thigh part and the other end reaches somewhere around the knee joint. Each artificial muscle consists of an internal bladder and an external polyester shell. When the compressed air enters the internal bladder, it will expand to deform the polyester shell and shorten it. When the air leaves the bladder, the muscle will shrink to its original shape. Surface electromyography (EMG) signals of patients' biological muscles are used to activate the four artificial muscles. The knee extensor is controlled by the Vastus Lateralis and the knee flexor is controlled by the medial

hamstrings. The physiologically-inspired controller is designed to synchronize the EMG signals so that it can supply and deplete the compressed air, adjusting the response time and the force magnitude of the muscles.

There are two control modes available in this pneumatically powered orthosis. The artificial knee extensor and flexor co-activate in the first mode. This means the four proportional pressure regulators always deliver the compressed air into the four artificial muscles. During the early stance and early swing phases, flexion motion is created by the two muscles of the knee flexor, which is resisted by extension moments from the other two muscles of the knee extensor. During the rest periods of the stance and swing phases, knee extension motion is generated by the two extensor muscles, which is conflicted by flexion moments from the two knee flexor muscles. The second operating mode prohibits the co-activation, which means only one muscle group can be engaged at a time. During the early stance and early swing phases, the knee joint is flexed by engaging the knee flexor muscles. During the rest periods of the stance and swing phases, the knee joint is extended by engaging the artificial extensor muscles.

The pneumatically powered KAFO can actively generate flexion and extension moments during the entire walking gait cycle. Therefore, it can be prescribed for individuals who are weak in both hamstrings and quadriceps, recovering their knee functionality after severe injuries. However, in order to operate the orthosis, an external air supply has to be used and it is not portable. So far, it is impossible to use the device in daily life due to its complex control system and bulky air supply equipment.

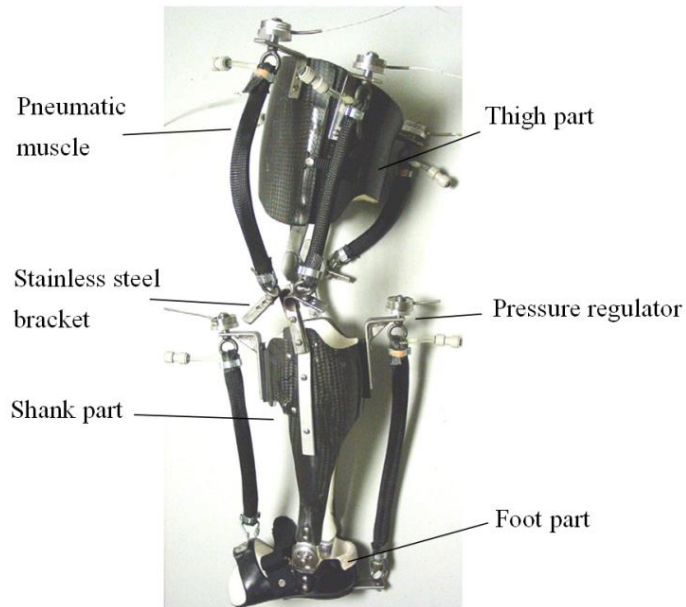


Figure 2-19. The Pneumatically Powered Knee-Ankle-Foot Orthosis. The Figure Is Adopted and Modified from Reference [75].

2.3.3 The C-brace®

OttoBock has launched the first commercial dynamic KAFO in the orthotic market, called C-brace® [77-81]. This orthosis uses a hydraulically powered actuator to control both the stance and the swing phases. In general, it consists of (1) a thigh part, (2) a shank part, (3) a foot part, (4) a sensor-integrated dynamic fiber composite spring that links the foot part and the shank part, and (5) a hydraulic powered knee unit that links the thigh and shank parts and is located at the lateral side of the orthosis, as shown in figure 2-20. The sensor integrated into the composite spring is an ankle movement sensor. The knee unit includes: (1) a knee angle sensor, (2) two control buttons, (3) a hydraulic mechanism, and (4) a microprocessor. The hydraulics generates flexion/ extension

damping moments around the knee joint and the microprocessor controls them according to signals from all the sensors discussed above. Users need to initiate all movements around the knee joint. Then, knee flexion motions are controlled by the flexion damping moments and knee extension motions are controlled by the extension damping moments, avoiding any abrupt behavior. Stance phase flexion damping starts at the initial contact moment, providing flexion resistance to compensate biological knee extending muscles. This protects users from falling down during the loading response. Stance phase extension damping acts to achieve smooth walking gaits during the mid-stance phase. Swing phase flexion damping initiates at the heel off and then gradually increases to decelerate flexion motion during the initial swing phase. Finally, swing phase extension damping starts from a low value to allow the pendulum motion of the leg during the mid-swing phase and later increases to slow down the extension movement before the next heel strike [16].

Due to all the sensors and the microcontroller, C-brace® can be controlled in real time to accommodate various walking environments, such as climbing stairs and slopes and even some sports activities. Smooth walking gait is produced when compared with the other KAFOs. By adjusting the flexion and extension damping moments, this design prevents patients from having abnormal and unstable gait. Also, this orthosis allows users to flex and extend during both the stance and swing phases. However, it is not suitable for those who lose quadriceps strength because the device cannot produce extension assistance. The knee unit cannot be covered under most pants because of the large size of the knee unit.

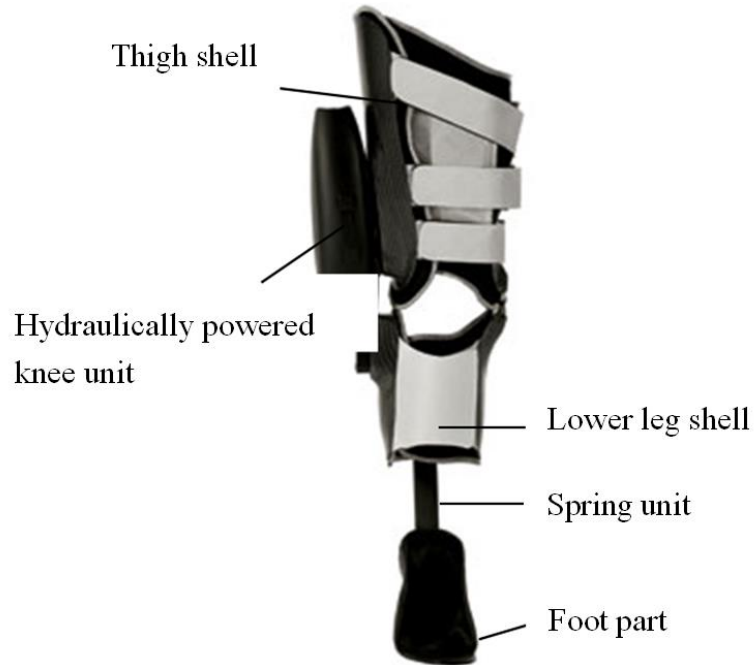


Figure 2-20. The C-brace® from OttoBock, Which Is Actuated by a Hydraulically Powered Mechanism. The Figure Is Adopted and Modified from Reference [77].

2.4 Problems and Limitations of Current KAFOs

An ideal KAFO reproduces normal knee behaviors over the walking gait cycle. Also it should be lightweight, convenient, comfortable, and have quick and smooth switching between different phases of the gait cycle. Based on the above literature review, problems and limitations of current KAFOs are discussed in this section. Passive KAFOs are the most commonly used type primarily due to their low cost and simplicity. Some of these devices produce enough support and stability by completely locking the knee joint. However, using such devices increases the energy consumption because of the associated body compensatory motions, such as hip hiking, circumduction, and vaulting

[53, 55, 56, 72]. In many cases, patients accept these devices for recovering in the early stage and later abandon them as they progress [64, 82]. On the contrary, other passive KAFOs always set the knee free, aiming at adjusting lower leg deformation. The flexible knee of these KAFOs provides limited support, therefore they cannot be prescribed for individuals with severe quadriceps weakness. Characteristics of the passive KAFOs that discussed in section 2.1 are summarized in table 2.1 [16].

Stance control KAFOs improve gait kinematics, provide more symmetric gaits, and require less energy consumption than the passive KAFOs [55, 56]. Generally, these orthoses lock the knee joint during the stance phase and allow for free rotation during the swing phase. However, abnormal walking patterns still exist because of the locked knee in the stance phase. The stiff knee causes abrupt striking and loading of the orthotic leg in the early stance and slight vaulting of the contralateral leg when it clears off the floor [55]. This also restricts the use of SCKAFOs on the level ground only. Next, in order to lock and unlock the knee joint, some SCKAFOs require the users to extend their knee joints intentionally, resulting in unsmooth gait. With such devices, patients have to pay attention when switching between different phases. Other SCKAFOs achieve the switching through specific ankle or hip angles, narrowing their use range within individuals who have normal ankle and hip functions. Additionally, in most SCKAFO devices, no extension assistance is available throughout the entire walking gait cycle, which is considered insufficient for users with severe quadriceps weakness. Characteristics of the stance control KAFOs discussed in section 2.2 are summarized in table 2.2 [16].

Dynamic KAFOs attempt to control the whole gait cycle, achieving normal walking patterns. Thus, they need to generate two different stiffnesses, since the normal knee joint exhibits a stiff behavior during the stance phase and a soft behavior during the swing phase. Three dynamic KAFOs have been reported in the literature. Two of them, actuated by a pneumatic system [75, 76] and a spring system [19, 74], are too bulky and heavy to be used in daily life with their complex mechanisms and non-portable control systems. The spring actuated device [19, 74] resists knee flexion, assists knee extension motions, and tends to reproduce the normal knee stiffness profile by reducing the nonlinear stiffness pattern into two linear sections. The pneumatically powered device [75, 76] mimics the functionality of both quadriceps and hamstrings using artificial muscles, and is the only KAFO that produces active flexion moments. The C-brace® [77, 80] utilizes a hydraulic system to generate flexion and extension damping moments to achieve stable and smooth gait. Therefore, the spring actuated KAFO can be prescribed for patients with weak quadriceps and healthy hamstrings, and C-brace® is suitable for those with medium-weak quadriceps and healthy hamstrings [16]. Only the pneumatically powered KAFO can be used on individuals have both weak quadriceps and hamstrings [16]. In general, dynamic KAFOs are bulky, cumbersome, and use complex control systems. Also, these orthoses are too expensive to be afforded by most users and this significantly restricts their widespread in the market. Furthermore, none of the three designs can be worn under clothes, which is cosmetically unacceptable. Characteristics of the dynamic KAFOs that discussed in section 2.3 are summarized in table 2.3 [16].

Table 2-1. The Summarization of Various Passive KAFOs. The Table Is Adopted from Reference [16].

Passive KAFO	Condition of the knee joint during the gait cycle	Locking position	Mechanism of locking/unlocking	Prescribed for those with knee flexion contractures
Straight set knee with drop lock [45]	The knee is locked during the entire gait cycle.	At full extension	The knee locks automatically when extending. It is unlocked manually by removing the drop ring.	No
Posterior offset knee [45]	The knee is locked in stance and moves freely in swing.	When the ground reaction force (GRF) is anterior to the knee hinge axis	Knee extension is maintained when the GRF is anterior to the hinge axis, which is accomplished by leaning the body slightly forward. The joint moves freely when the GRF moves posteriorly.	No
Polycentric knee [45]	The knee moves freely during the entire gait cycle.	When the GRF is anterior to the knee center of rotation	Knee extension is maintained when the GRF is anterior to the knee center of rotation. The joint moves freely when the GRF moves posteriorly.	Yes

Bail lock KAFO [45]	The knee is locked during the entire gait cycle.	At full extension	The knee is locked by the bail lock when extending. It is unlocked manually by lifting up the bail.	No
Ratchet lock KAFO [45]	The knee extends freely but flexion is blocked during the entire gait cycle.	At any specified knee flexion angle	The knee locks automatically due to the ratchet lock. It is unlocked by pressing down the release lever of the ratchet lock.	Yes
Dial lock KAFO [45]	The knee is locked during the entire gait cycle.	At any specified knee flexion angle	The knee locks automatically when extending. It is unlocked by pulling up the dial of the KAFO.	Yes

Table 2-2. The Summarization of Various Stance Control KAFOs. The Table Is Adopted from Reference [16].^{1, 2}

SCKAFO	Engaging mechanism	Condition of the knee joint during the gait cycle	Locking position	Maximum user weight	Knee Flexion Contracture	Knee valgum/varum
Otto Bock Free Walk/Becker Orthopedic UTX [55]	Spring-loaded pawl lock	The knee is locked in stance and moves freely in swing.	From 0° to 10° of knee flexion [83]	265 lbs [83]	≤10° [83]	≤10° [83]
Fillauer® swing KAFO [55]	Weighted pawl	The knee is locked in stance and moves freely in swing.	From 0° to 10° of knee flexion [84]	/	≤10° [84]	/
Becker 9001 E-Knee Orthosis [55]	Magnetically activated clutch	The knee can extend but flexion is blocked in stance. It moves freely in swing.	From 0° to 15° of knee flexion [83]	187 lbs [83]	≤15° [83]	≤15° [83]
Horton SCKAFO [55]	Eccentric cam mechanism	The knee can extend but flexion is blocked in stance. It moves freely in swing.	From 0° to 10° of knee flexion [84]	225 lbs [84]	≤10° [84]	≤10° [84]

¹ All SCKAFOs listed in this table require knee extension in late stance to switch between the stance and swing phases except for the Sensor Walk® [67].

² All SCKAFOs listed in this table do not provide knee extension assistance except for the quasi-passive compliant SCKAFO [70] which assists extension during the entire gait cycle and the motor powered KAFO [72] which assists extension in swing.

Belt-clamping SCKAFO [58]	Friction-based belt-clamping mechanism	The knee can extend and slight flexion is allowed in stance. It moves freely in swing.	Any knee flexion angle at heel strike	198 lbs [58]	Allows knee flexion contracture	/
Hydraulic SCKAFO [63]	Hydraulically powered mechanism	The knee is locked in stance and moves freely in swing.	At full extension	/	Does not allow knee flexion contracture	/
Sensor walk® [67]	Electronically controlled wrap-spring clutch	The knee can extend but flexion is blocked in stance. It moves freely in swing.	From 0° to 15° of knee flexion [83]	300 lbs [83]	≤15° [83]	≤10° [83]
Quasi-passive compliant SCKAFO [70]	Electronically controlled mechanism	The knee can flex and is assisted to extend during the entire gait cycle.	Any knee flexion angle at heel strike	/	Allows knee flexion contracture	/
Motor powered KAFO [72]	Motor powered mechanism	The knee is locked in stance. It is assisted to flex and extend in swing.	At full extension	/	No knee flexion contracture	/

Table 2-3. The Summarization of Various Dynamic KAFOs. The Table Is Adopted from Reference [16].

Dynamic KAFO	Operation	Extension assistance	Flexion assistance	Switching from stance to swing	Knee extension requirement at late stance	Prescription
Compression springs actuated KAFO [19]	The non-linear normal knee stiffness profile is reduced into two linear patterns using compression springs.	Extension moments are provided during both stance and swing phases.	No flexion assistance	Uses signals from a foot switch	Yes	For people with weak quadriceps and healthy hamstrings
Pneumatically powered KAFO [75]	Biological muscles signals are used to produce knee joint moments.	Extension moments are provided during both stance and swing phases.	Flexion moments are provided during both stance and swing phases.	No switching	No	For people with weak quadriceps and hamstrings
C-brace® with hydraulics mechanism [77]	Flexion and extension damping moments are produced to avoid any uncontrolled knee motion.	Extension damping moments are provided during both stance and swing phases.	Flexion damping moments are provided during both stance and swing phases.	No switching	No	For people with medium level of quadriceps and hamstrings weakness

2.5 Summary

There are three types of KAFOs presently available in the market: passive, stance control, and dynamic. Several typical designs of each type have been discussed in this chapter. Although these designs can improve ambulation, they have limitations that prevent them from being widely accepted by potential users. It is very critical for researchers to study the functions and limitations of current KAFOs in order to continue with further improvements.

Chapter 3

Development of the Dynamic Knee Actuator

The dynamic knee actuator is the core mechanism of the UT dynamic KAFO. It aims at reproducing normal knee behavior for individuals with weak quadriceps. This chapter presents the development of the dynamic knee actuator. In the beginning, a conceptual design for the knee actuator was proposed. Two actuating units were combined to meet the requirements for the different phases during the walking cycle. For each part of the gait, this actuating system combined one superelastic torsional rod and one torsional spring. There was a switching mechanism to engage the proper actuation mechanism in each portion of the gait. For each of the two portions of the gait, a superelastic rod and a torsional spring were designed respectively. In order to determine the geometries of the superelastic rods, a 3D constitutive model for Nitinol was used to simulate the material behavior. Since the superelastic alloys show different responses according to different loading/ unloading rates and the knee actuator works under fast loading rates, the adiabatic simulation method was conducted in this research and thermal effects were taken into consideration [85-87]. Proper dimensions for the two superelastic rods were found via the numerical simulations. The two torsional springs were created using rubber tubes based on the dimensions of the superelastic rods.

3.1 Conceptual Design of the Dynamic Knee Actuator

3.1.1 Determine the Proper Material and Loading Condition

Nitinol was chosen to develop this specified knee actuator due to the similarity between the behavior of the normal knee joint and the materials. As described in section 1.4, Nitinol has two distinct properties: shape memory effect and superelastic effect. The shape memory effect represents the temperature-induced transformation and the superelastic effect represents the stress-induced transformation. Several applications of Nitinol in rehabilitation devices have been reported in the literature [32, 35, 37, 39, 41]. The devices actuated by shape memory alloys require special control systems. Shape memory alloys are activated by increasing the temperature of the materials and then their original shapes can be recovered via cooling down for the next actuation cycle. The response time of shape memory alloys depends on the speed of heating up and cooling down. The heating speed is restricted by the maximum current that is allowed to pass through the materials. The higher current provides for faster heating. The current threshold is limited by the properties and geometries of the materials. The main limitation in repeated shape memory based actuation is in the cooling phase. External convection mechanisms can be used in order to speed up the cycling time of the materials, however, this may make the whole system more complex and impractical as assistive devices. On the contrary, using superelastic alloys does not involve the heating and cooling issues that exist for shape memory alloys. A pure mechanical load leads to a stress-induced transformation and creates a large strain (about 8%) as almost constant resistive loading, which can be recovered by unloading. This makes superelastic Nitinol suitable in the

situations where large deformations and quick responses are requested. Based on the above discussion, it was determined that the dynamic knee actuator should be developed with superelastic Nitinol so that it could respond quickly while not imposing a large level of stress on the knee joint. Using such materials also simplified the design of the actuator and reduced the weight of the whole KAFO. Superelastic alloys give the knee actuating system the potential of reproducing the non-linear stiffness profile of a normal knee joint and being lightweight and inexpensive.

Superelastic alloy actuators can be fabricated in the form of both wires and rods. Wire actuators, which are typically loaded in tension, are the most common type in lower leg brace applications, as presented in section 1.4. However, the required long wires limit their practical use. For our specific design, the dynamic knee actuator was made of superelastic rods, due to the large angular rotation and the high torque requirements at the knee joint [17, 88-91]. The use of torsional superelastic actuators also allowed for miniaturization of the resulting KAFO.

3.1.2 Conceptual Design of the Dynamic Knee Actuator

In this study, the dynamic knee actuator was developed to reproduce the normal knee stiffness profile during both the stance and swing phases. As discussed in section 1.2, the normal knee stiffness is almost linear with a small hysteretic character during the early stance and mid-stance phases. It also can be considered linear with a lower slope and more hysteretic character during the rest of the stance phase and the swing phase. This indicates that the dynamic knee actuator needs two different sections to match the

two stiffness patterns respectively. The first part, which is called the stance actuating part, gets activated only during the early stance and mid-stance phases, while the second part, called the swing actuating part, functions only during the late stance, pre-swing, and swing phases. The switching between these two parts occurs at the heel strike and the heel off of the orthotic leg.

To realize the required stiffness profile, both the stance and swing actuating parts were composed of a linear torsional spring and a superelastic torsional rod. Combining springs and superelastic rods with different dimensions in parallel made it possible to reproduce the two distinct knee stiffness profiles of the stance and swing phases. Fundamental design specifications of the dynamic knee actuator are illustrated in figure 1-4. The actuator was designed on the basis of the assumption that the patient had no extension ability at the knee. Thus the actuator was required to deliver the knee extension moment, and in doing so, replace the activity of the quadriceps by providing the complete extension torque. For a person who weighs 60 kg (135 lbs), figure 1-4 shows that the stance actuating part is required to produce about 40 Nm torque via 15 degrees of rotation. Figure 1-4 also shows that the swing actuating part needs to produce about 10 Nm torque via 60 degrees of rotation. The 3D constitutive model discussed in the next section was used to simulate the superelastic Nitinol rods in the actuating parts, to calculate the geometry of these Nitinol parts.

3.2 Design of the Nitinol Knee Actuator

3.2.1 A 3D Constitutive Model for Nitinol

In the literature, several mathematical models to simulate the response of Nitinol have been built and reported. These models are classified into two general groups: micro-mechanical based models [92-94] and macroscopic phenomenological based models [95-102]. The 3D phenomenological constitutive model used in this work is a macroscopic phenomenological based model and was first proposed by a research group from Texas A&M University [27]. Based on this preliminary model, a set of MATLAB based code for adiabatic loadings [39, 85, 87, 103-109] was developed at the University of Toledo. This model is appropriate for different working temperatures and various loads in tension and torsion.

3.2.2 Calibrating the Properties of the Superelastic Nitinol

Fort Wayne Metals NiTi#1 superelastic alloys were used to develop the dynamic knee actuator in this study. The material properties for the adiabatic model are reported in this section.

3.2.2.1 Calibration Setup and Procedure

The experimental setup for calibrating the superelastic rods included an ElectroForce BOSE® machine (BOSE Corporation, United States), a temperature controlled environmental chamber (BOSE Corporation, United States), an IR Camera

(Micro-Epsilon, Germany), and a computer interface. The BOSE machine enables us to apply both tensional and torsional loads. Since the superelastic alloy elements in the knee actuator worked only in torsion, the sample's material properties were obtained through torsional calibration tests. The calibration had to be conducted under several different temperatures [27]. The IR Camera measured the surface temperatures of the sample over the calibration process to ensure that the tests were under the slow loading (isothermal) condition. The experimental setup is shown in figures 3-1 and 3-2. A superelastic Nitinol rod with a diameter of 3.43 mm (0.15 inch) and a length of 25.2 mm (0.992 inch) was used to collect the parameters. The three temperatures used for the tests were 24⁰C, 35⁰C, and 45⁰C as listed in table 3-1.

Table 3-1. The Calibration Conditions of the NiTi#1 Superelastic Rod Sample.

	Maximum deformation (deg)	Loading/ unloading rates (deg/sec)	Temperature (°C)
Calibration cycle 1	40	0.168	24
Calibration cycle 2	40	0.168	35
Calibration cycle 3	40	0.168	45

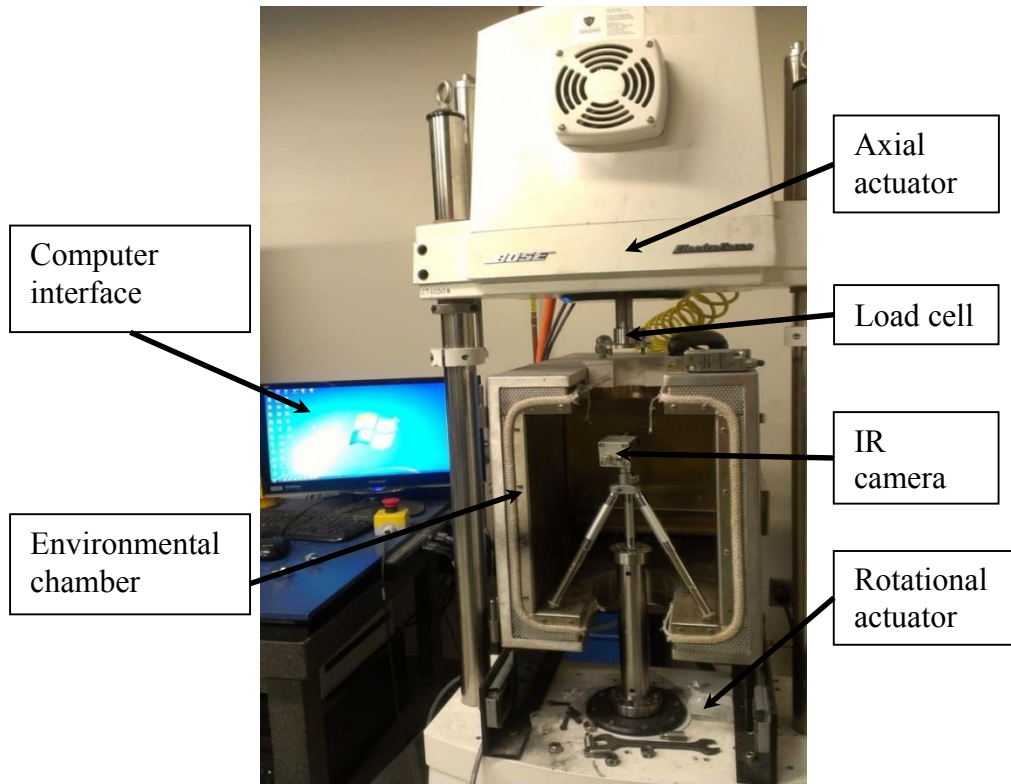


Figure 3-1. The Experimental Setup for Calibrating the NiTi#1 Superelastic Rod Sample.

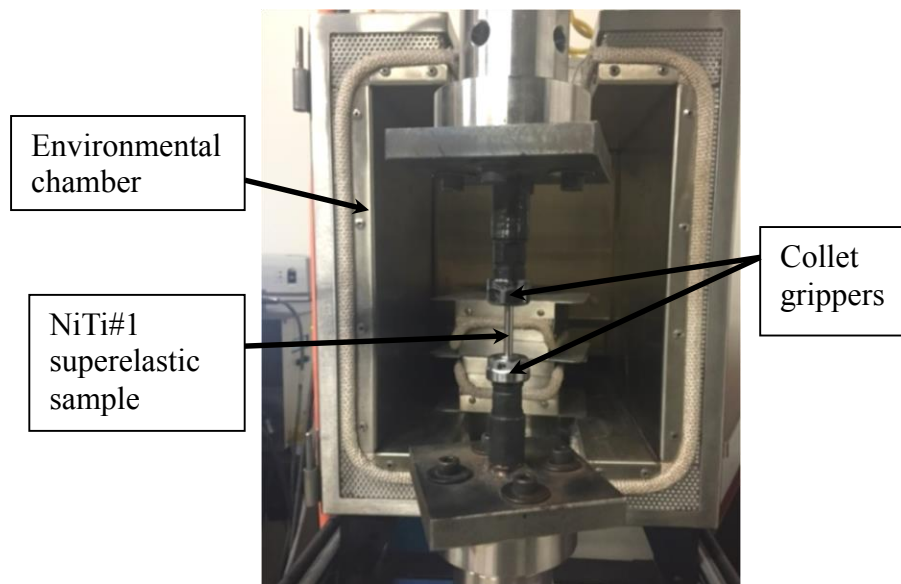


Figure 3-2. The Experimental Setup for Sample Calibration: the NiTi#1 Superelastic Sample is Mounted on the Grippers.

3.2.2.2 Calibration Results

The material properties that were measured are listed as follows: (1) martensite start temperature M_s , (2) martensite finish temperature M_f , (3) austenite start temperature A_s , (4) austenite finish temperature A_f , (5) martensite modulus of elasticity E^M , (6) austenite modulus of elasticity E^A , (7) stress influence coefficient of martensite C^M , (8) stress influence coefficient of austenite C^A , and (9) maximum transformation strain ϵ at a given stress. The test results are shown in figure 3-3 and table 3-2. Then the material properties in table 3-2 were used as parameter inputs in the 3D constitutive model to simulate this sample, indicating that the experimental and simulation results were matching. The comparison between the simulation and experimental results for the three calibration cases are shown in figures 3-4, 3-5, and 3-6.

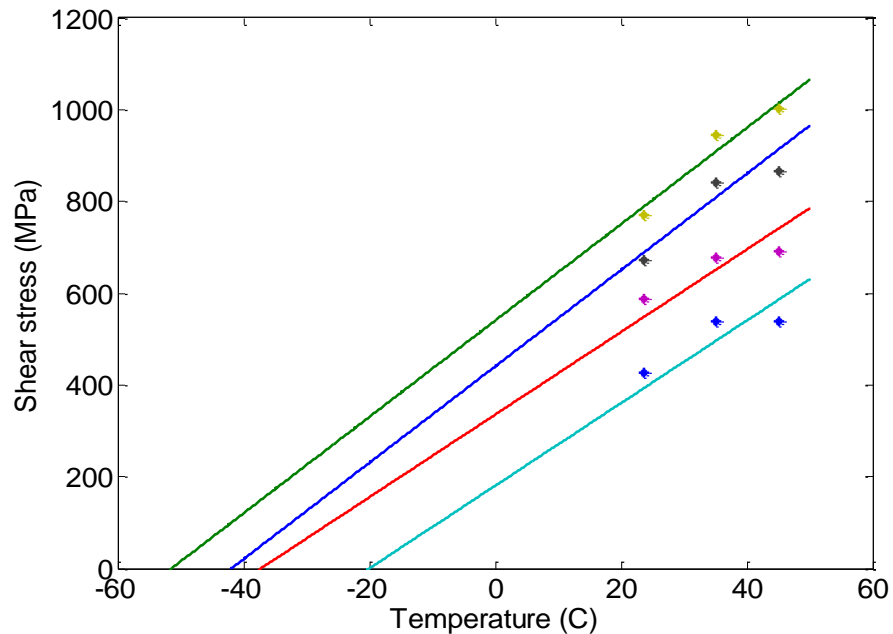


Figure 3-3. Calibrated Phase Diagram for the NiTi#1 Superelastic Rod Sample.

Table 3-2. Material Properties of the NiTi#1 Superelastic Rod Collected from Calibration.

Parameter	NiTi#1 rod	Unit
M_f	-51.4	$^{\circ}\text{C}$
M_s	-42	$^{\circ}\text{C}$
A_s	-37.2	$^{\circ}\text{C}$
A_f	-19	$^{\circ}\text{C}$
E^A	32	GPa
E^M	17	GPa
C^A	10.5	$\text{MPa}\cdot\text{K}^{-1}$
C^M	9	$\text{MPa}\cdot\text{K}^{-1}$
ϵ	2.62	%

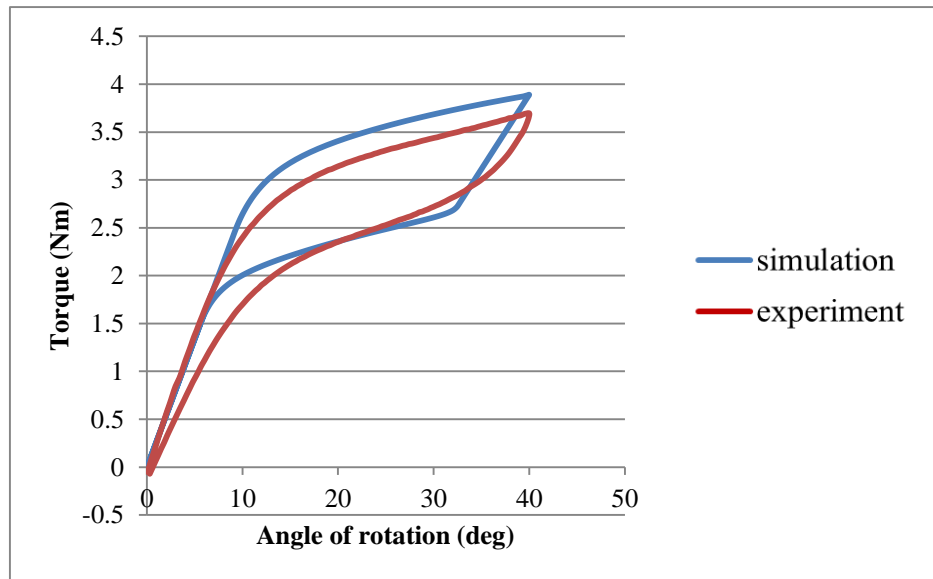


Figure 3-4. Comparison of the Torque vs. Angle of Rotation of the NiTi#1 Superelastic Rod Sample between the Experimental and Simulation Results. The Calibration Temperature Is 24°C .

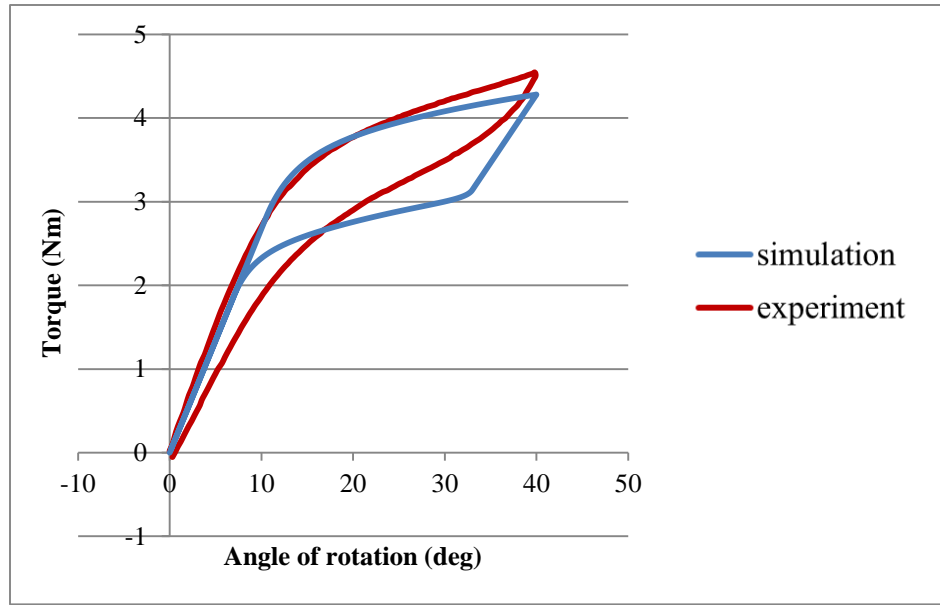


Figure 3-5. Comparison of the Torque vs. Angle of Rotation of the NiTi#1 Superelastic Rod Sample between the Experimental and Simulation Results. The Calibration Temperature Is 35°C.

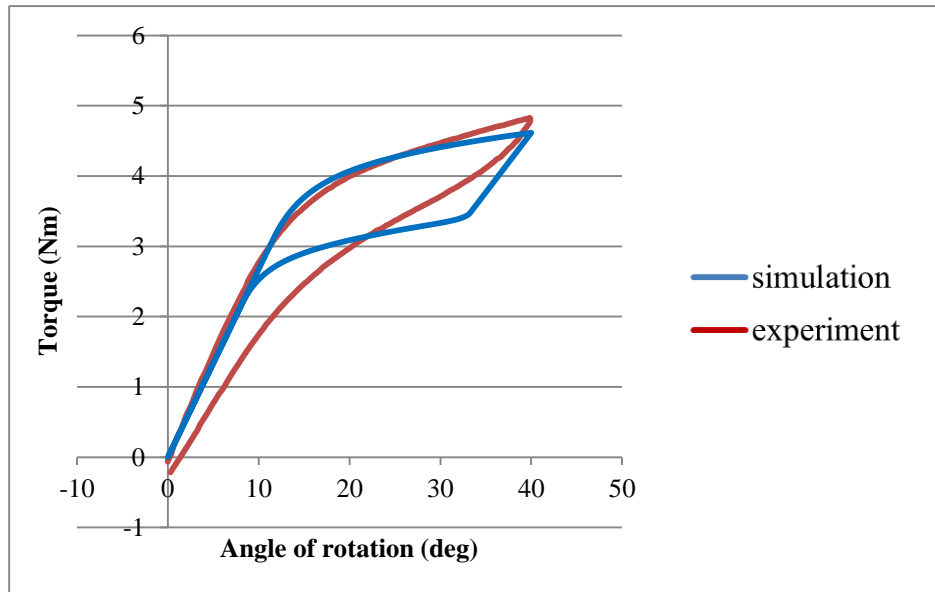


Figure 3-6. Comparison of the Torque vs. Angle of Rotation of the NiTi#1 Superelastic Rod Sample between the Experimental and Simulation Results. The Calibration Temperature Is 45°C.

3.2.3 Numerical Simulation Results of the Nitinol Rods

Numerical simulations were used to determine the dimensions of the two superelastic rods and to verify whether the normal knee stiffness could be reproduced using the dynamic knee actuator. Since one average walking cycle takes about 1.2 seconds [37, 110, 111], the Nitinol actuator response time should be around 1.2 seconds to address the requirements of normal walking. Therefore, the adiabatic simulation that represents fast loading rates was been conducted in this research. In such simulations, the forward transformation from austenite into detwinned martensite releases energy while the reverse transformation from detwinned martensite to austenite absorbs energy. The simulations used the material properties shown in table 3-2 as input parameters in the MATLAB based 3D phenomenological constitutive model.

The dimensions of the two superelastic rods were determined via the adiabatic simulations so that the rods could deliver the required level of torque during the rotation. It was determined that the stance rod should have a 6.40 mm diameter and an 11.75 mm length, and the swing rod should have a 3.80 mm diameter and a 26.7 mm length. Figures 3-7, 3-8, and 3-9 show the simulation results of the two superelastic rods and the combined stiffness profile of the dynamic knee actuator. Figure 3-7 shows the adiabatic response of the superelastic rod used in the stance actuating part and figure 3-8 shows that of the superelastic rod used in the swing actuating part. Both the stance and swing superelastic rods were simulated under the loading rate of 0.5 seconds per cycle. This matches the response time in normal walking. Figure 3-7 illustrates that an 18 Nm torque was generated on the stance superelastic rod by applying 15 degrees of rotation. Figure 3-8 shows that a 5.5 Nm torque was generated on the swing superelastic rod by applying 60

degrees of rotation. As long as the response of the superelastic rods was simulated in the adiabatic situation, no significant difference could be observed in the results, even when changing the loading rate. Hence, this actuator was assumed to be appropriate for accommodating all walking speeds. However, the dimensions of the two superelastic rods might need some modification in practical use, since they did not work in the adiabatic surroundings.

As discussed in the section 3.1.2, the stance and swing actuating parts were designed to produce about 40 Nm and 12 Nm, respectively. The additional torque needed to be provided by the two linear torsional springs. Hence, the stiffnesses of the two torsional springs were calculated as 1.4 Nm/deg and 0.11 Nm/deg, respectively.

Figure 3-9 compares the stiffness of the dynamic knee actuator and that of a normal knee joint. There are three curves in this figure. The pink curve represents the normal knee stiffness pattern. The blue curve represents the response of the stance actuating part and the red curve is for the response of the swing actuating part. When the stance actuator was twisted by 15 degrees, it generated a 40 Nm torque, and when the swing actuator was twisted by 60 degrees, it generated a 10 Nm torque. The simulation results indicated that there was a good match between the stiffness of the dynamic knee actuator and that of a normal knee joint in the early stance and mid-stance phases. So enough support could be provided by the stance actuating part during these two periods. During the late stance, pre-swing, and early swing phases, the swing actuator induced less resistance, thus not blocking normal flexion motions. In the mid-swing and terminal swing phases, the swing actuator assisted knee extension before the next foot contact.

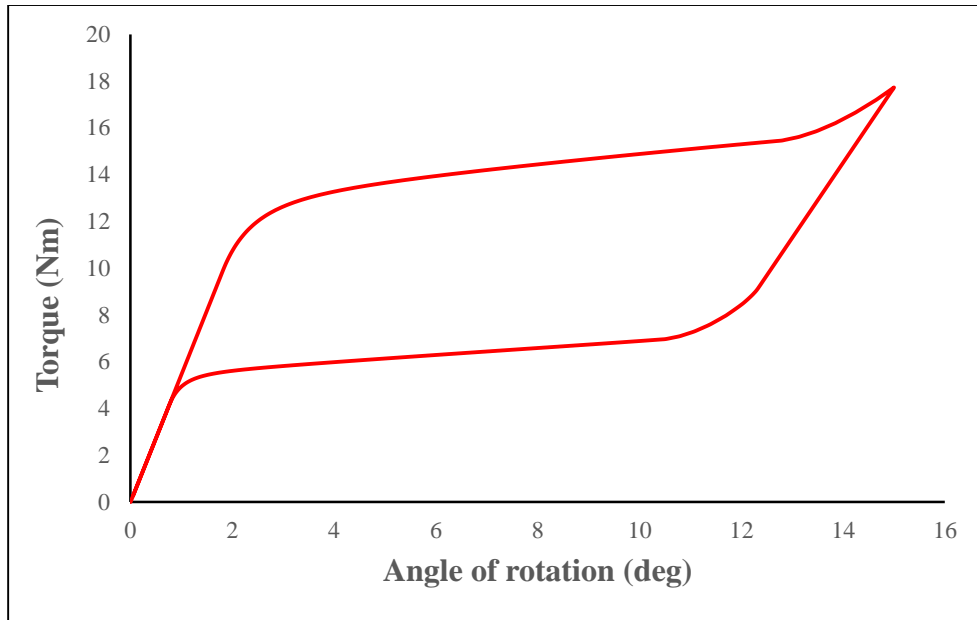


Figure 3-7. Adiabatic Simulation Result for the Superelastic Nitinol Rod Used in the Stance Actuating Part: Torque vs. Angle of Rotation.

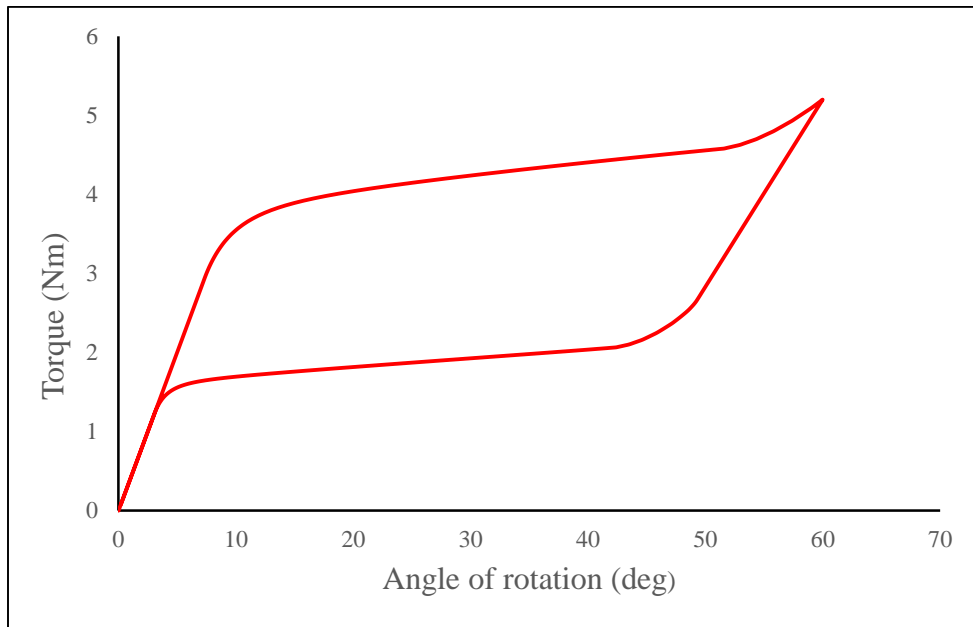


Figure 3-8. Adiabatic Simulation Result for the Superelastic Nitinol Rod Used in the Swing Actuating Part: Torque vs. Angle of Rotation.

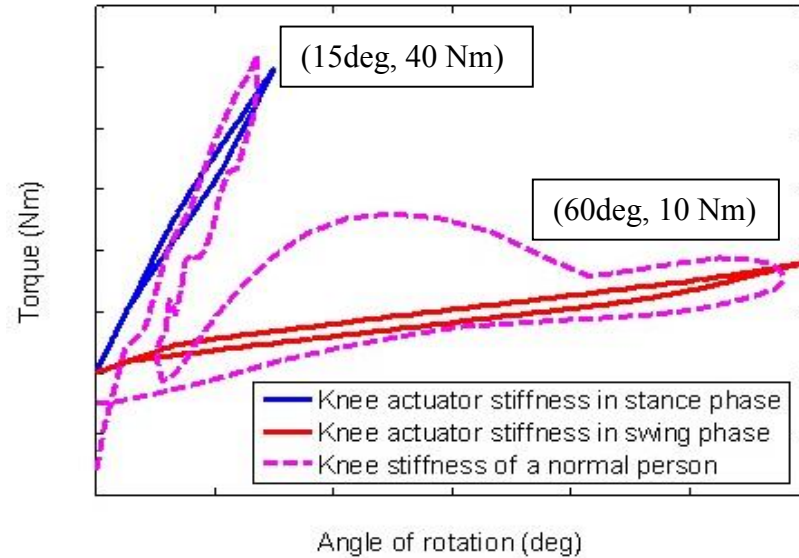


Figure 3-9. The Stiffness Profile of the Dynamic Knee Actuator and that of a Normal Knee Joint. Pink Dash Curve: Normal Knee Stiffness Profile. Blue Curve: Stance Actuator Response. Red Curve: Swing Actuator Response. The Figure Is Adopted from Reference [89].

Ideally, the dynamic knee actuator should have a long service life. If the superelastic Nitinol rods work in the elastic deformation region, their fatigue life can reach as high as 10^7 cycles [27]. On the contrary, if the rods are applied to significantly higher loads, it is likely that they will fail much sooner [27]. Therefore, the stress-strain relationships for both superelastic rods were studied. Figure 3-10 shows the stress-strain curves of the superelastic rod in the stance actuator and figure 3-11 represents that of the superelastic rod in the swing actuator. The same loading rates were set in the simulations to match normal walking. In the adiabatic conditions, the stance rod reached about 8% shear strain and 380 MPa shear stress, and the swing rod reached about 8% shear strain and 330 MPa shear stress. These two figures indicate that both superelastic rods worked

within the elastic deformation region.

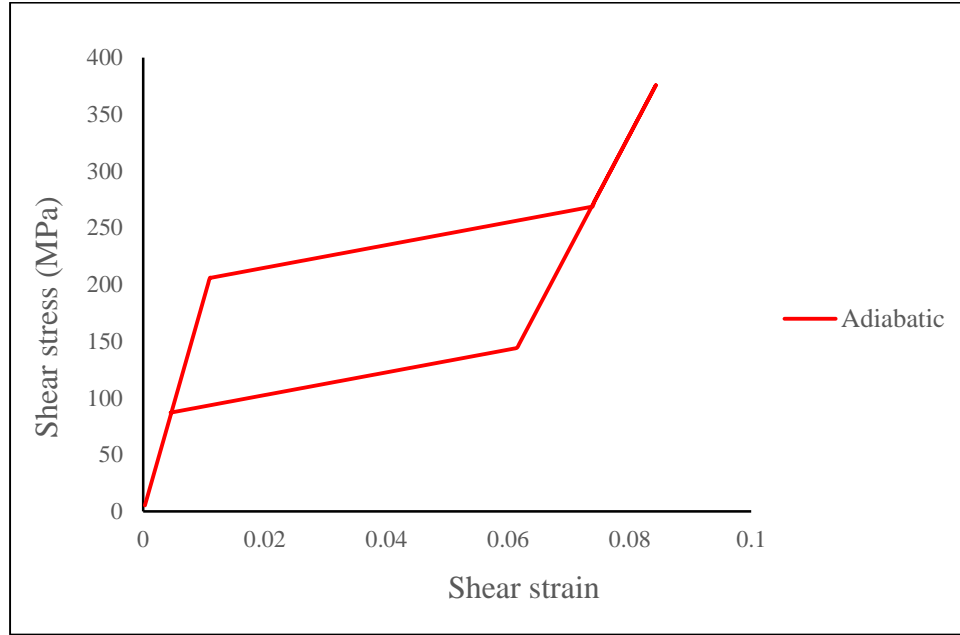


Figure 3-10. Adiabatic Simulation Result for the Superelastic Nitinol Rod Used in the Stance Actuating Part: Shear Stress vs. Shear Strain.

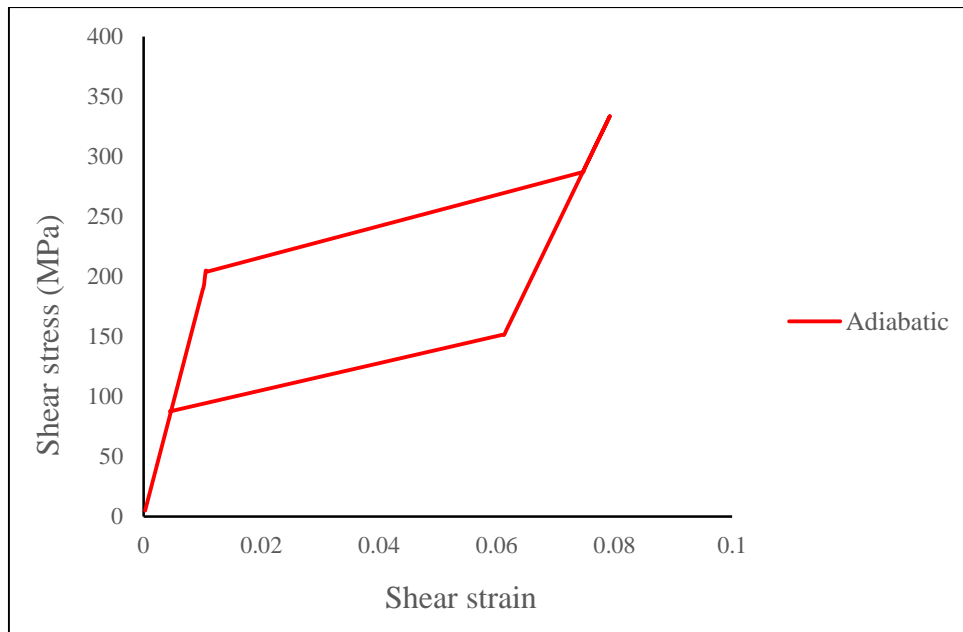


Figure 3-11. Adiabatic Simulation Result for the Superelastic Nitinol Rod Used in the Swing Actuating Part: Shear Stress vs. Shear Strain.

3.2.4 Training the Nitinol Rods

The two NiTi#1 superelastic rods have to be trained to stabilize their cyclic behaviors before any practical application can be made of them. The highest possible load must be used to train the materials [27] so that they can accommodate the working environment later. Also, training should be done at low frequency (strain rate = 0.0001/sec), preventing any latent heat effect on the specimens. Table 3-2 shows the dimensions and training parameters of the two NiTi#1 superelastic rods.

Table 3-2. The Dimensions and Training Parameters of the Two NiTi#1 Superelastic Rods.

	Diameter (mm)	Length (mm)	Deformation (deg)	Strain rate (/sec)	Loading rate (deg/sec)
The SE rod used in the stance actuator	6.40	11.75	15	0.0001	0.021
The SE rod used in the swing actuator	3.80	26.7	60	0.0001	0.081

The loading rate that was used to train the superelastic rods in the stance actuating part was calculated from equations 3-1 to 3-4. One complete cycle of loading and unloading required about 1426 sec and ten training cycles took more than 4 hours.

$$d_1 = 6.4 \text{ mm}, \quad \theta_1 = 15 \text{ deg} = \frac{\pi}{12} \text{ rad}, \quad L_1 = 11.75 \text{ mm} \quad (3-1)$$

$$\gamma_1 = \frac{r_1 \theta_1}{L_1} = \frac{3.2 \times \frac{\pi}{12}}{11.75} = 0.0713 = 7.13\% \quad (3-2)$$

$$\dot{\gamma} = 0.0001 = \frac{0.0713}{T_1}, \quad T_1 = 713 \text{ sec} \quad (3-3)$$

$$\text{loading rate} = \frac{15 \text{ deg}}{713 \text{ sec}} = 0.021 \text{ deg/sec} \quad (3-4)$$

The loading rate used to train the superelastic rod in the swing actuating part was calculated from equations 3-5 to 3-8. One complete cycle of loading and unloading took about 1490 sec and ten training cycles required more than 4 hours.

$$d_2 = 3.8 \text{ mm}, \quad \theta_2 = 60 \text{ deg} = \frac{\pi}{3} \text{ rad}, \quad L_2 = 26.7 \text{ mm} \quad (3-5)$$

$$\gamma_2 = \frac{r_2 \theta_2}{L_2} = \frac{1.9 \times \frac{\pi}{3}}{26.7} = 0.0745 = 7.45\% \quad (3-6)$$

$$\dot{\gamma} = 0.0001 = \frac{0.0745}{T_2}, \quad T_2 = 745 \text{ sec} \quad (3-7)$$

$$\text{loading rate} = \frac{60 \text{ deg}}{745 \text{ sec}} = 0.081 \text{ deg/sec} \quad (3-8)$$

3.2.4.1 Training Setup and Procedure

The MTS 858 Mini Bionix® II Biomaterials Testing System (MTS Systems Corporation, MN, United States) was used to train the two superelastic Nitinol rods, as shown in figures 3-12 and 3-13. The machine can provide both tensional and torsional loads. In this study, only torsional training was applied on the samples. Figure 3-14 shows that the two NiTi#1 superelastic rods were assembled with their fixtures. Both testing samples were loaded under pure torsion, and the training results are shown in the next section.

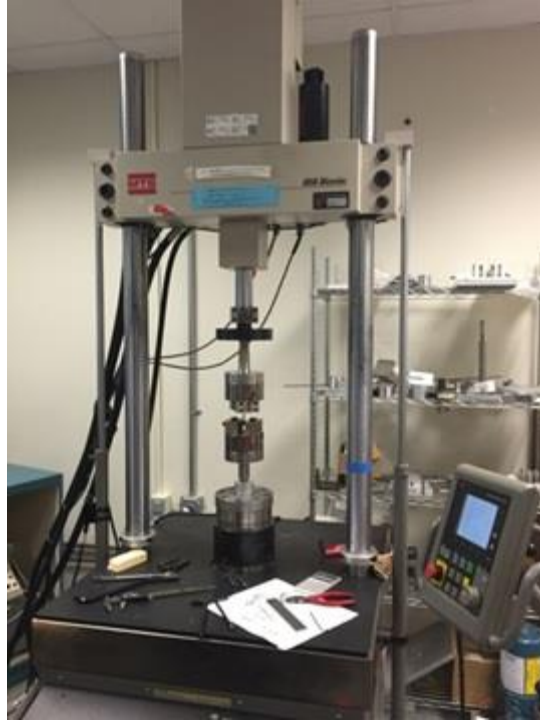


Figure 3-12. The MTS 858 Mini Bionix® II Biomaterials Testing System.

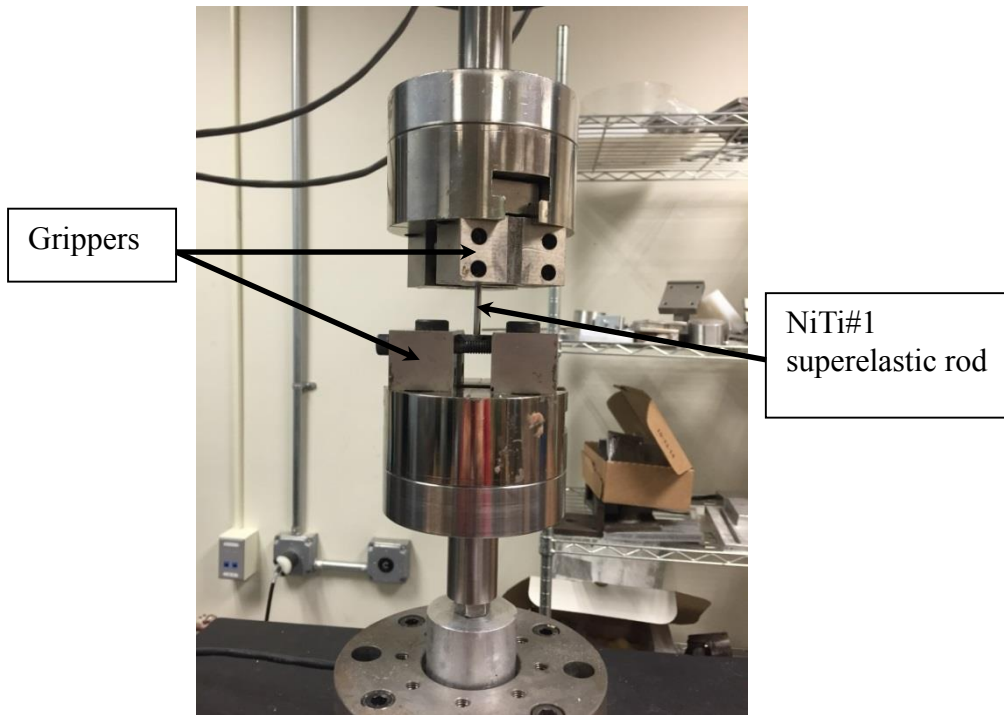


Figure 3-13. The NiTi#1 Superelastic Rod Is Installed on the MTS 858 Testing Machine.

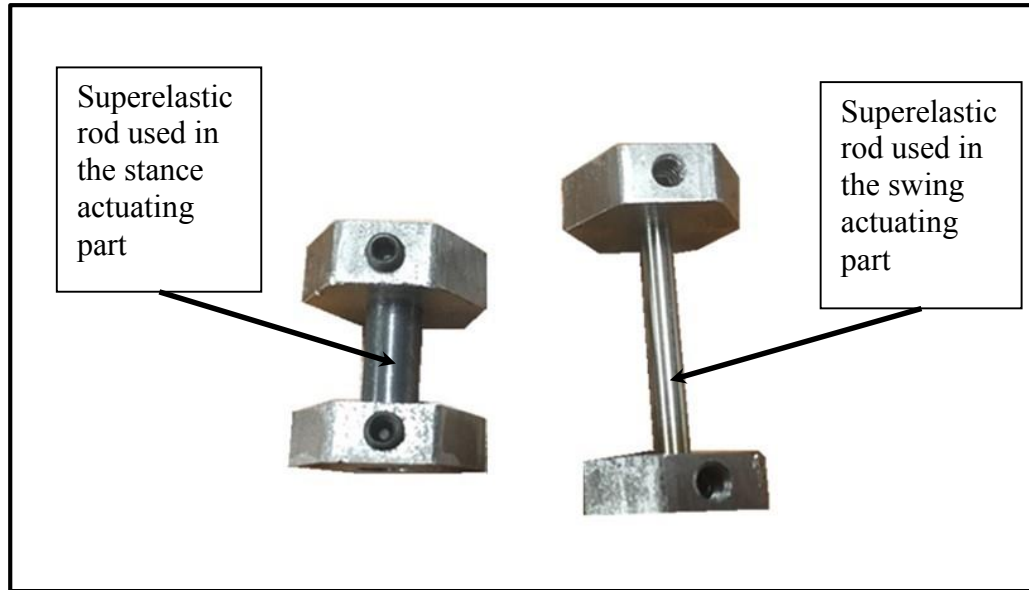


Figure 3-14. The Two NiTi#1 Superelastic Rods Assembled with the Alloy Fixtures.

3.2.4.2 Training Results

Material training must be conducted before any practical application of the superelastic Nitinol rods can be made. The training results are shown in this section. In order to avoid latent heat effect during the training processes, the loading rates followed the 0.0001/sec isothermal strain rate. For the stance superelastic rod, the loading rate was 0.021 degrees/sec and the total deformation was 15 degrees. For the swing superelastic rod, the loading rate was 0.081 degrees/sec and the total deformation was 60 degrees. Ten training cycles were completed for both rods so that the repeatable hysteretic behaviors could be achieved. The training process of the two superelastic rods is shown in figures 3-15 and 3-16. And their first and final cycles are highlighted in these two figures.

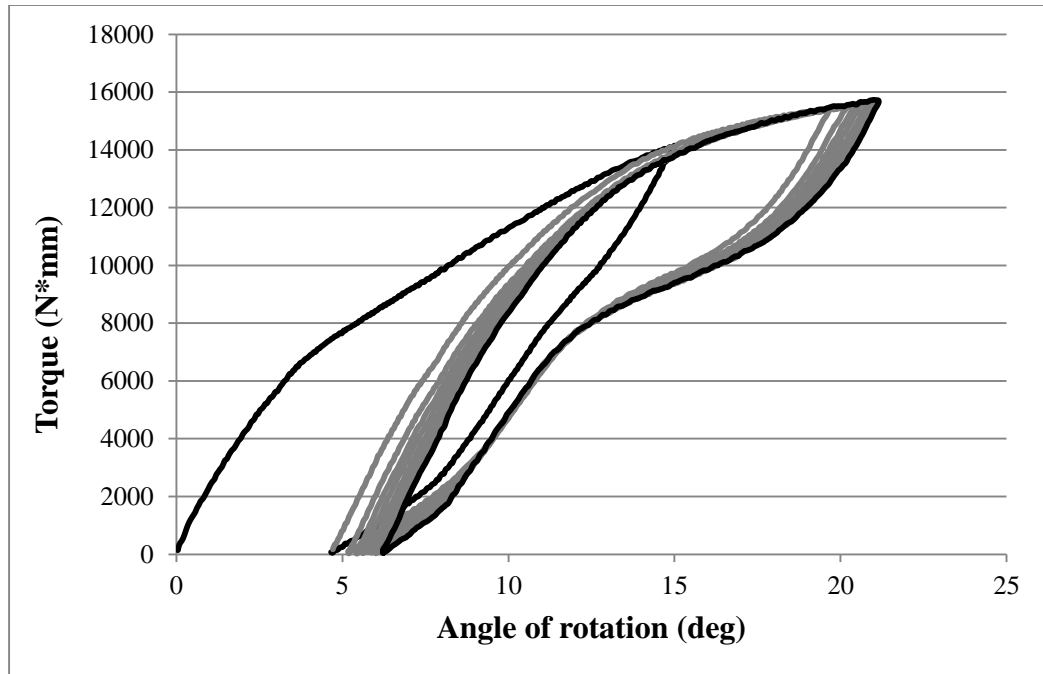


Figure 3-15. The Training Process of the Superelastic Nitinol Rod Used in the Stance Actuating Part. The 1st and the 10th Cycles Are Highlighted.

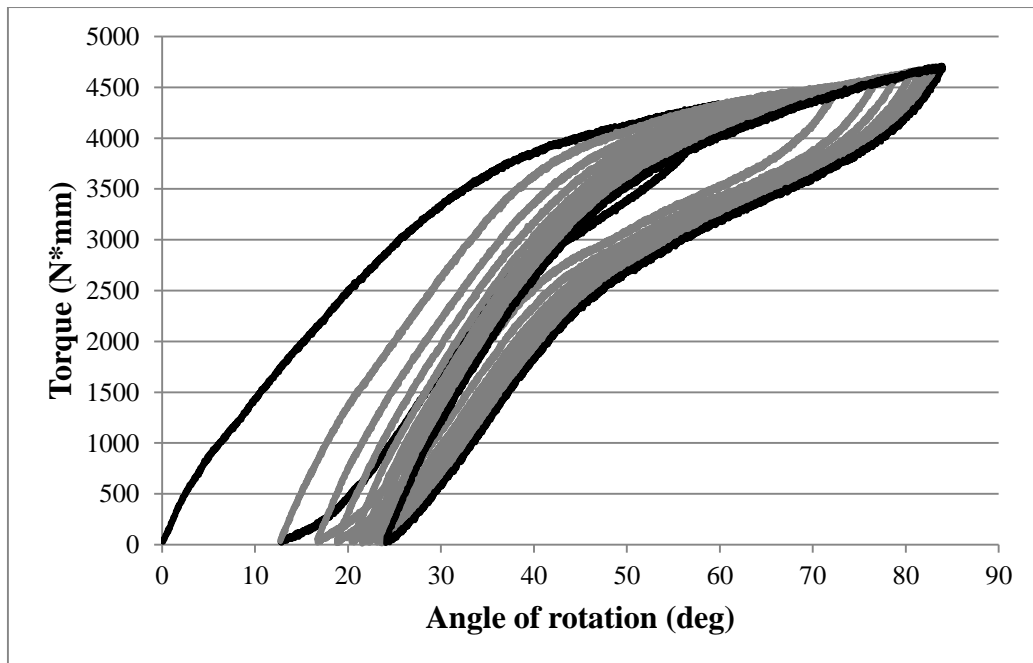


Figure 3-16. The Training Process of the Superelastic Nitinol Rod Used in the Swing Actuating Part. The 1st and the 10th Cycles Are Highlighted.

3.3 Design of the Torsional Springs in the Knee Actuator

In order to mimic the normal knee stiffness pattern, the stance actuating part was designed to provide about 40 Nm torque, while the swing actuating part needed to generate around 10 Nm torque. As the adiabatic simulation results have shown, the two superelastic rods used in the stance and swing actuating parts were able to produce 18 Nm and 5.5 Nm torque, respectively. Thus the remaining torque had to be compensated for by the two torsional springs. However, the stiffnesses of the two torsional springs had been calculated as 1.4 Nm/deg and 0.11 Nm/deg, respectively, which was too high to be achieved by conventional helical springs. Hence, neoprene spring rubber and 60A polyurethane in tube shapes were used in developing the two torsional springs.

Shear modulus G values of neoprene spring rubber and 60A polyurethane were calibrated by a torsion test so that they could be used to determine the geometries of the torsional springs. The testing setup included a torque wrench and an angle meter, as shown in figure 3-17. The parts used to calibrate are shown in figure 3-18. The neoprene spring rubber that was used in the calibration had a 76.2 mm outside diameter, a 23.1 mm inside diameter, and an 80.4 mm gauge length. It generated about 41 Nm torque in 20 degrees of rotation. The 60A polyurethane had a 63.7 mm outside diameter, a 25.2 mm inside diameter, and a 92 mm gauge length. It was twisted in 40 degrees and generated about 13.6 Nm torque. The geometries and calibrating results are listed in table 3-4. Then the shear modulus for these two material types was calculated and is shown in equations 3-9 to 3-14.

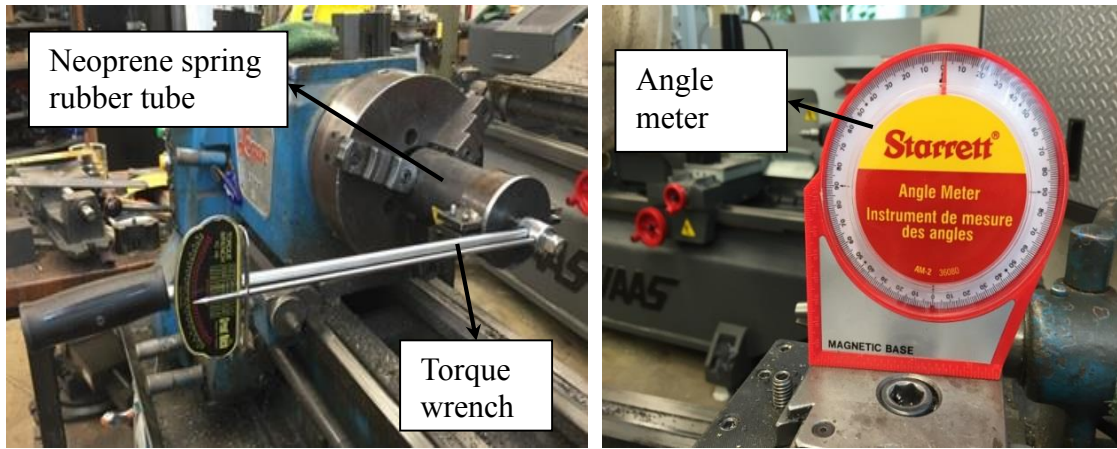


Figure 3-17. The Testing Setup Used to Calibrate the Shear Modulus of the Two Rubber Tubes.

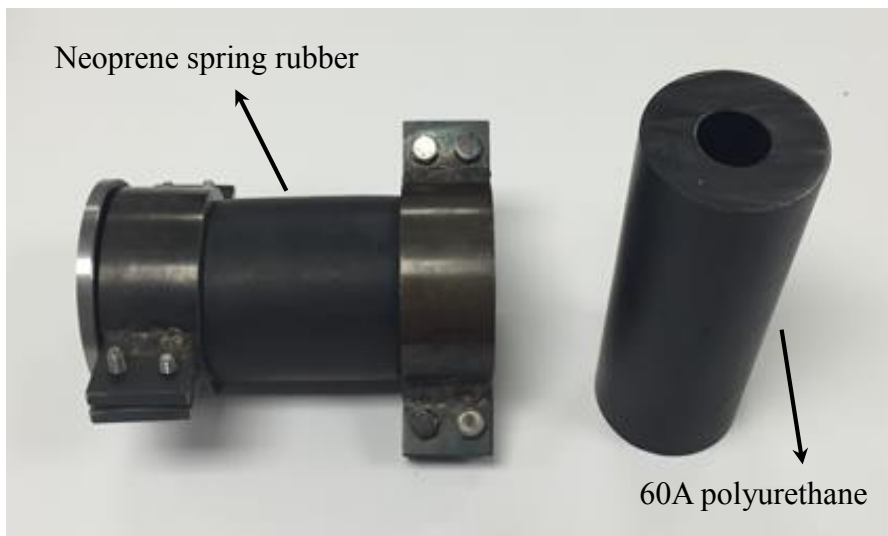


Figure 3-18. The Neoprene Spring Rubber Tube and the 60A Polyurethane Tube Used in the Calibration Tests.

Table 3-4. Geometries and Calibrating Results of the Neoprene Spring Rubber Tube and the 60A Polyurethane Tube.

	Outside diameter (mm)	Inside diameter (mm)	Gauge length (mm)	Angle of rotation (deg)	Torsional load (Nm)
Neoprene Spring Rubber	76.2	23.1	80.4	20	41
Polyurethane Tube	63.7	25.2	92	40	13.6

Calculating the shear modulus of the Neoprene spring rubber tube:

$$D_o = 76.2 \text{ mm}, D_i = 23.1 \text{ mm}, L = 80.4 \text{ mm}, T = 41 \text{ Nm} \quad (3-9)$$

$$J = \frac{\pi}{32} (D_o^4 - D_i^4) = 3281983.15 \text{ mm}^4 \quad (3-10)$$

$$G = \frac{TL}{J\theta} = \frac{41 \times 80.4 \times 10^{-3}}{3281983.15 \times 10^{-12} \times \frac{\pi}{9}} = 0.003 \times 10^9 \quad (3-11)$$

Calculating the shear modulus of the polyurethane tube (60A):

$$D_o = 63.71 \text{ mm}, D_i = 25.23 \text{ mm}, L = 92 \text{ mm}, T = 13.6 \text{ Nm} \quad (3-12)$$

$$J = \frac{\pi}{32} (D_o^4 - D_i^4) = 1577667.6 \text{ mm}^4 \quad (3-13)$$

$$G = \frac{TL}{J\theta} = \frac{13.6 \times 92 \times 10^{-3}}{1577667.6 \times 10^{-12} \times \frac{2\pi}{9}} = 0.0011 \times 10^9 \quad (3-14)$$

In the dynamic knee actuator, the stiff torsional spring used in the stance actuating part was developed with neoprene spring rubber and the soft torsional spring used in the swing actuating part was made by 60A polyurethane. By using the shear modulus results in equations 3-11 and 3-14, the dimensions, shear stresses, and generated torque of the

two torsional springs were calculated and are shown from equations 3-15 to 3-22.

For the torsional spring used in the stance actuating part:

$$D_o = 1.5 \text{ in} = 38.1 \text{ mm}, D_i = \frac{3}{8} \text{ in} = 9.525 \text{ mm} \quad (3-15)$$

$$J = \frac{\pi}{32} (D_o^4 - D_i^4) = 206063 \text{ mm}^4 \quad (3-16)$$

$$T = \frac{GJ\theta}{L} = \frac{0.003 \times 10^9 \times 206063 \times 10^{-12} \times \frac{\pi}{12}}{11.75 \times 10^{-3}} = 20 \text{ Nm} \quad (3-17)$$

$$\tau = \frac{Tr}{J} = \frac{20 \times 19.05 \times 10^{-3}}{206063 \times 10^{-12}} = 1.84 \text{ MPa} \quad (3-18)$$

For the torsional spring used in the swing actuating part:

$$D_o = 1.25 \text{ in} = 31.75 \text{ mm}, D_i = 0.5 \text{ in} = 12.25 \text{ mm} \quad (3-19)$$

$$J = \frac{\pi}{32} (D_o^4 - D_i^4) = 97553.45 \text{ mm}^4 \quad (3-20)$$

$$T = \frac{GJ\theta}{L} = \frac{0.0011 \times 10^9 \times 97553.45 \times 10^{-12} \times \frac{\pi}{3}}{26.7 \times 10^{-3}} = 5 \text{ Nm} \quad (3-21)$$

$$\tau = \frac{Tr}{J} = \frac{5 \times 15.875 \times 10^{-3}}{97553.45 \times 10^{-12}} = 0.81 \text{ MPa} \quad (3-22)$$

The dimensions of the two torsional springs were determined according to the above calculation. The length of the springs maintained consistency with that of the superelastic rods. In conclusion, the stance torsional spring had a 38.1 mm outside diameter, a 9.525 mm inside diameter, and an 11.75 mm length. It produced about 20 Nm torque in 15 degrees of rotation. The swing torsional spring had a 31.75 mm outside diameter, a 12.25 mm inside diameter, and a 26.7 mm length, providing about 5 Nm torque in 60 degrees of rotation.

3.4 Summary

Development of the dynamic knee actuator has been presented in this chapter. Two actuating parts in the actuator acted for different phases during walking. Each part combined a superelastic torsional rod and a torsional spring in parallel. The development process was divided into two major portions: design of the superelastic Nitinol rods and design of the torsional springs. The geometries and specific materials of the rods and the springs were determined, completing the knee actuator design. The numerical simulation results indicated that the dynamic knee actuator was able to reproduce the normal knee joint stiffness profile.

Chapter 4

Development of the Dynamic Knee Module

Chapter 3 discussed the design of the superelastic dynamic knee actuator. The supporting parts in the knee module are studied in this chapter. Since there were two actuating parts working for different gait phases, a control system was necessary to operate them properly. Discussion of this logic is also included in this chapter. The knee module parts were first fabricated via additive manufacturing (AM) technology. This prototype provided the possibility of assessing the design and verifying its feasibility. Then the final knee module prototype was built by traditional manufacturing and mounted on a conventional KAFO for motion analysis tests.

4.1 Design of the Dynamic Knee Module

In most studies of KAFOs, hinged joints are considered to provide a good approximation of joint motion, which minimizes the size, weight, and cost of the devices. Therefore, the dynamic knee module presented in this research was designed to have a single axis of rotation. In general, the dynamic knee joint module consisted of two frames, as conceptually shown in figure 4-1. These were referred to as the internal and

external frames (parts 1 and 2) of the knee module, and were connected with the shank and the thigh segments of the KAFO, respectively. The two knee actuating parts (parts 3 and 4) were housed between the two frames to provide the desired level of stiffness across the entire walking gait cycle. The stance actuating part (part 3) was engaged only during the early and mid-stance phases, while the swing actuating part (part 4) functioned for the rest of the gait cycle. Each of these two parts combined a superelastic Nitinol rod and a linear torsional spring in parallel.

Two solenoids (part 5) controlled the two actuating parts, engaging and disengaging them based on the signals from a force sensitive resistor (FSR) that was attached at the heel of the KAFO. The dynamic knee module had three working modes: free mode, locked mode, and dynamic mode. In the free mode, both of the actuating parts were disengaged so that the thigh and shank segments could rotate freely around the axis of the knee module, which also was the knee motion center. In the locked mode, the knee joint was maintained in the locked position, and the device functioned as a conventional drop lock KAFO. Both actuators were engaged in this mode, which provided the most stability for the joint. In the dynamic mode, the two actuators interacted between each other, based on the signals of the FSR switch. The stance actuating part was engaged at the heel strike of the orthotic leg. Through absorbing energy in the actuator, it generated adequate support and allowed the knee to flex to facilitate smooth shock absorption during the loading response. Then the stance actuating part assisted the knee extension motion during the mid-stance phase by releasing the saved energy. Switching between the two actuating parts occurred at the heel off of the orthotic leg. The swing actuating part controlled knee flexion and assisted knee extension during the late stance, pre-swing, and

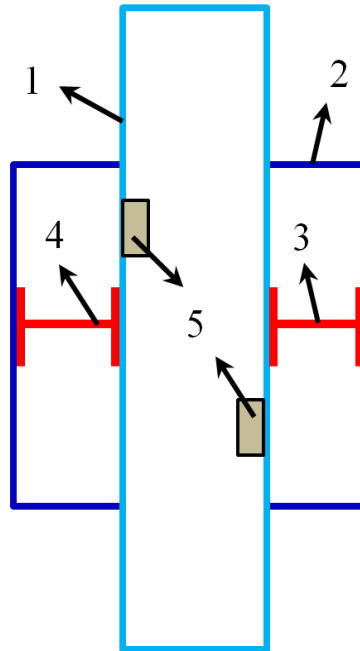


Figure 4-1. The Conceptual Design of the Dynamic Knee Module: 1) the Internal Frame of the Knee Module That Is Connected to the Shank Segment; 2) the External Frame of the Knee Module That Is Connected to the Thigh Segment; 3) the Stance Actuating Part That Combines a Stiff Superelastic Nitinol Rod and a Stiff Torsional Spring In Parallel; 4) the Swing Actuating Part That Combines a Soft Superelastic Nitinol Rod and a Soft Torsional Spring in Parallel; 5) Two Push-Pull Solenoids. This Figure Is Adopted from Reference [16].

swing phases.

The dynamic knee joint module was been modeled and assembled in SolidWorks. The cross-sectional view of the assembly is shown in figure 4-2. All parts of the knee module are listed in table 4-1.

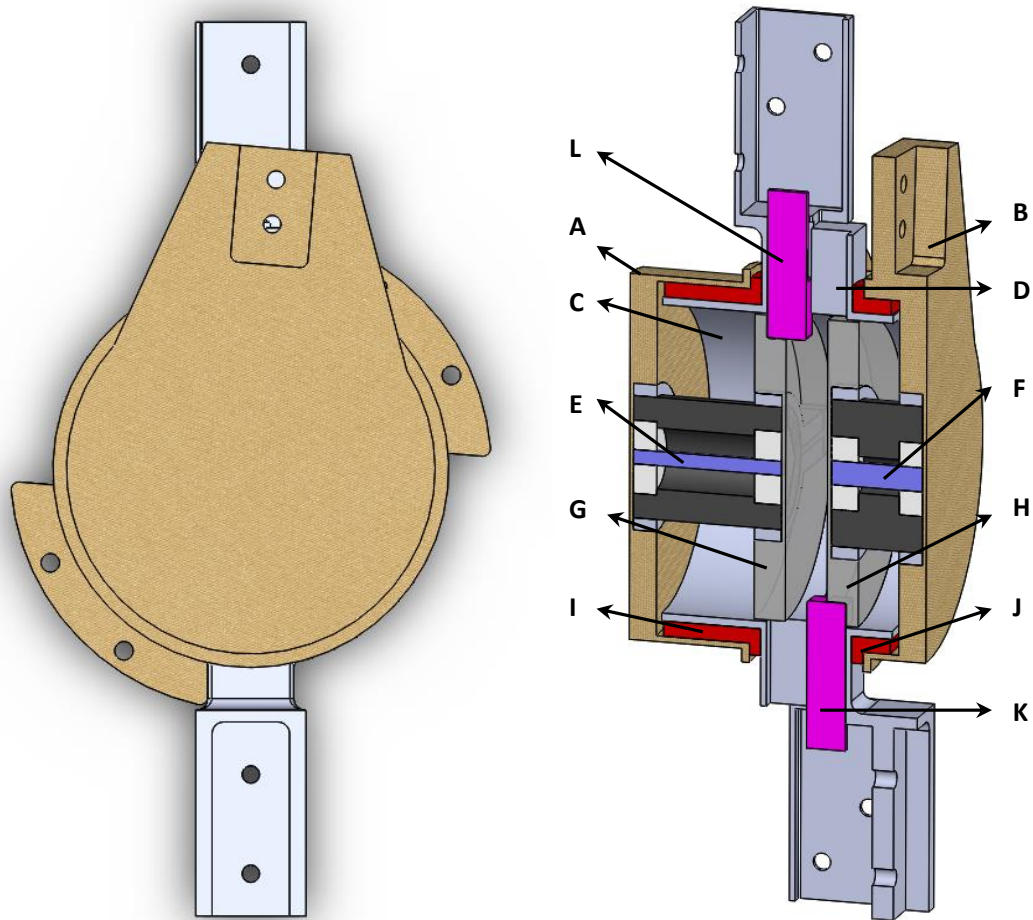


Figure 4-2. The Dynamic Knee Module Assembly. (A) Swing Side of the External Frame of the Knee Module; (B) Stance Side of the External Frame of the Knee Module; (C) Swing Side of the Internal Frame of the Knee Module; (D) Stance Side of the Internal Frame of the Knee Module; (E) Swing Actuating Part; (F) Stance Actuating Part; (G) Swing Support Disk; (H) Stance Support Disk; (I) Swing Sleeve Bearing; (J) Stance Sleeve Bearing; (K) Stance Engagement Mechanism; (L) Swing Engagement Mechanism.

Table 4-1. Description of All Parts in the Dynamic Knee Joint Module.

Part	Description	Material	Weight (g)
A: Swing side of the external frame of the knee module	Parts A and B compose the external frame of the dynamic knee module that connects to the thigh segment.	Aluminum 6061-T6	110.8
B: Stance side of the external frame of the knee module	Parts A and B compose the external frame of the dynamic knee module that connects to the thigh segment.	Aluminum 6061-T6	139.7
C: Swing side of the internal frame of the knee module	Parts C and D compose the internal frame of the dynamic knee module that connects to the shank segment.	Aluminum 6061-T6	98.4
D: Stance side of the internal frame of the knee module	Parts C and D compose the internal frame of the dynamic knee module that connects to the shank segment.	Aluminum 6061-T6	101.7

E: Swing actuating part	Part E consists of two hexagon fixtures, one soft superelastic Nitinol rod, and one soft torsional spring. It acts during the swing phase to control knee motion.	Alloy 4140 cold finished annealed; Fort Wayne NiTi#1; Polyurethane (60A tubes)	132
F: Stance actuating part	Part F consists of two hexagon fixtures, one stiff superelastic Nitinol rod, and one stiff torsional spring. It acts during the stance phase to control knee motion.	Alloy 4140 cold finished annealed; Fort Wayne NiTi#1; Neoprene spring rubber	145
G: Swing support disk	Part G is connected to the part E, supporting the internal frame of the knee module (part C).	Aluminum 6061-T6	40.2
H: Stance support disk	Part H is connected to the part F, supporting the internal frame of the knee module (part D).	Aluminum 6061-T6	40.2
I: Swing sleeve bearing	Part I reduces the rotation friction between the external and internal frames.	PTFE	62

J: Stance sleeve bearing	Part J reduces the rotation friction between the external and internal frames.	PTFE	24.5
K: Stance engagement mechanism	Part K is composed of one slider and one push-pull solenoid, functioning to activate and inactivate the stance actuating part.	Alloy 4140 cold finished annealed	33.2
L: Swing engagement mechanism	Part L is composed of one slider and one push-pull solenoid, functioning to activate and inactivate the swing actuating part.	Alloy 4140 cold finished annealed	33.2

4.2 FEM Analyses of the Dynamic Knee Module

Finite element analysis was used to ensure the safety of the dynamic knee module. All material properties used to simulate the knee module are listed in table 4-2. Optimal structures and factors of safety were obtained for all parts. Simulation results for the dynamic knee module are described in this section and indicate that all the parts worked in the elastic deformation range and had good repeatability.

Table 4-2. Material Properties Used to Simulate the Parts of the Dynamic Knee Module.

Material	Young's modulus (GPa)	Poisson's ratio	Yield strength (MPa)	Density (g/cm³)
Aluminum 6061-T6	68.9	0.33	276	2.70
Alloy steel 4140 cold finished annealed	190-210	0.29	415	7.85
Superelastic Nitinol	Austenite: 75-83 Martensite: 28-40	0.33	Austenite: 195-690 Martensite: 70-140	6.45

4.2.1 The External Frame of the Dynamic Knee Module

The stance side part and the swing side part of the external frame were combined into an integrated unit in the dynamic knee module via screws. In the simulations, the swing side part was fixed on the screw holes and a 20 Nm torque was applied where it connected with the swing actuating part, which was the maximum load the part needed to bear. As shown in figures 4-3 and 4-4, the maximum von Mises stress generated on the

swing side part was about 32.2 MPa and the factor of safety was 8.57. The stance side part connected the whole external frame onto the thigh segment of the KAFO. When simulating this part, the boundary conditions were set on the connecting surfaces. The maximum torque on the stance side part was about 50 Nm and was loaded where it connected with the stance actuating part. Figures 4-5 and 4-6 show that the maximum von Mises stress on the stance side part of the external frame was about 102.9 MPa and the factor of safety was 2.68.

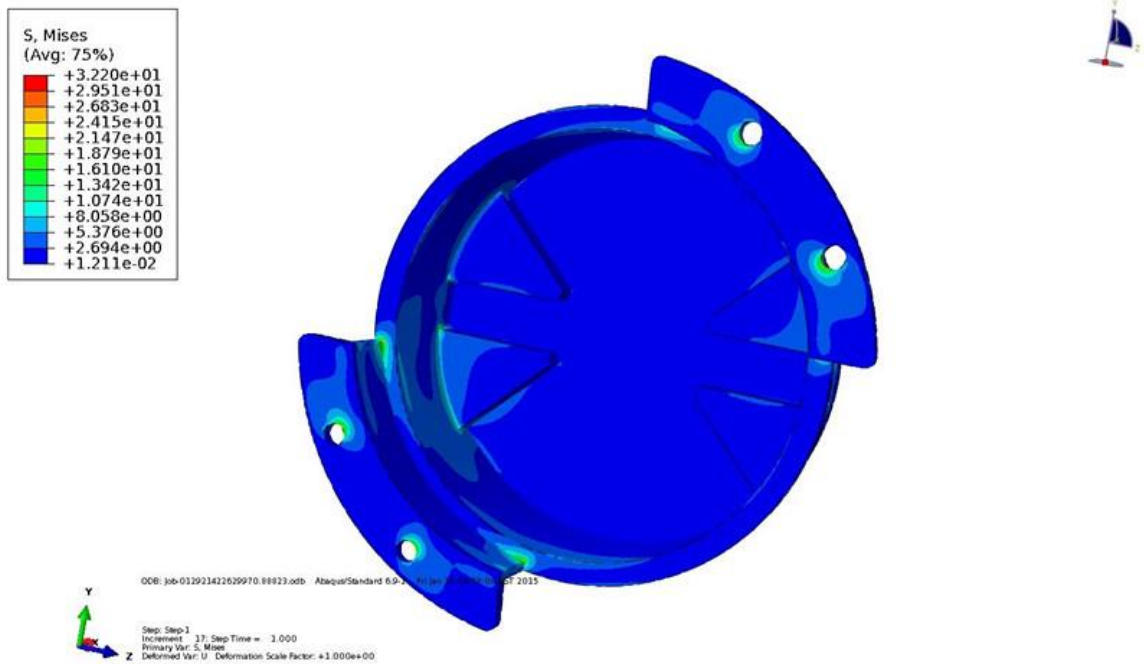


Figure 4-3. The FEA Simulation Result of the Swing Side Part of the External Frame.

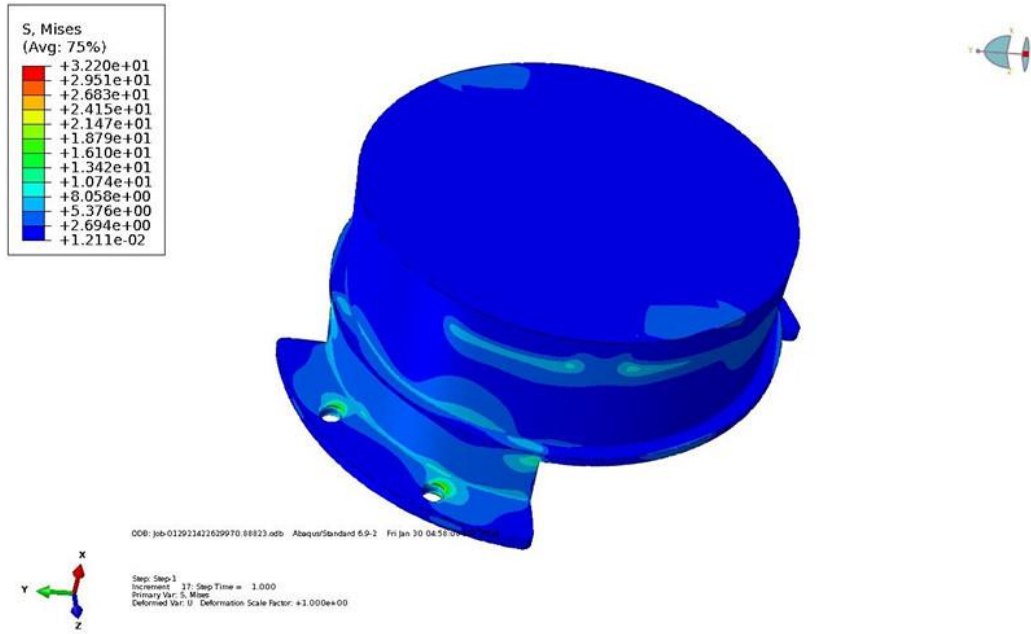


Figure 4-4. The FEA Simulation Result of the Swing Side Part of the External Frame.

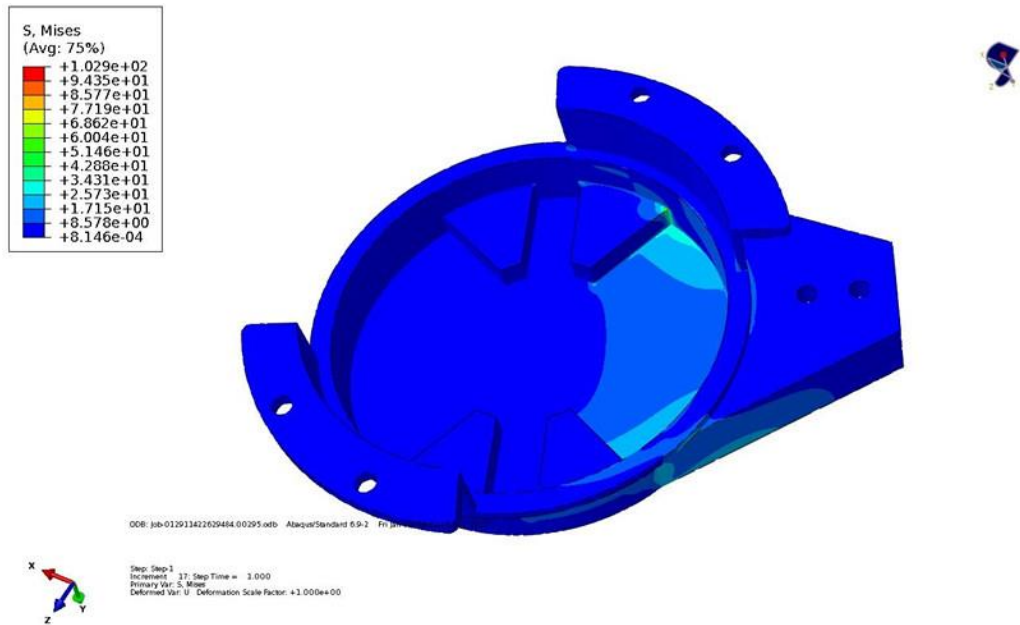


Figure 4-5. The FEA Simulation Result of the Stance Side Part of the External Frame.

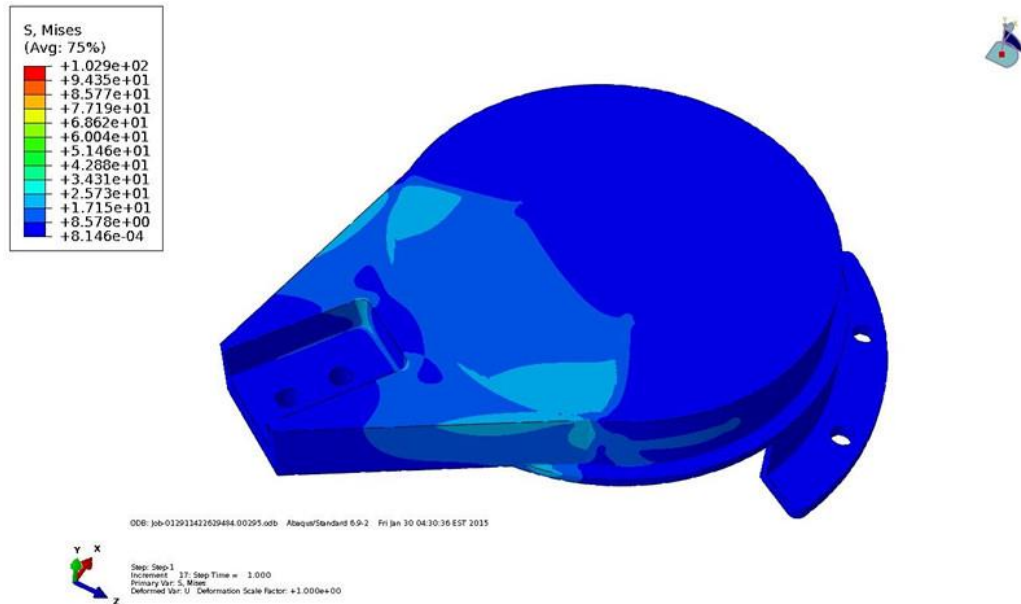


Figure 4-6. The FEA Simulation Result of the Stance Side Part of the External Frame.

4.2.2 The Actuating Fixtures of the Dynamic Knee Module

Four actuating fixtures were designed in hexagon shapes in order to mount the superelastic Nitinol rods inside the dynamic knee module, to prevent relative rotary motions between the superelastic rods and the supporting parts. Two of the fixtures were for the stance superelastic rod and bear a torsion load (about 20 Nm) that is the maximum amount of torque produced by the stiff superelastic rod. The other two were used on the swing superelastic rod, and a low torque (about 10 Nm) was applied on them. These fixtures were simulated with 4140 alloy steel and fixed on their outside surfaces. The maximum von Mises stresses generated on the stance and swing fixtures were 363.9 MPa and 264.3 MPa, respectively. And the factors of safety for the stance and swing fixtures were 1.14 and 1.57, respectively. The simulation results are shown in figures 4-7, 4-8, 4-9, and 4-10.

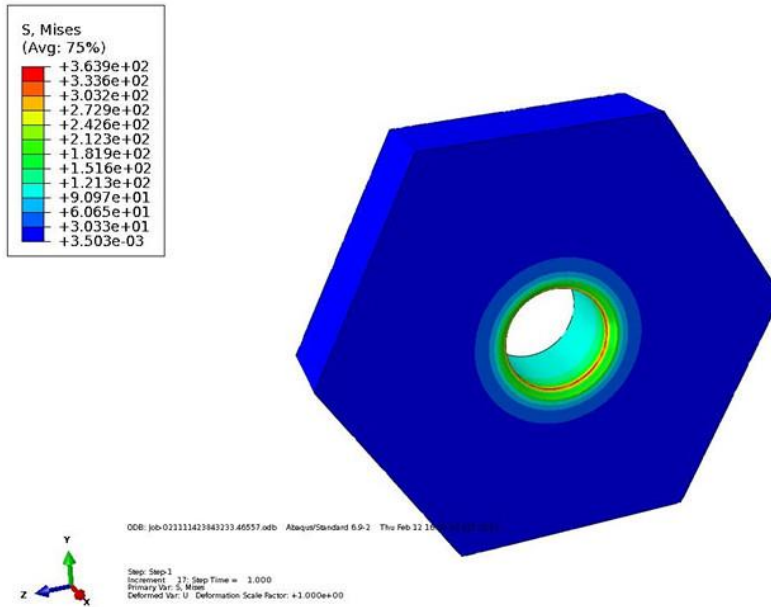


Figure 4-7. The FEA Simulation Result of the Stance Fixture That Connects the Stance Superelastic Rod to the Dynamic Knee Module.

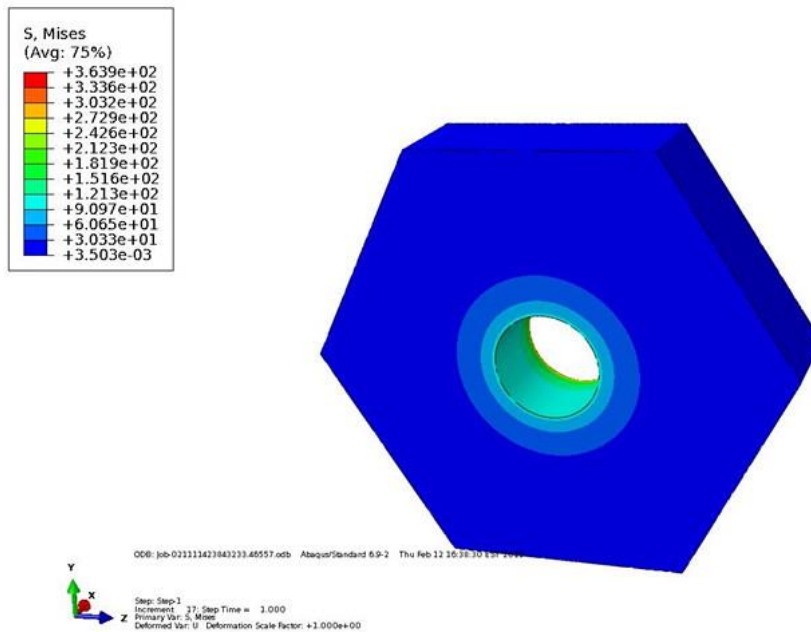


Figure 4-8. The FEA Simulation Result of the Stance Fixture That Connects the Stance Superelastic Rod to the Dynamic Knee Module.

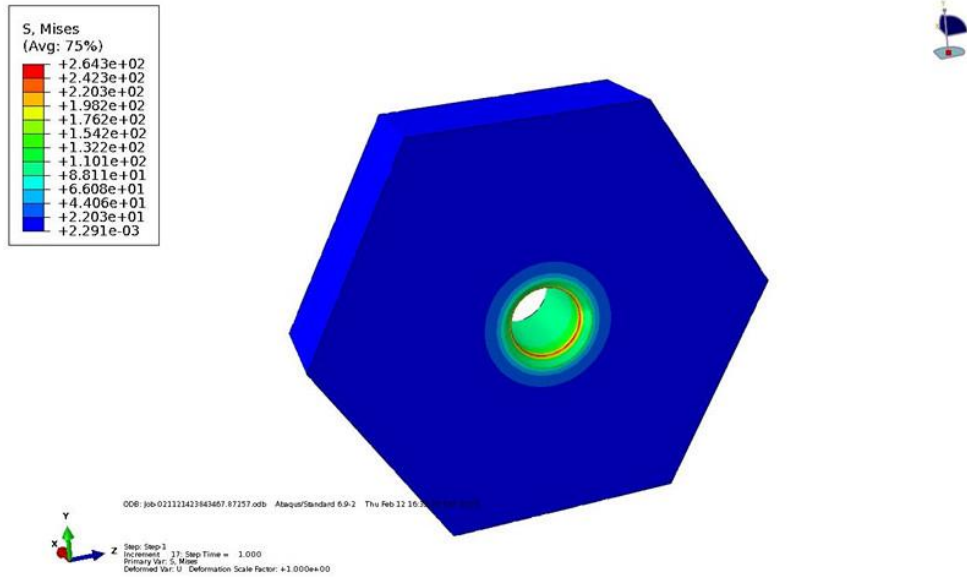


Figure 4-9. The FEA Simulation Result of the Swing Fixture that Connects the Swing Superelastic Rod to the Dynamic Knee Module.

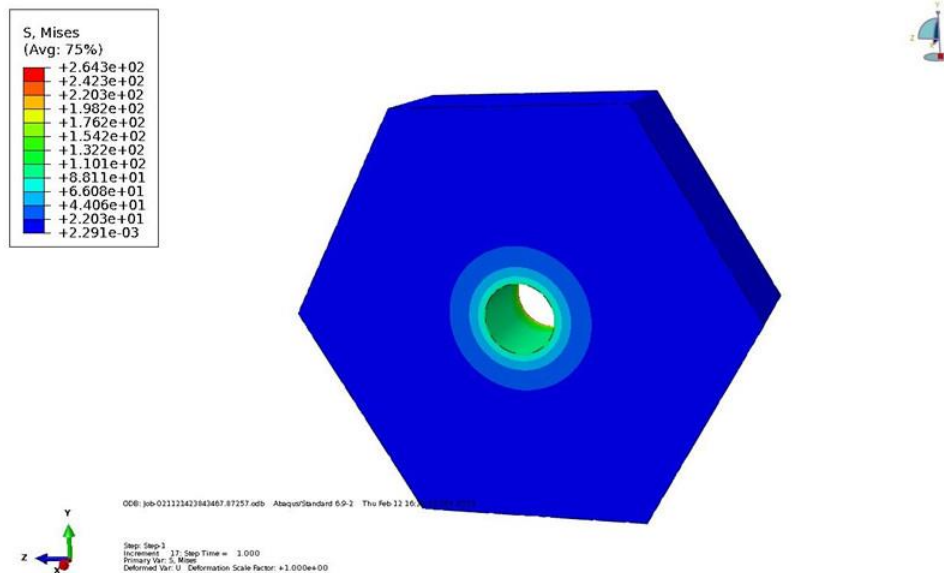


Figure 4-10. The FEA Simulation Result of the Swing Fixture That Connects the Swing Superelastic Rod to the Dynamic Knee Module.

4.2.3 The Support Disks and the Internal Frame of the Dynamic Knee Module

Two support disks were designed to increase the strength of the internal frame of the dynamic knee module: one for the stance side and the other for the swing side. As mentioned before, one end of the stance and swing actuating parts was connected with the external frame of the knee module. The other end of the two actuators was connected with the support disks. The stance side part and the swing side part of the internal frame were combined into an integrated part in the dynamic knee module, attaching to the shank segment of the KAFO. The support disks and the internal frame were bound through the engaging mechanisms. When the thigh and shank segments of the passive KAFO rotated around the knee joint, it caused rotary motions between the two frames, twisting the stance or swing actuating parts to generate torques. Assemblies of the support disks and the internal frame parts for both sides were studied in this research. These parts were simulated with aluminum alloys in order to reduce the overall weight of the knee module and simplify the manufacturing processes. The boundary conditions were set on the surfaces of the support disks and the internal frames where they connected to the actuating parts and the shank segment, respectively. When the stance actuator was engaged, the stance engagement mechanism applied 34.76 MPa and 11.52 MPa of pressure on the stance support disk and the stance internal frame, respectively. When the swing actuator was engaged, the swing engagement mechanism applied 13.25 MPa and 3.33 MPa of pressure on the swing support disk and the swing internal frame, respectively. These values were calculated from the parts' dimensions and the generated torques in the actuators. The maximum von Mises stresses on the stance and swing side assemblies were about 193.8 MPa and 54.0 MPa, respectively. And the factors of safety

were 1.42 and 5.11, respectively. The simulation results are shown in figures 4-11, 4-12, 4-13, and 4-14.

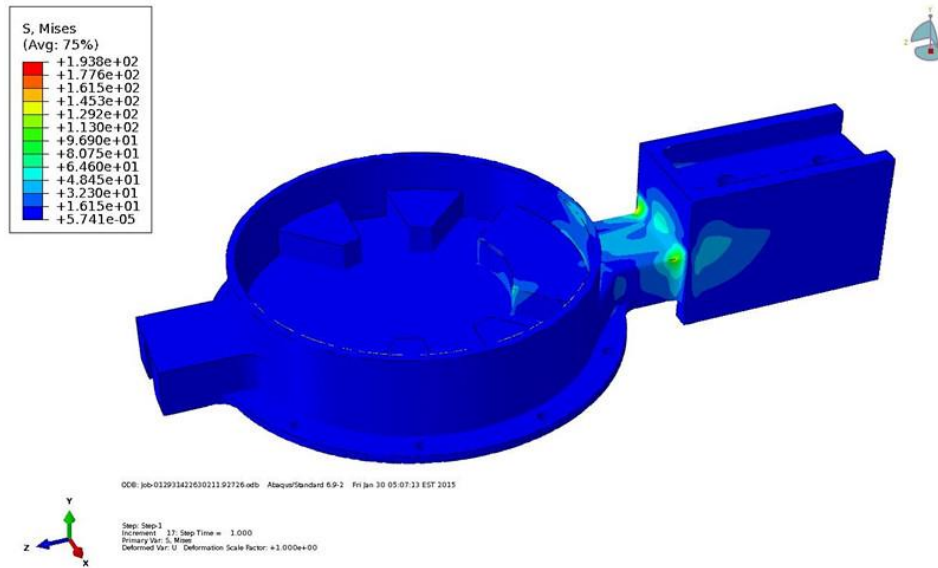


Figure 4-11. The FEA Simulation Result of the Stance Side Assembly Combining the Stance Support Disk and the Stance Internal Frame.

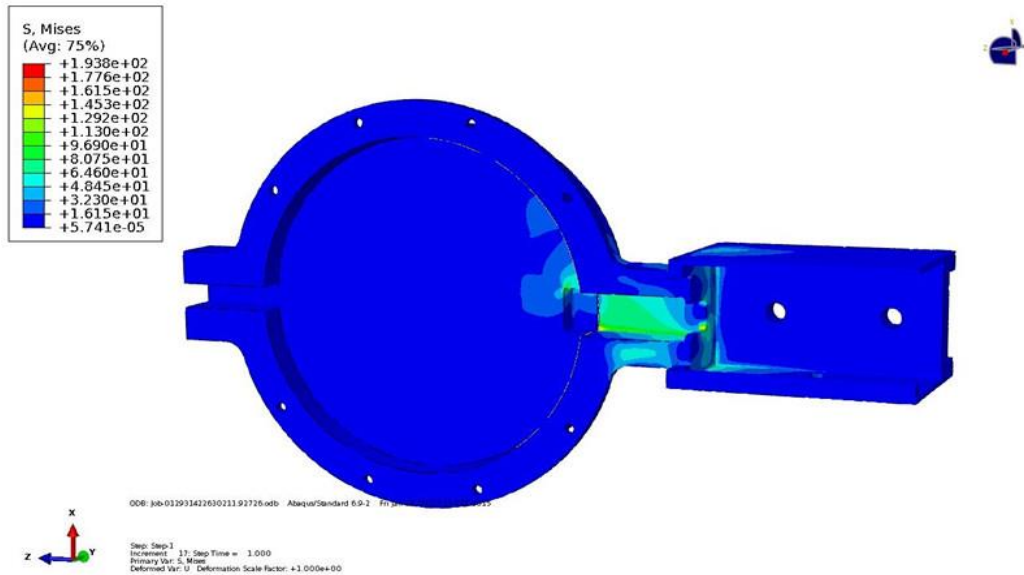


Figure 4-12. The FEA Simulation Result of the Stance Side Assembly Combining the Stance Support Disk and the Stance Internal Frame.

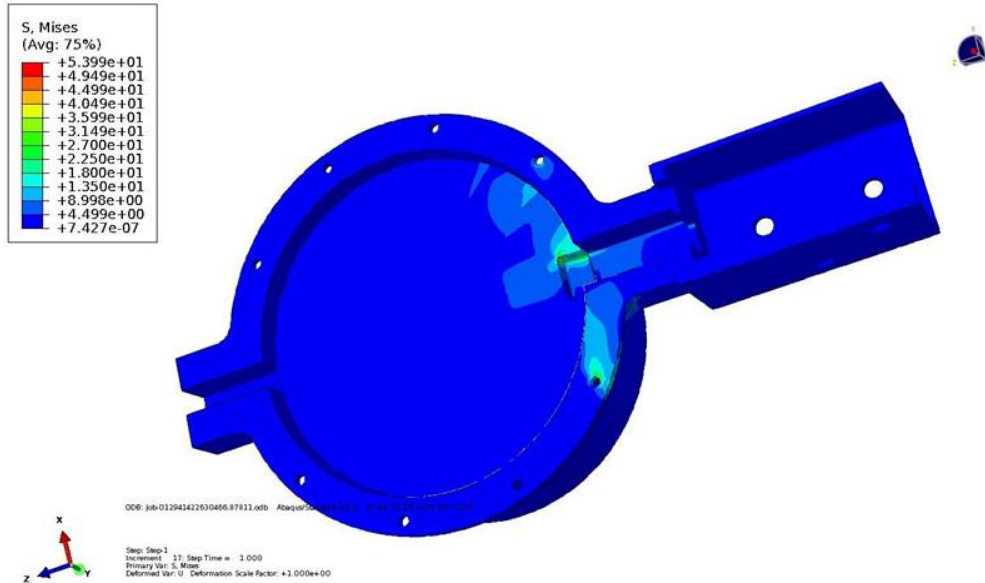


Figure 4-13. The FEA Simulation Result of the Swing Side Assembly Combining the Swing Support Disk and the Swing Internal Frame.

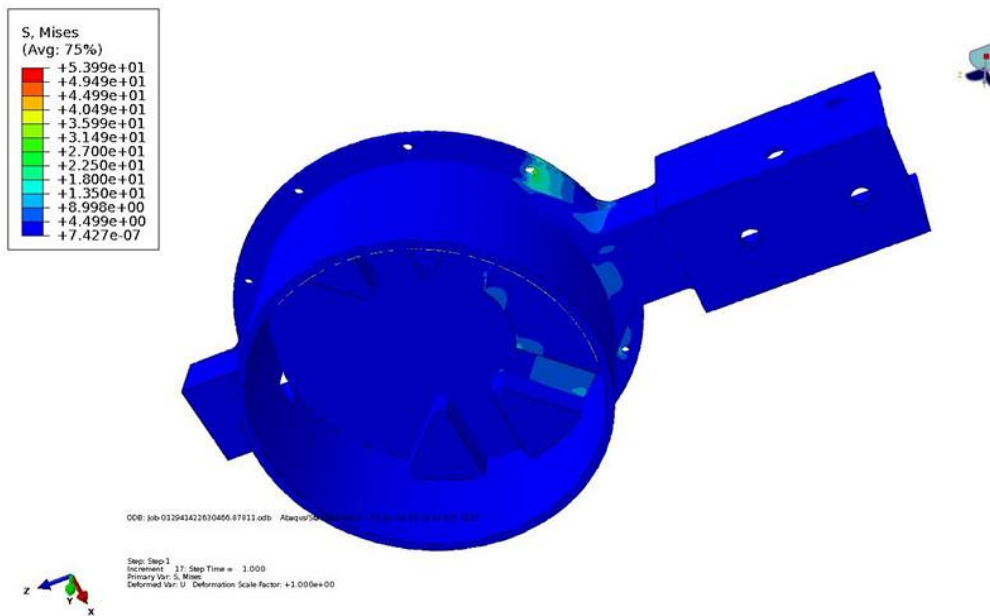


Figure 4-14. The FEA Simulation Result of the Swing Side Assembly Combining the Swing Support Disk and the Swing Internal Frame.

4.2.4 The Engagement Mechanisms of the Dynamic Knee Module

Both the stance and swing engagement mechanisms were composed of one slider and one push-pull solenoid. The sliders moved along the radial direction of the knee joint, triggering the engagement of the actuators. When the sliders moved towards the joint center, they connected the support disks and the internal frame, making them rotate as one part. Therefore, the two sliders endured high compression forces to prohibit relative rotations between the support disks and the internal frame. The sliders were simulated with 4140 alloy steel. A 34.76 MPa pressure and a 13.25 MPa pressure were applied on the sliders of the stance and swing engagement mechanisms, respectively. The maximum von Mises stresses generated on the two sliders were 356.7 MPa and 130.1 MPa, respectively. And the factors of safety were 1.16 and 3.19, respectively. The simulation results are shown in figures 4-15 and 4-16.

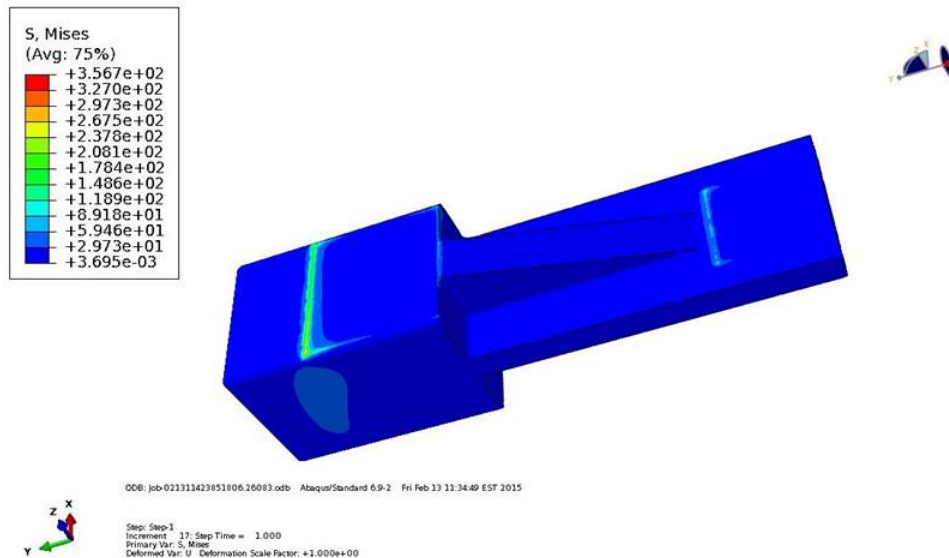


Figure 4-15. The FEA Simulation Result of the Slider in the Stance Engagement Mechanism.

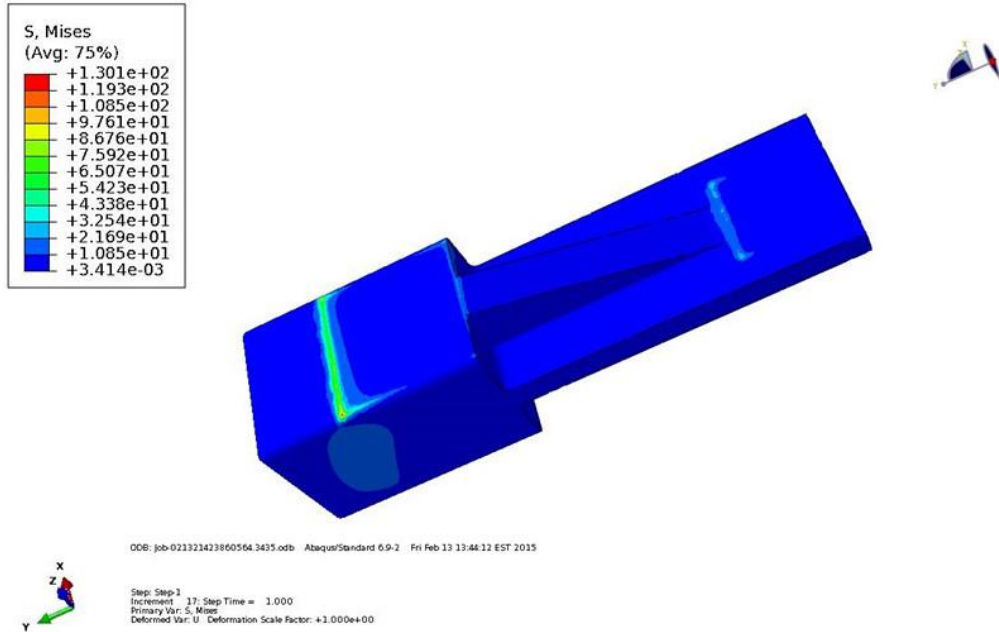


Figure 4-16. The FEA Simulation Result of the Slider in the Swing Engagement Mechanism.

4.3 Design of the Control System

As mentioned in section 4.2, there were three working modes available in the dynamic knee module: free mode, locked mode, and dynamic mode. So a control system was necessary to enable the conversion from one mode to another.

The control system included: (1) a control circuit, (2) an Arduino Uno board (Arduino LLC, United States), (3) a breadboard to build the control circuit on, and (4) a 12 VDC power supply (Keysight Technologies, Inc., California, United States). The control circuit was associated with the Arduino Uno board, which consisted of (1) two 12VDC solenoid electromagnets (Jifa Electric LLC, China), (2) a 0.5” force sensitive resistor (FSR) (Sparkfun Electronics, United States), (3) a tactile button switch, (4) two

TIP 122 transistors, (5) two light emitting diodes, and (6) two 10K resistances. The Arduino Uno board was programmed in advance. The two push-pull solenoids, which had a 10 mm rated stroke and a 20 N attraction force, were used in the dynamic knee module to engage and disengage the stance and swing actuating parts. The FSR had a resistance larger than $1M\Omega$ under zero pressure. It was able to be attached on the orthotic sole as a foot switch and the resistance changed according to the amount of pressure applied on its sensing area. The larger the force applied to it, the lower the resistance was set.

This system switched among the three working modes of the actuator by operating the two solenoids. The connections of the microcontroller are illustrated in figure 4-17.

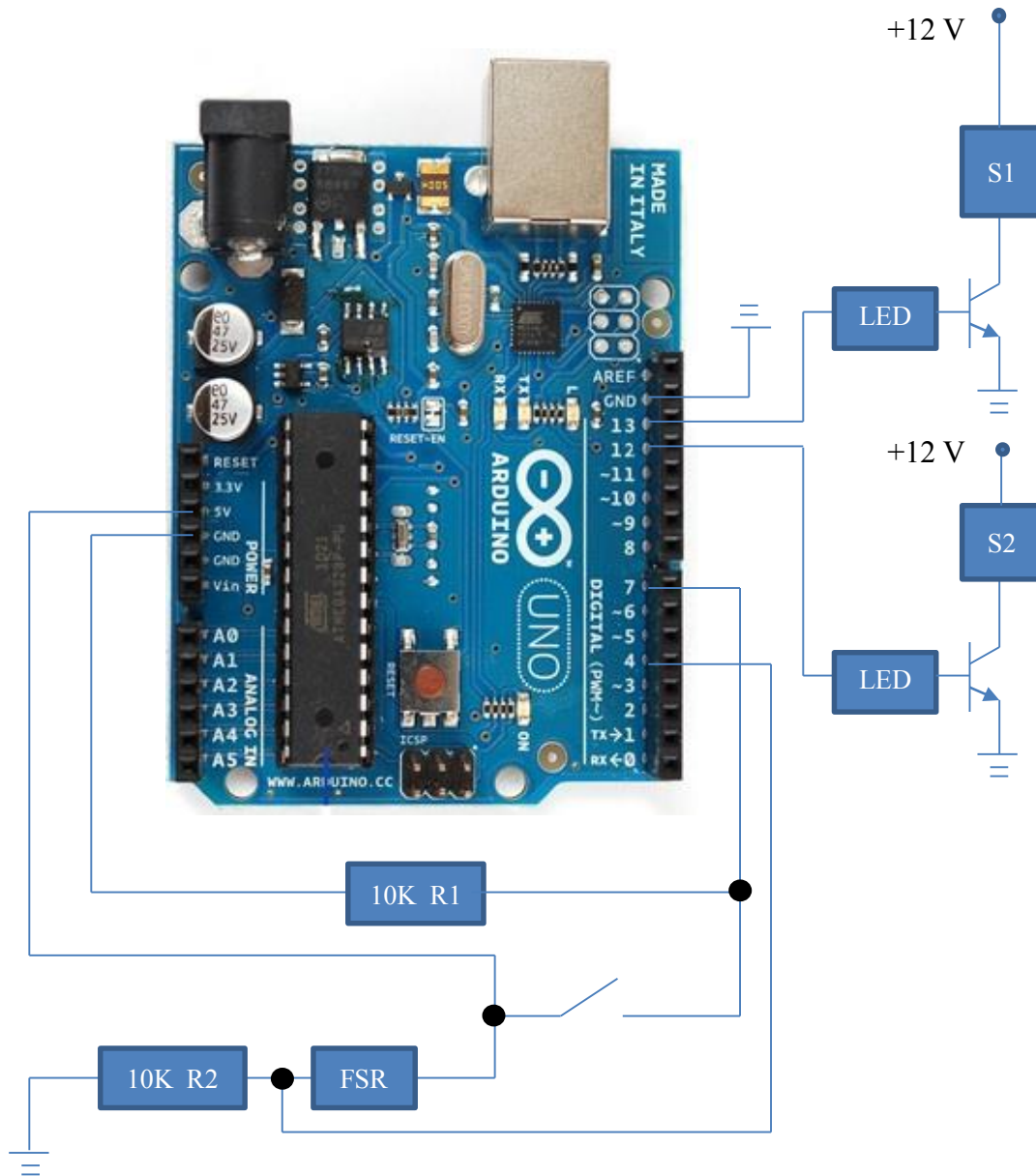


Figure 4-17. The Connection of the Arduino UNO Board and Control Circuit.

4.4 Prototypes of the Dynamic Knee Module

A ULTRA® 3SP™ from EnvisionTEC, Germany was used to fabricate the preliminary prototype of the dynamic knee module in this research [112-118]. The preliminary prototype is shown in figures 4-18 and 4-19.



Figure 4-18. The Preliminary Prototype of the Dynamic Knee Module.



Figure 4-19. The Connection between the Dynamic Knee Module and the Microcontroller.

The final prototype was improved and machined, based on the assessment of the plastic prototype. This metallic device was attached to a conventional drop lock KAFO (Marshall Kloene, OH, USA), which includes (1) four aluminum side brackets, (2) four stainless steel hinged joints (ankle and knee), (3) three polypropylene braces for foot, (4) calf and thigh segments, (5) two straps, and (6) one drop lock on the lateral knee joint. The lateral knee joint of the KAFO was replaced by the dynamic knee module.

The two assemblies of the stance and swing actuating parts are illustrated in figure 4-20. Figures 4-21 and 4-22 show the parts of the knee module and the complete knee module assembly, respectively. Figure 4-23 shows the UT dynamic KAFO which includes the knee module, the control system, the FSR switch, and a 12VDC battery.

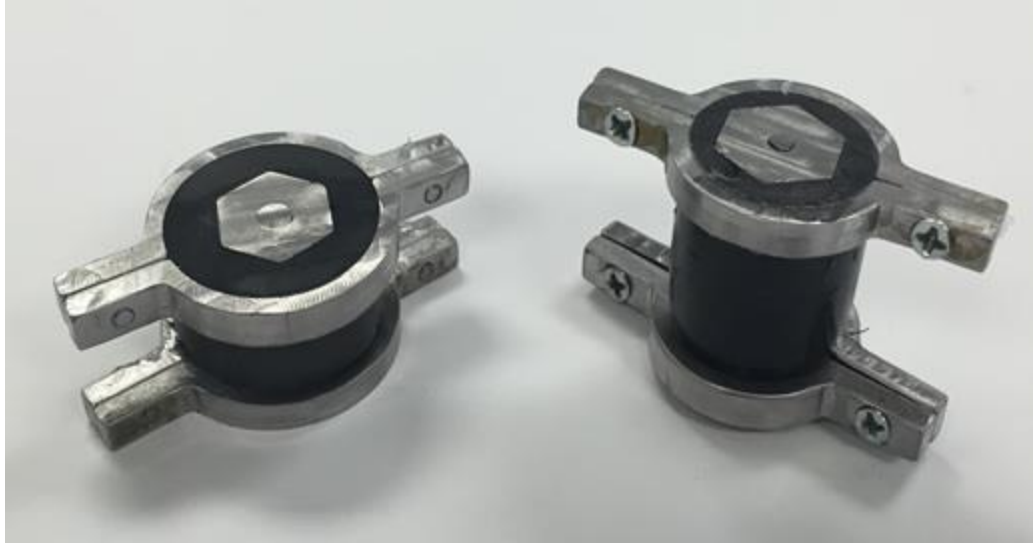


Figure 4-20. The Stance and Swing Actuating Parts with Fixtures at Both Ends.

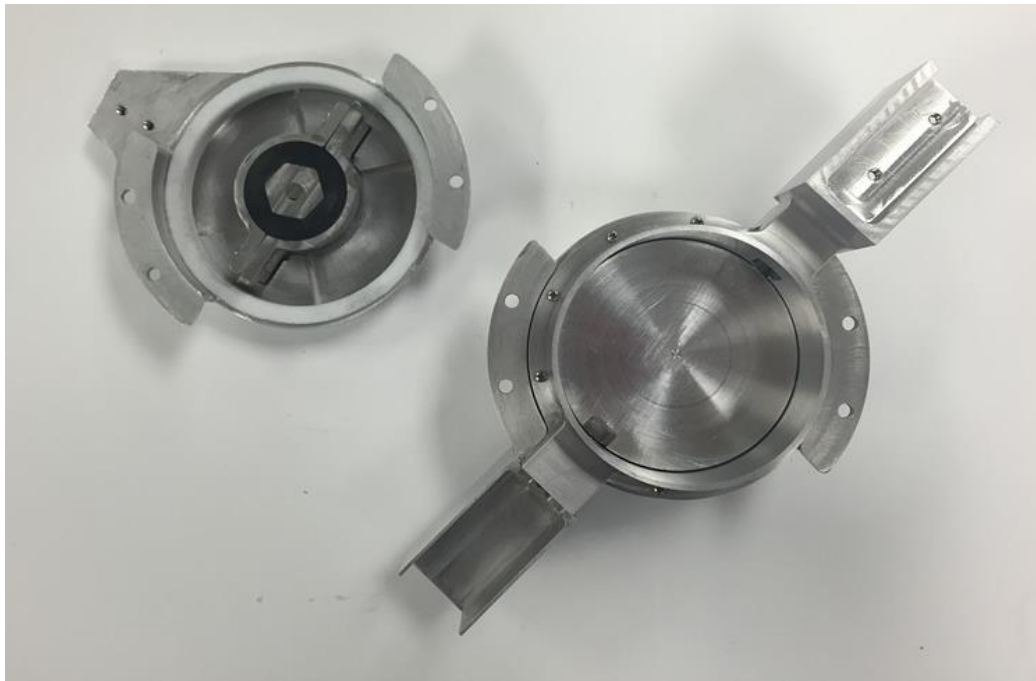


Figure 4-21. The Parts of the Dynamic Knee Joint Module.

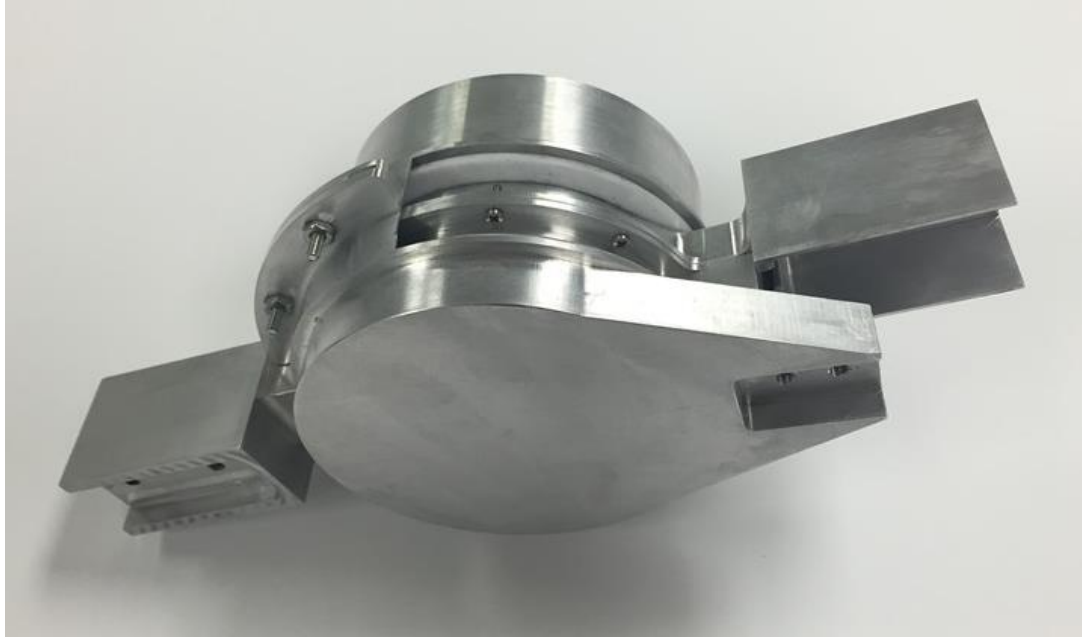


Figure 4-22. The Final Prototype of the Dynamic Knee Joint Module.

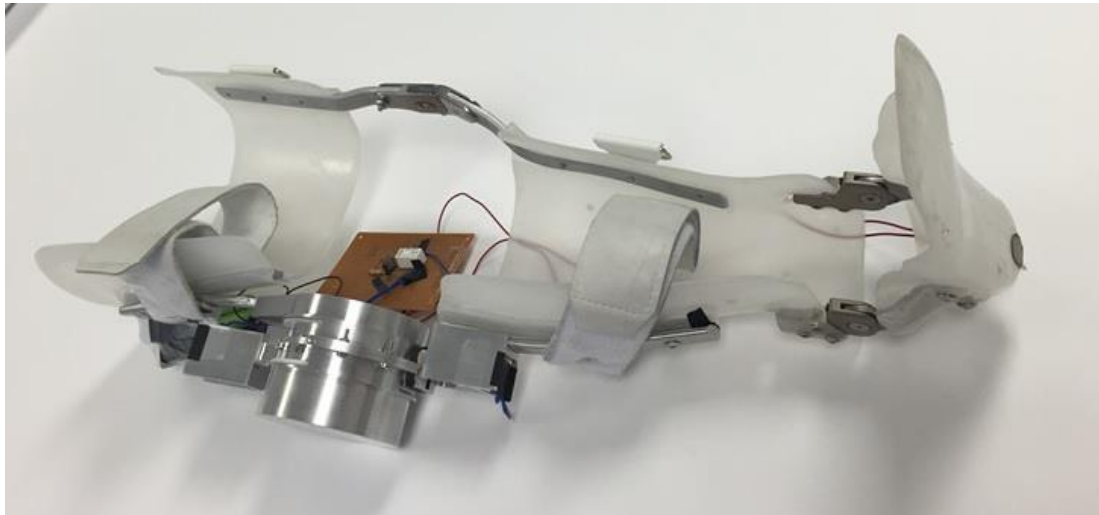


Figure 4-23. The UT Dynamic KAFO Prototype with the Knee Module, the Control System, the Foot Switch, and the 12VDC Battery.

4.5 Summary

The dynamic knee module was proposed and described in this chapter. The knee module had three distinct working modes: free mode, locked mode, and dynamic mode. A microcontroller switched between these three modes to make the device meet various requirements from different KAFO users. A preliminary prototype of the dynamic knee module was fabricated by additive manufacturing technology to verify the concept. Then, a final prototype was made by traditional manufacturing and the device was ready for motion analysis tests.

Chapter 5

Results

5.1 Hypothesis of the Motion Analysis Tests

To evaluate the applicability of the UT dynamic KAFO, motion analysis tests were conducted on a healthy subject in three different walking conditions: walking without the KAFO, walking with the UT dynamic KAFO in the locked mode, and walking with the UT dynamic KAFO in the dynamic mode. Several hypotheses were proposed before the tests, and are listed as follows.

(1) Walking without the KAFO and walking with the UT dynamic KAFO in the locked mode will show significantly different gait patterns.

(2) Walking with the UT dynamic KAFO in the locked mode will cause a rigid, asymmetric gait pattern as well as some compensation motions such as hip hiking and leg circumduction on the orthotic side.

(3) Walking with the UT dynamic KAFO in the dynamic mode will allow knee flexion and assist with knee extension throughout the gait cycle, producing a gait pattern that is close to normal.

(4) Walking with the UT dynamic KAFO in the dynamic mode will improve the

gait abnormalities caused by the locked mode and relieve the related compensation motions, generating a symmetric walking pattern.

5.2 Experimental Setup and Procedure of the Motion Analysis Tests

One healthy subject (female, age 29, weight 102 lbs) was involved in this research, with the intention of wearing the UT dynamic KAFO on the right leg. The subject has no neuromuscular issues that in any way will impair normal walking. The study was approved by the University of Toledo Biomedical IRB (Institutional Review Board, IRB #200204) and the subject signed the approved consent form before completing the motion tests.

The motion tests were conducted under three different conditions: a) walking without the KAFO; b) walking with the UT dynamic KAFO in the locked mode; (c) walking with the UT dynamic KAFO in the dynamic mode. They will be referred as slow walking, locked mode, and dynamic mode in the following discussion. It is worth noting that in the locked mode the dynamic KAFO behaves similarly to that of a passive KAFO device. The difference is that the UT dynamic KAFO is heavier than a typical passive device by approximately 2.5 lb. A consistent walked speed (0.2 m/s) was established for each condition along a 6m walkway. This allowed us to compare the testing results between the three cases and avoid extra influences from different walking speeds. For each of the three conditions, data for five trials was collected and the five trails were averaged to produce a data set reflective of each of the three conditions.

For the testing, reflective markers were placed on the subject to identify relevant

anatomical landmarks on the lower limb segments. The Helen Hayes marker set was used to define the specific marker locations for the motion analysis tests [119]. This included 21 markers in all, each with a diameter of 13 mm. When testing without the KAFO, all markers were applied directly on both limbs, as shown in figure 5-2. When testing with the UT dynamic KAFO, the markers on the limb with the orthosis were attached to the orthosis (on the orthotic leg) and to the skin (on the contralateral leg), as shown in figure 5-3. On the orthotic leg, the markers were placed on the fifth metatarsal, the heel of the foot part of the KAFO, the medial and lateral sides of the knee and ankle joints of the KAFO, and the lateral brackets of the shank and thigh segments of the KAFO. On the contralateral leg, markers were placed on the fifth metatarsal, the heel, the medial and lateral malleolus (ankle), the medial and lateral epicondyle of the thigh (knee), and on the lateral sides of the shank and thigh segments. Markers were also placed on the left and right great trochanter, left and right anterior superior iliac spines, and on the middle of the two posterior superior iliac spines. In addition, two wireless EMG sensors were placed on the belly of the rectus femoris of both legs to detect quadriceps muscle activity.



Figure 5-1. The Marker Setup and EMG Sensors When Walking without the KAFO.

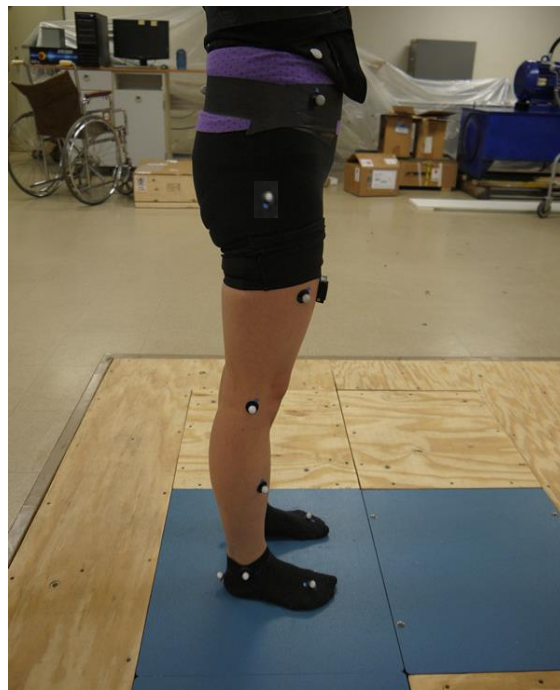


Figure 5-2. The Marker Setup and EMG Sensors When Walking without the KAFO.



Figure 5-3. The Marker Setup and EMG Sensors When Testing with the UT Dynamic KAFO.

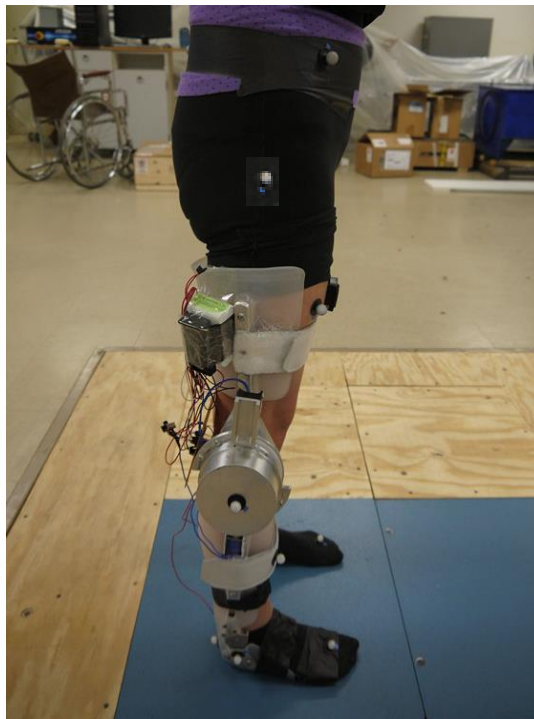


Figure 5-4. The Marker Setup and EMG Sensors When Testing with the UT Dynamic KAFO.

The motion tests were conducted in the Biomechanics and Assistive Technology Laboratory of the College of Engineering at the University of Toledo. The experimental setup included a calibrated ten-camera Raptor-E digital real-time analysis system (Motion Analysis, Inc., California, USA), two Optima 464508-200 Force Plates (Advanced Mechanical Technology, Inc., Massachusetts, USA), and a Trigno™ Wireless Electromyography (EMG) System (Delsys Inc., Massachusetts, USA). The sampling rates for the three systems were 120 Hz for the video, 720 Hz for the force plates, and 720 Hz for the EMG respectively.

Camera calibration had been completed before the motion testing was initiated. Firstly, an L-frame with four reflective markers was placed at the corner of one of the two force plates, to establish a global coordinate that included both the video data and the force platform data. This was then followed by a wand calibration to expand the entire capture volume (7.35m*2.8m*2m). Several warm-up walks were completed by the subject before the tests so that the subject could get familiar with the UT dynamic KAFO, finding a proper starting position to achieve good strike on the two force plates, and establishing a comfortable walking speed. During all of the actual data collection trials, 3D position data of all the markers was collected by the camera system, also synchronized muscle activation data from the EMG sensors and ground reaction force data from the force plates was collected. During post-processing of these data, a 6Hz low pass Butterworth filter was used to smooth all the data. Post processing was conducted using the Cortex® software, which included calculating the kinematic and kinetic characteristics of the subject's lower extremities (hip, knee, and ankle) in all testing conditions. Paired t-tests ($p < 0.05$) among different trials were used to determine the

significance of the difference in selected gait characteristics between walking without the KAFO and walking with the UT dynamic KAFO. All the experimental results are reported in section 5.3.

5.3 Experimental Results of the Motion Analysis Tests

Experimental results of the motion analysis tests were classified into three sections: (1) spatiotemporal parameters, (2) kinematic characteristics, and (3) kinetic characteristics. Spatiotemporal parameters were calculated for both legs, including the step length, stride length, cadence, single limb support, double limb support, and stance phase percentage. The kinematic characteristics of the orthotic leg that were measured included the ankle angle in the sagittal plane, the knee angle in the sagittal plane, the hip angle in the sagittal and frontal planes, and the pelvic obliquity. The kinetic characteristics of the orthotic leg that were measured included the knee moment pattern and the knee stiffness profile. When calculating these parameters and joint profiles, the average was taken from the five trials for each case.

5.3.1 Spatiotemporal Parameters

Step length

In slow walking, a symmetric step length was expected between the two legs. While walking in the locked mode and in the dynamic mode, significant differences were shown ($p=0.0005$ and $p<0.0001$, respectively) between the two legs. Also significant step

length differences existed between the slow walking and the locked mode (p=0.0254 on the right side and p=0.0109 on the left side), and between the slow walking and the dynamic mode (p=0.0093 on the right side and p=0.0471 on the left side). These results are summarized in table 5-1 and figure 5-5.

Table 5-1. Average Step Length with One Standard Deviation in the Three Testing Conditions. The Right and Left Sides Represent the Orthotic and Sound Legs, Respectively.

	Average step length \pm 1SD on the right side (m) (percentage difference from the base line)	Average step length \pm 1SD on the left side (m) (percentage difference from the base line)
Slow walking	0.33 \pm 0.01 (base line)	0.25 \pm 0.01 (base line)
The UT dynamic KAFO (locked mode)	0.35 \pm 0.01 (7.51% more)	0.21 \pm 0.01 (16.52% less)
The UT dynamic KAFO (dynamic mode)	0.36 \pm 0.02 (10.28% more)	0.24 \pm 0.01 (6.18% less)

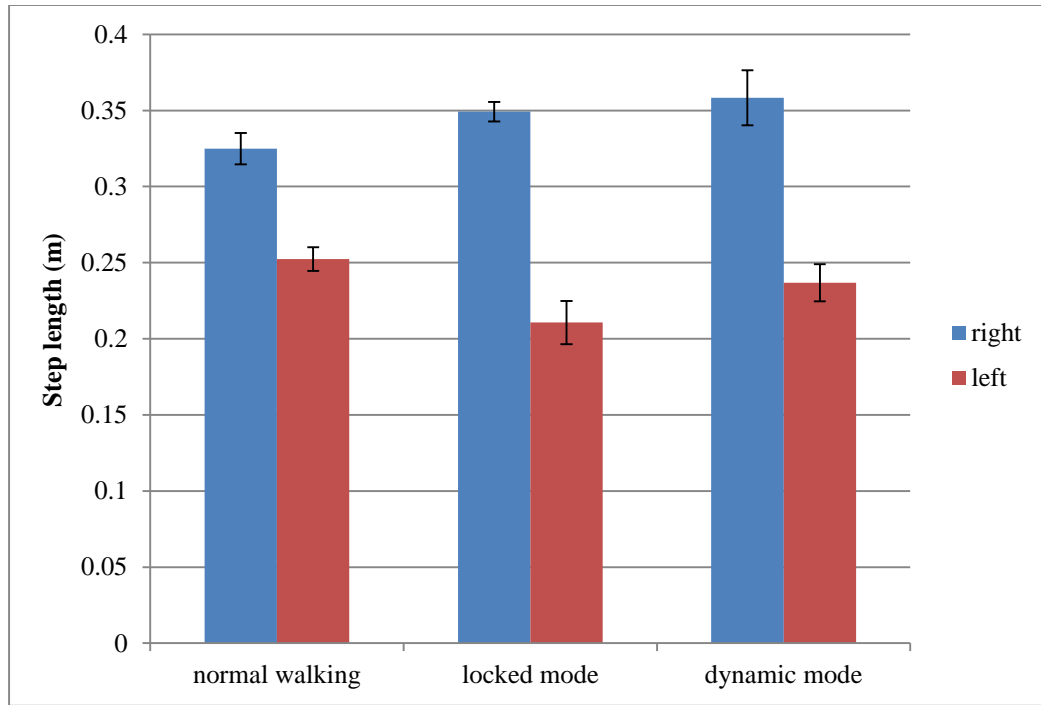


Figure 5-5. Average Step Length with One Standard Deviation in the Three Testing Conditions. The Right and Left Sides Represent the Orthotic and Sound Legs, Respectively.

Stride length

In the locked mode, a symmetric stride length was observed between the two legs. When comparing the slow walking and the dynamic walking conditions, significant differences were shown between the two sides ($p=0.0208$ and $p=0.0210$, respectively). No significant stride length differences were observed between the slow walking and the locked mode, and between the slow walking and the dynamic mode on either side. The results are summarized in table 5-2 and figure 5-6.

Table 5-2. Average Stride Length with One Standard Deviation in the Three Testing Conditions. The Right and Left Sides Represent the Orthotic and Sound Legs, Respectively.

	Average stride length\pm1SD on the right side (m) (percentage difference from the base line)	Average stride length\pm1SD on the left side (m) (percentage difference from the base line)
Slow walking	0.57 \pm 0.02 (base line)	0.62 \pm 0.01 (base line)
The UT dynamic KAFO (locked mode)	0.55 \pm 0.03 (3.21% less)	0.59 \pm 0.02 (6.01% less)
The UT dynamic KAFO (dynamic mode)	0.59 \pm 0.03 (4.10% more)	0.65 \pm 0.05 (4.24% more)

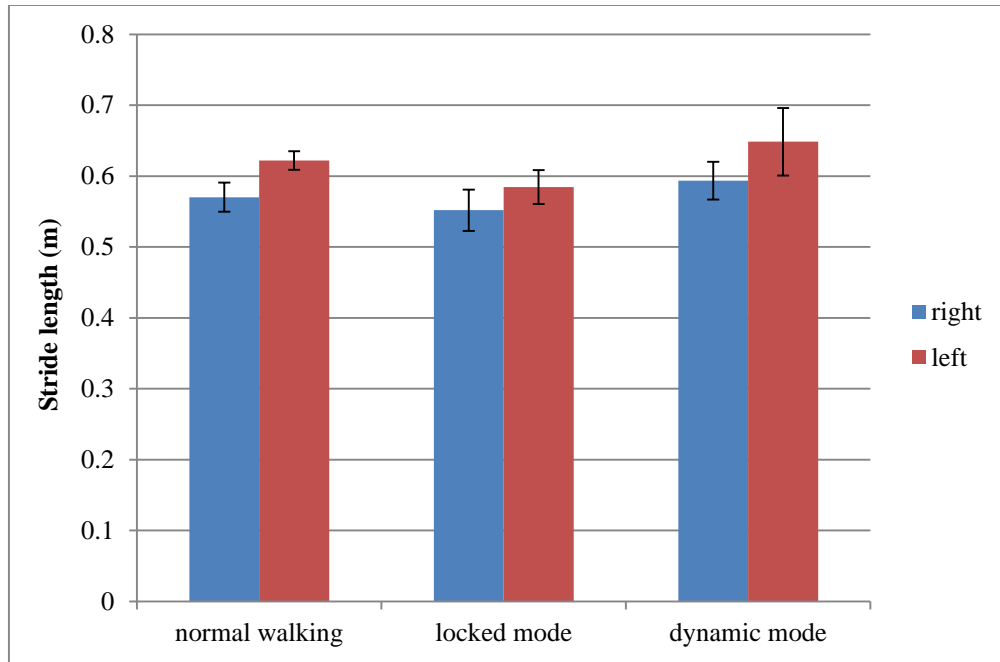


Figure 5-6. Average Stride Length with One Standard Deviation in the Three Testing Conditions. The Right and Left Sides Represent the Orthotic and Sound Legs, Respectively.

Cadence (steps per minute)

In slow walking, symmetry of cadences was observed between the two legs. When walking in the locked mode and in the dynamic mode, significant differences were present ($p < 0.0001$ and $p = 0.0005$, respectively). Also there were significant cadence differences between the slow walking condition and the locked mode condition ($p = 0.0113$ on the right side and $p = 0.0005$ on the left side), and between the slow walking mode and the dynamic mode ($p = 0.0363$ on the right side and $p = 0.0156$ on the left side). These results are summarized in table 5-3 and figure 5-7.

Table 5-3. Average Cadence with One Standard Deviation in the Three Testing Conditions. The Right and Left Sides Represent the Orthotic and Sound Legs, Respectively.

	Average cadence\pm1SD on the right side (step/min) (percentage difference from the base line)	Average cadence\pm1SD on the left side (step/min) (percentage difference from the base line)
Slow walking	127.3 \pm 8.7 (base line)	136 \pm 5.2 (base line)
The UT dynamic KAFO (locked mode)	160.2 \pm 9.4 (25.79% more)	101.7 \pm 2.1 (25.25% less)
The UT dynamic KAFO (dynamic mode)	149.4 \pm 9.6 (17.30% more)	121.5 \pm 8.6 (10.66% less)

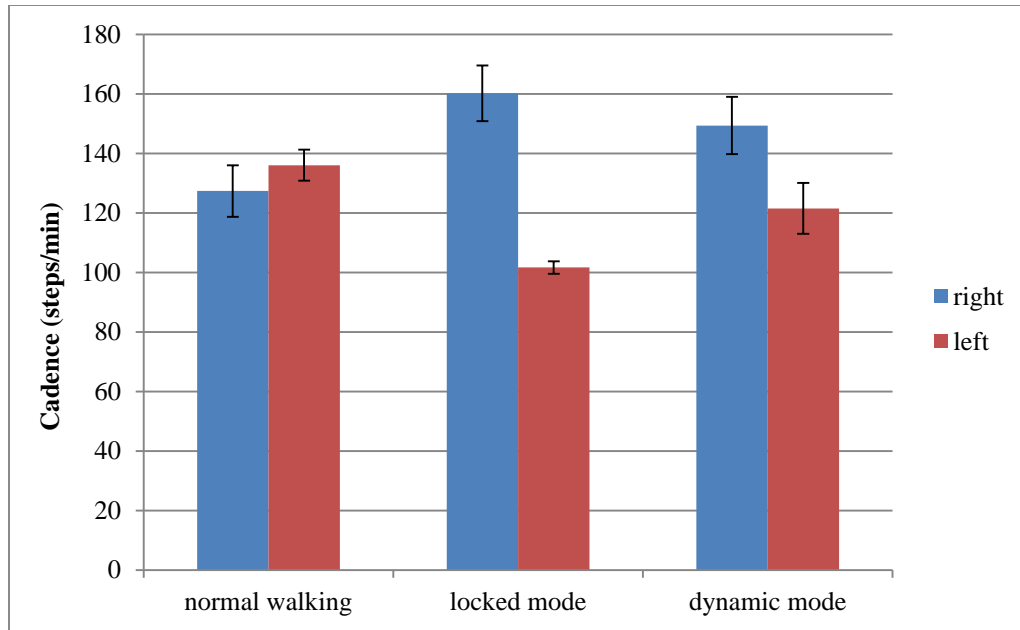


Figure 5-7. Average Cadence with One Standard Deviation in the Three Testing Conditions. The Right and Left Sides Represent the Orthotic and Sound Legs, Respectively.

Percentage of stance phase

In the slow walking condition, the duration of the stance phase on both sides was symmetric and occupied about 79% of gait cycle, due to the relatively slow walking speed. When walking in the locked mode and in the dynamic mode, significant differences were shown between the right and left legs ($p < 0.0001$ in both cases). Also significant differences in the stance period could be observed between the slow walking and the locked mode ($p < 0.0001$ on the right side and $p = 0.0013$ on the left side), and between the slow walking and the dynamic mode ($p = 0.0002$ on the right side and $p = 0.0043$ on the left side). The results are summarized in table 5-4 and figure 5-8.

Table 5-4. Stance Phase Percentage with One Standard Deviation in the Three Testing Conditions. The Right and Left Represent the Orthotic and Sound Legs, Respectively.

	Stance percentage\pm1SD on the right side (%) (percentage difference from the base line)	Stance percentage\pm1SD on the left side (%) (percentage difference from the base line)
Slow walking	79.5 \pm 0.7 (base line)	78.5 \pm 1.3 (base line)
The UT dynamic KAFO (locked mode)	57.4 \pm 1.3 (27.90% less)	84.7 \pm 0.5 (7.92% more)
The UT dynamic KAFO (dynamic mode)	66.2 \pm 1.9 (16.80% less)	84.3 \pm 1.6 (7.33% more)

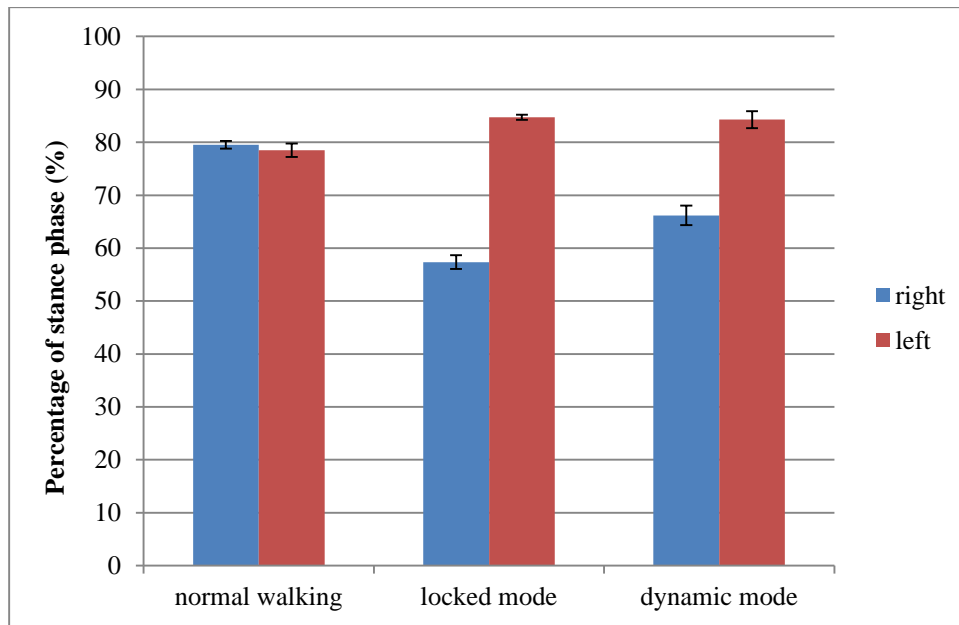


Figure 5-8. Average Stance Phase Percentage with One Standard Deviation in the Three Testing Conditions. The Right and Left Represent the Orthotic and Sound Legs, Respectively.

Double limb support (DLS)

Double limb support (DLS) in the gait cycle indicates when both legs are in contact with the ground. In slow walking, there are two DLS periods over the stance phase and each takes about 10-11% of the gait cycle. Due to the low walking speed in this study, the slow walking condition had about 26.8% of the gait cycle in DLS on the orthotic side. When walking in the locked mode and in the dynamic mode conditions, double limb support decreased to around 19.2% and 22.0% on the orthotic side, respectively. On the left side, the slow walking condition had 27.9% DLS, and the locked and the dynamic modes had 19.5% and 22.9% DLS, respectively. Significant differences were observed between the slow walking and the locked mode conditions ($p=0.0240$ on the right side and $p=0.0179$ on the left side), and between the slow walking and the dynamic mode conditions ($p=0.0011$ on the right side and $p=0.0040$ on the left side). These results are summarized in table 5-5 and figure 5-9.

Table 5-5. Average of Double Limb Support with One Standard Deviation in the Three Testing Conditions. The Right and Left Sides Represent the Orthotic and Sound Legs, Respectively.

	DLS±1SD on the right side (%) (percentage difference from the base line)	DLS±1SD on the left side (%) (percentage difference from the base line)
Slow walking	26.8 ± 0.6 (base line)	27.9 ± 1.6 (base line)
The UT dynamic KAFO (locked mode)	19.2 ± 3.7 (28.39% less)	19.6 ± 3.4 (29.88% less)
The UT dynamic KAFO (dynamic mode)	22.0 ± 2.2 (17.83% less)	22.9 ± 2.8 (17.72% less)

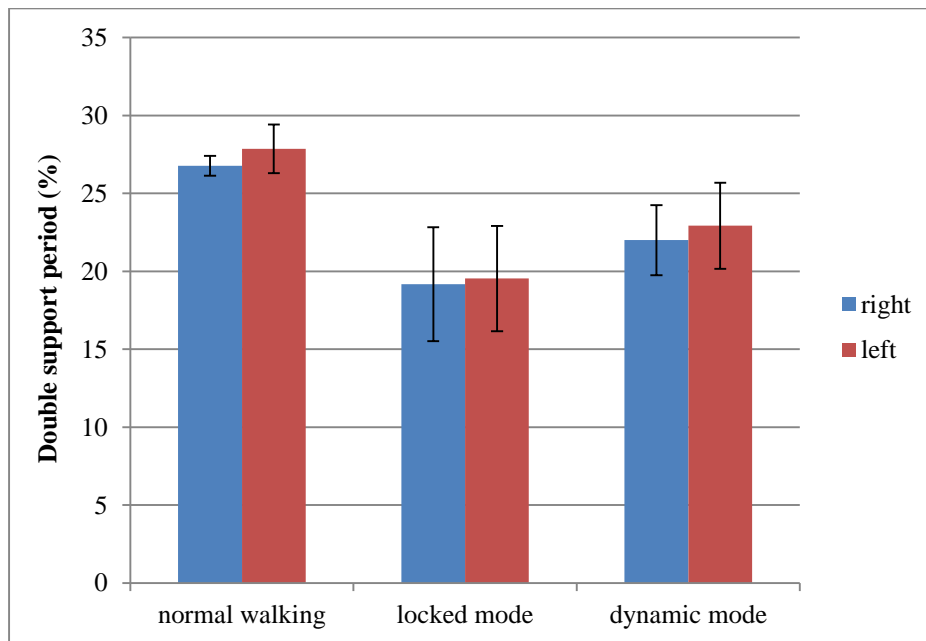


Figure 5-9. Average Double Limb Support with One Standard Deviation for the Orthotic Leg in the Three Testing Conditions.

Single limb support (SLS)

Single limb support (SLS) in the gait period is when only one leg is in contact with the ground. In the slow walking condition, SLS took about 51.7% of the gait cycle on the orthotic side. When walking in the locked mode and in the dynamic mode, single limb support on the orthotic side decreased to around 39.0% and 44.0%, respectively. On the left side, the slow walking had about 50.6% SLS, and the locked and the dynamic modes had 64.2% and 61.0% SLS, respectively. Significant differences were observed between the slow walking and the locked mode ($p=0.0009$ on the right side and $p=0.0015$ on the left side), and between the slow walking and the dynamic mode ($p=0.0012$ on the right side and $p=0.0014$ on the left side). The results are listed in table 5-6 and figure 5-10.

Table 5-6. Single Limb Support with One Standard Deviation in the Three Testing Conditions. The Right and Left Represent the Orthotic and Sound Legs, Respectively.

	SLS±1SD on the right side (%) (percentage difference from the base line)	SLS±1SD on the left side (%) (percentage difference from the base line)
Slow walking	51.7 ± 1.7 (base line)	50.6 ± 0.5 (base line)
The UT dynamic KAFO (locked mode)	39.0 ± 1.8 (24.57% less)	64.2 ± 3.0 (21.16% more)
The UT dynamic KAFO (dynamic mode)	44.0 ± 2.2 (14.89% less)	61.0 ± 3.6 (20.61% more)

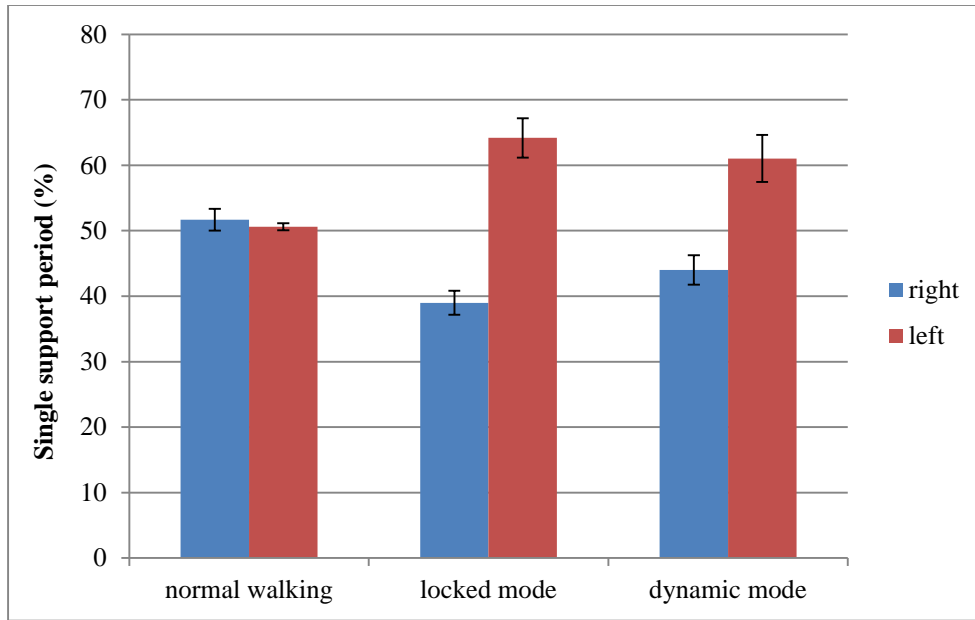


Figure 5-10. Average Single Limb Support with One Standard Deviation in the Three Testing Conditions. The Right and Left Sides Represent the Orthotic and Sound Legs, Respectively.

5.3.2 Kinematic Characteristics

Knee angle profiles in the sagittal plane

The knee angle profiles on the right leg were calculated and the results are shown in figure 5-11. There are three graphs included in this figure. The red one shows knee motion for the slow walking. The green and blue graphs represent walking with the UT dynamic KAFO in the locked mode and the dynamic mode, respectively. In slow walking, the knee angle pattern showed two peaks over the gait cycle. The subject reached about 9 degrees of flexion during the stance phase and about 52 degrees during the swing phase. When walking in the locked mode, the knee angle was around zero

because the knee was fixed in the full extension position. The locked mode therefore generated a walking gait pattern that was different from the slow walking condition. When walking in the dynamic mode, the knee angle pattern was closer to that of the slow walking condition. The maximum knee flexion angle during the stance phase was about 6 degrees, and that during the swing phase was about 42 degrees, which represented a 33% and 20% reduction compared to those in the slow walking condition, respectively. Maximum knee angles on the orthotic leg during the stance and swing phases were recorded and the average was taken for the five trials in each case. In the stance phase, significant differences were shown between the right and left legs for the three testing conditions ($p=0.0462$ for the slow walking, $p=0.0002$ for the locked mode, and $p=0.0213$ for the dynamic mode). In the swing phase, symmetry was observed for the slow walking condition. However, significant differences existed for the locked mode and the dynamic mode ($p=0.0001$ and $p=0.0019$, respectively). The results are listed in tables 5-7 and 5-8, and figures 5-12 and 5-13.

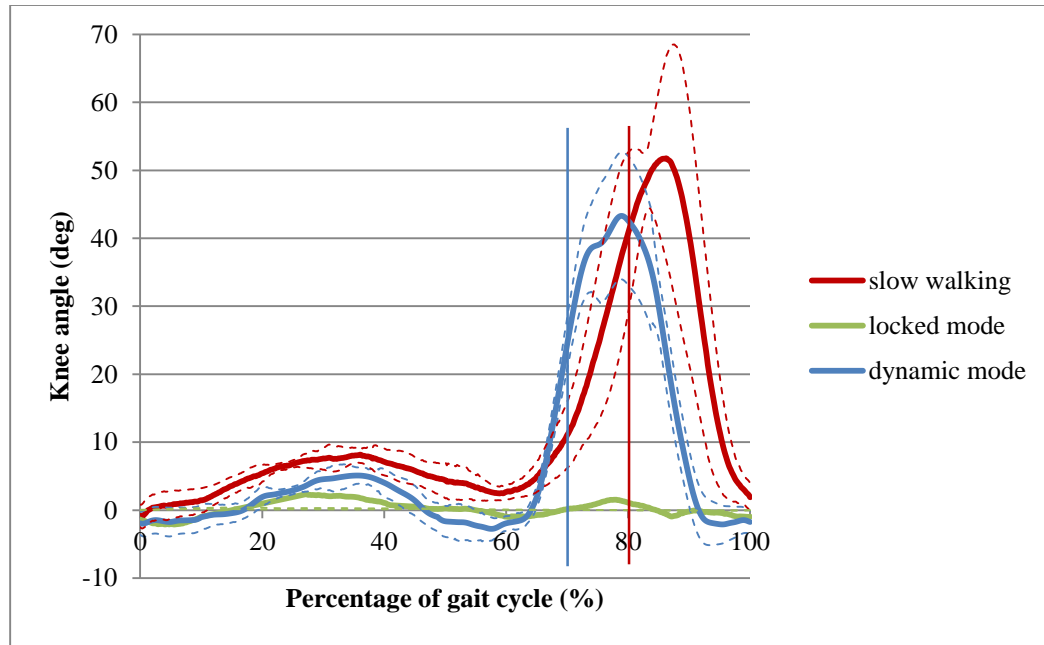


Figure 5-11. Knee Angle Change over the Entire Gait Cycle with One Standard Deviation in the Three Testing Conditions. The Red and Blue Solid Lines Represent the End of Stance Phase for the Slow Walking and the Dynamic Walking, Respectively.

Table 5-7. Maximum Knee Flexion Angle during the Stance Phase in the Three Testing Conditions. The Right and Left Represent the Orthotic and Sound Legs, Respectively.

	Max knee angle\pm1SD on the right side (%) (percentage difference from the base line)	Max knee angle\pm1SD on the left side (%) (percentage difference from the base line)
Slow walking	9.3 \pm 0.4 (base line)	7.1 \pm 1.3 (base line)
The UT dynamic KAFO (locked mode)	2.2 \pm 0.3 (76.38% less)	6.3 \pm 0.4 (10.72% less)
The UT dynamic KAFO (dynamic mode)	6.1 \pm 0.5 (34.68% less)	8.3 \pm 1.0 (17.05% more)

Table 5-8. Maximum Knee Flexion Angle during the Swing Phase in the Three Testing Conditions. The Right and Left Represent the Orthotic and Sound Legs, Respectively.

	Max knee angle\pm1SD on the right side (%) (percentage difference from the base line)	Max knee angle\pm1SD on the left side (%) (percentage difference from the base line)
Slow walking	60.6 \pm 1.9 (base line)	58.9 \pm 1.8 (base line)
The UT dynamic KAFO (locked mode)	2.2 \pm 0.3 (96.36% less)	42.3 \pm 4.6 (28.25% less)
The UT dynamic KAFO (dynamic mode)	41.0 \pm 4.3 (32.26% less)	47.6 \pm 2.7 (19.25% less)

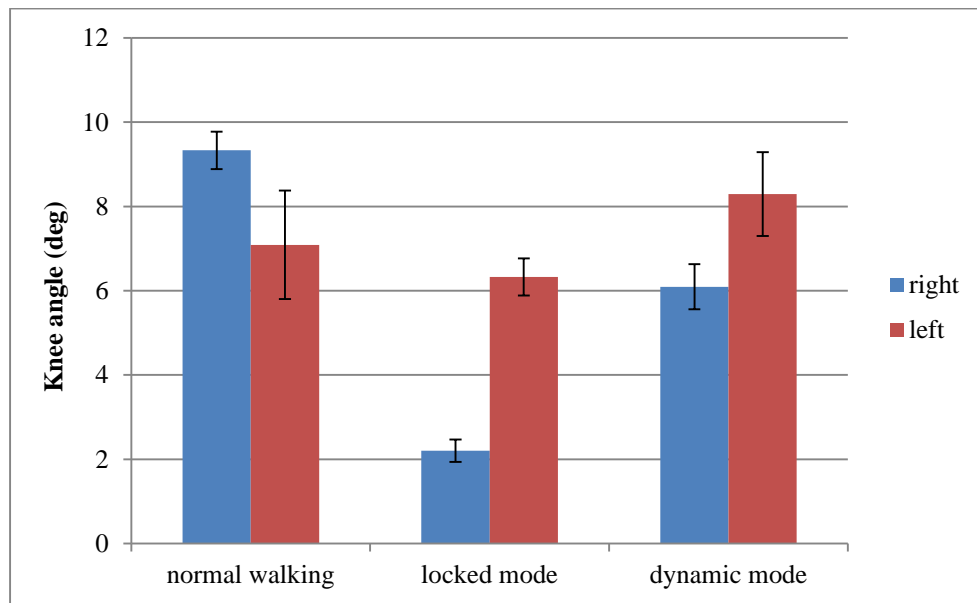


Figure 5-12. Maximum Knee Stance Flexion Angles with One Standard Deviation in the Three Testing Conditions. The Right and Left Sides Represent the Orthotic and Sound Legs, Respectively.

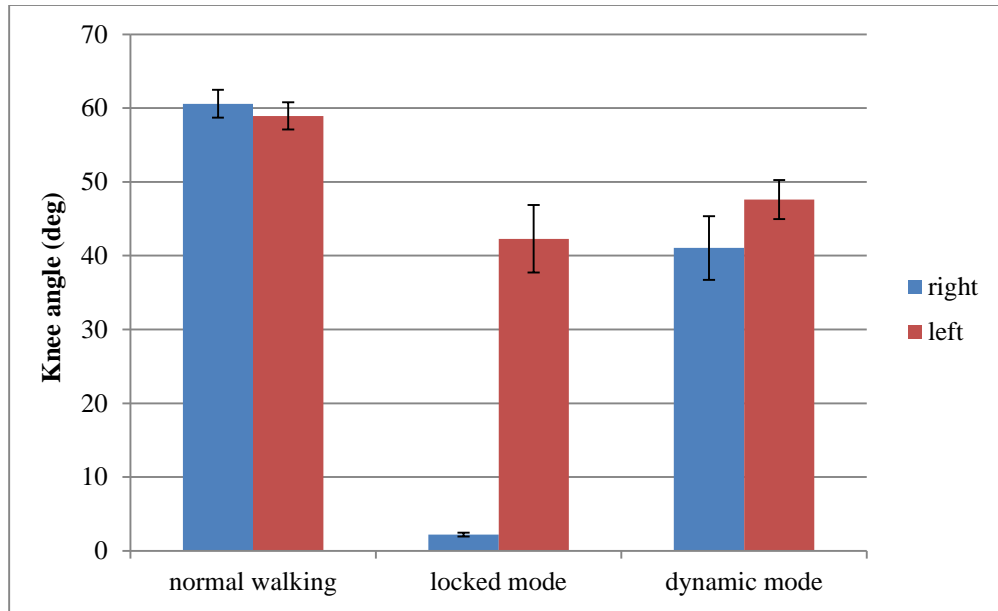


Figure 5-13. Maximum Knee Swing Flexion Angles with One Standard Deviation in the Three Testing Conditions. The Right and Left Sides Represent the Orthotic and Sound Legs, Respectively.

Ankle angle profiles in the sagittal plane

The UT dynamic KAFO supports the ankle while allowing for free motions of the joint in the sagittal plane. The ankle angle profiles for the right leg were calculated and the results are shown in figure 5-14. There are three graphs included in this figure. The red one shows ankle motion for the slow walking condition without wearing the KAFO. The green and blue graphs represent walking with the UT dynamic KAFO in the locked mode and in the dynamic mode, respectively. In the slow walking, the ankle plantarflexed to about 7 degrees in the loading response and then reached about 8 degrees of dorsiflexion in late stance. The maximum plantarflexion (about 20 degrees) occurred right after toe off. When walking in the locked mode, for almost the whole curve the

ankle was in the dorsiflexion region. The maximum dorsiflexion angle in late stance was about 16 degrees (100% more than that in slow walking). Then the dorsiflexion angle decreased gradually during the swing phase. When walking in the dynamic mode, an ankle profile similar to that of the slow condition was observed, but with less plantar flexion (about 5 degrees which is 75% less than that in the healthy walking) at the push off and more dorsiflexion during the mid-stance and the swing phases (about 12 degrees and 10 degrees, respectively, which is 50% and 100% higher than those in the healthy walking).

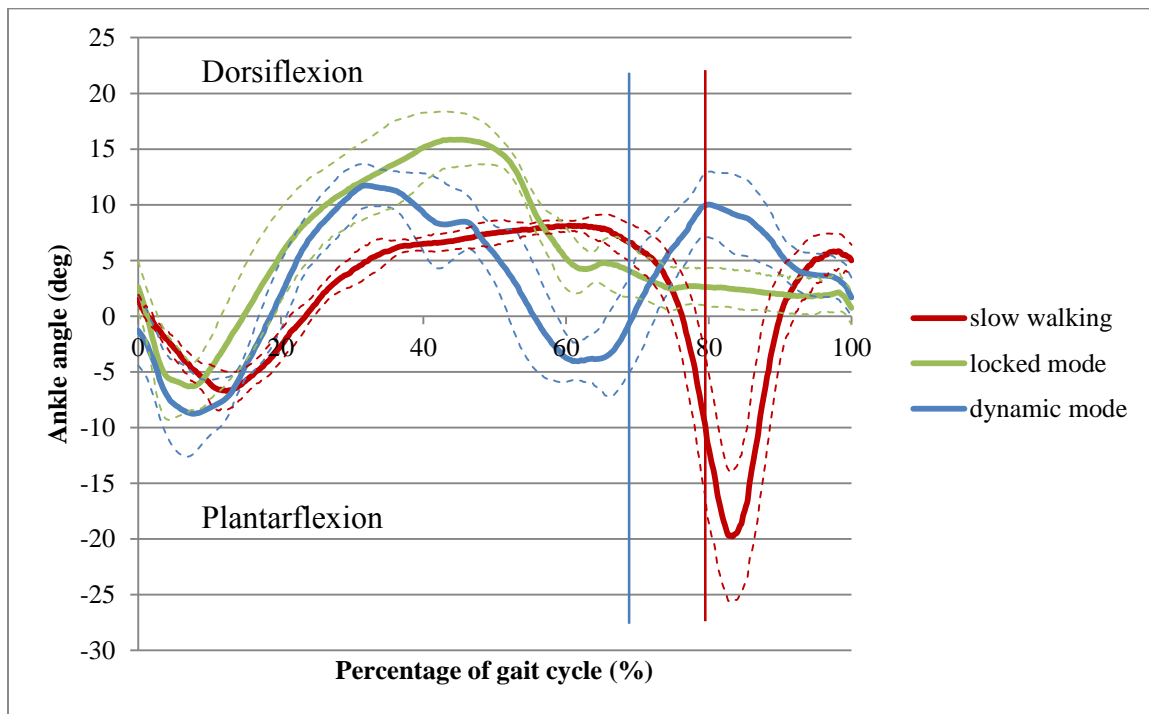


Figure 5-14. Ankle Angle Change over the Entire Gait Cycle with One Standard Deviation in the Three Testing Conditions. The Red and Blue Solid Lines Represent the End of Stance Phase for the Slow Walking and the Dynamic Walking, Respectively.

Hip angle profiles in the sagittal and frontal planes

Hip motions were also studied in this research since motion of both the ankle and the knee affects hip joint behavior. When using the locked KAFO, some compensatory motions were involved at the hip, such as circumduction, in order to clear the foot during swing. Analyzing hip profiles in the frontal plane could help us understand this issue by determining the potential improvements brought about by the UT dynamic KAFO. The changes of hip range of motion in both the sagittal and frontal planes are presented in figures 5-15 and 5-16, respectively. There are three graphs included in each figure. The red one shows hip motion for the slow walking condition. The green and blue graphs represent walking in the locked mode and the dynamic mode, respectively.

In the sagittal plane, the hip movements are described as hip flexion and extension. In the slow walking condition, the hip started from about 20 degrees of flexion and moved to approximately 3 degrees of extension near 50% of the gait cycle. Then the leg moved forward, up to 27 degrees of hip flexion in mid-swing. At the end of the gait cycle, the hip slightly extended in order to allow for the proper positioning of the foot for the next foot strike. The hip angle patterns are very similar among the three testing conditions, although the curves are shifted substantially. When walking in the locked mode, the hip started from 10 degrees of flexion (50% less than that in the slow walking condition), reached about 5 degrees of extension (66% higher than that in the slow walking condition) in mid-stance and 17 degrees of flexion (37% less than that in the slow walking condition) before the next heel strike. When walking in the dynamic mode, the hip started from 15 degrees of flexion (25% less than that in the slow walking condition), reached about 7 degrees of extension (133% higher than that in the slow

walking condition) in the late stance and 22 degrees of flexion (19% less than that in the slow walking condition) before the next heel strike as shown in figure 5-15.

In the frontal plane, the hip motions that occur are described as abduction and adduction. Circumduction, which reflects a combination of all four hip joint motions, can be evaluated using the hip angle graphs [120]. The results are illustrated in figure 5-16. In the slow walking condition, the right leg stayed in adduction throughout the whole gait cycle. And the maximum hip adduction angle was around 10 degrees and occurred in late stance. However, in the locked and dynamic walking conditions, the orthotic leg remained in an abducted position. When using the KAFO, the orthotic leg tended to move laterally in order to avoid the conflict between the orthosis and the sound leg in the medial side. Especially in the swing phase of the locked mode, the orthotic leg showed a semicircular motion curve.

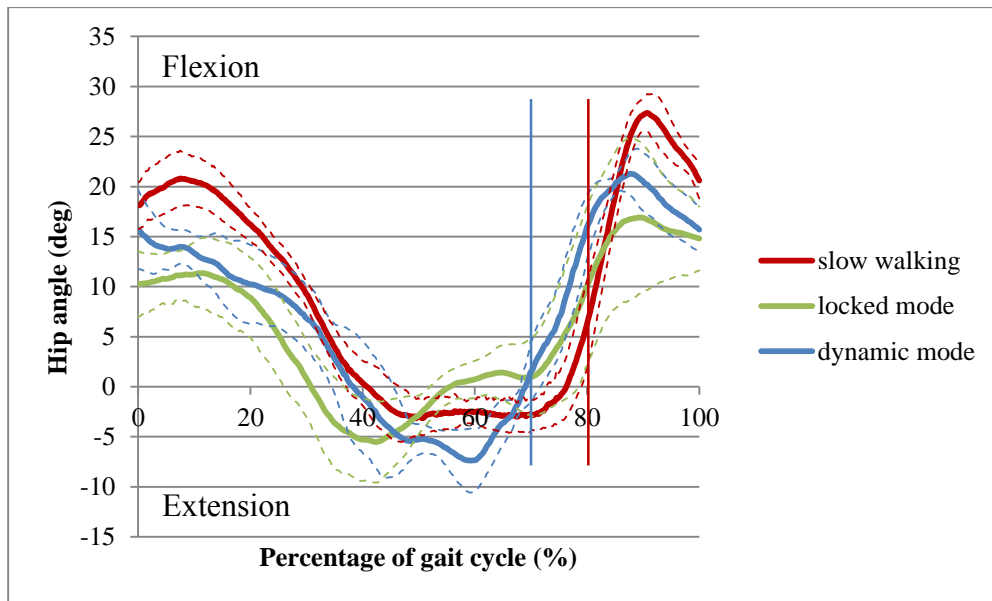


Figure 5-15. Sagittal Hip Angle Change over the Entire Gait Cycle with One Standard Deviation in the Three Walking Conditions. The Red and Blue Solid Lines Represent the End of Stance Phase for the Slow Walking and the Dynamic Walking, Respectively.

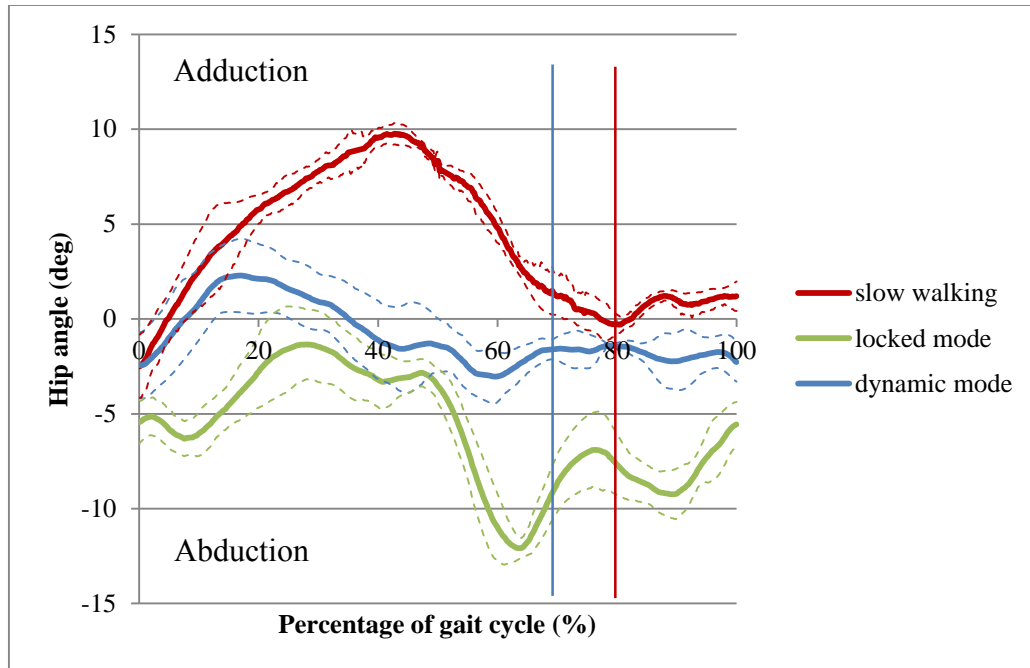


Figure 5-16. Frontal Hip Angle Change over the Entire Gait Cycle with One Standard Deviation in the Three Testing Conditions. The Red and Blue Solid Lines Represent the End of Stance Phase for the Slow Walking and the Dynamic Walking, Respectively.

Pelvic obliquity in the frontal plane

Hip hiking is another common compensation motion associated with conventional KAFOs. The patients elevate their pelvis on the orthotic side to clear the leg off the ground [121]. Pelvic obliquity is the parameter used to determine hip hiking. Pelvic obliquity shows pelvic rotation in the frontal plane, which is the angle between the line of the two ASIS markers and the transverse plane. The angle is zero when the two ASIS markers are on the same level. And positive angles represent the positions when the marker on the orthotic (right) side rises higher than that on the left side [122].

The pelvic obliquity profiles for the three testing conditions are illustrated in figure 5-17. There are three graphs included in each figure. The red one is for the slow

walking condition. The green and blue graphs represent walking with the UT dynamic KAFO in the locked mode and the dynamic mode, respectively. In the slow walking condition, the pelvis was almost neutral at the heel contact of the right leg. During the loading response of the right leg, the hip of the left leg started to rise, increasing the pelvic obliquity in the negative direction. After the toe off of the left leg, pelvic obliquity decreased gradually since the left leg swung forward. The left hip reached the neutral position at its heel contact. Then, the right hip was lifted, increasing the obliquity amount in the positive direction. Again after the toe off of the right leg, its hip returned back to the neutral position at the next heel strike to complete one gait cycle. The pelvic obliquity pattern was symmetric around the neutral position in the slow walking condition. The range of the pelvic obliquity was between -5 to 5 degrees, as shown in figure 5-17. When walking in the locked mode and the dynamic mode conditions, asymmetric pelvic obliquity patterns were generated. During the swing phase of the left leg, no significant hip hiking could be observed in the three walking conditions. The maximum pelvic obliquity angles were about 5 degrees, 5 degrees, and 7 degrees in the slow walking, dynamic walking, and locked knee walking, respectively. However, during the swing phase of the right leg, its hip hiking motions caused about 27 degrees and 12 degrees of pelvic obliquity in the locked mode and the dynamic mode, respectively, which is about 440% and 140% higher than that in the slow walking condition. Also, the right hip was about 5 degrees higher than the neutral position at heel strike in these two cases, and it was in the neutral position in the slow walking condition.

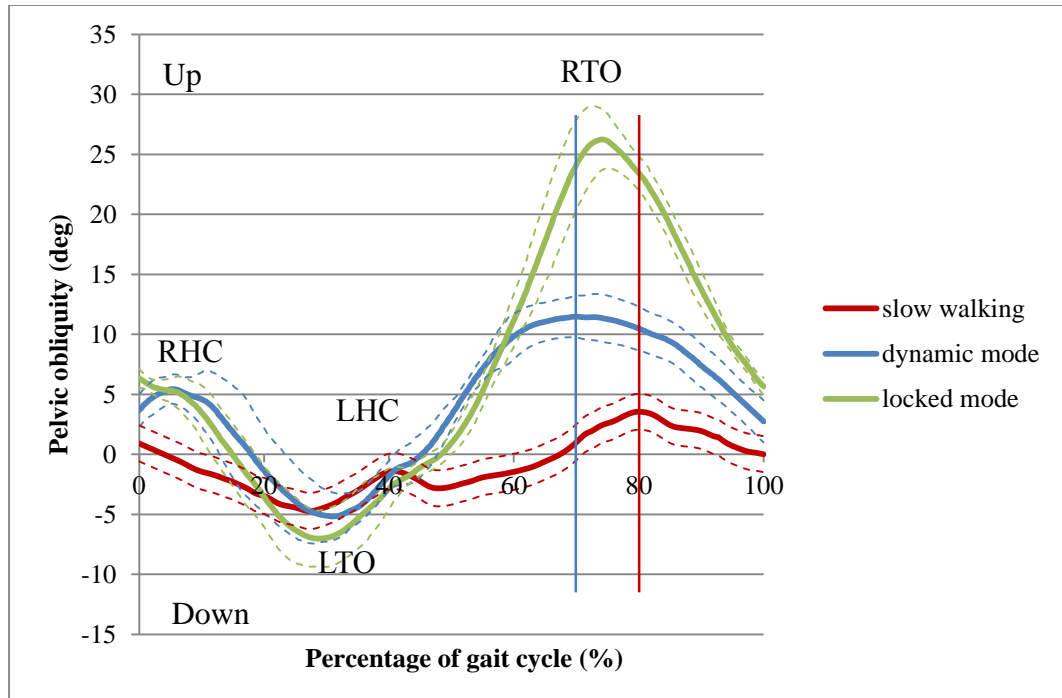


Figure 5-17. Pelvic Obliquity over the Entire Gait Cycle with One Standard Deviation in the Three Walking Conditions. The Red and Blue Solid Lines Represent the End of Stance Phase for the Slow Walking and the Dynamic Walking, Respectively.

5.3.3 Kinetic Characteristics

Knee moment profiles

Weight-normalized knee moment profiles for the three walking conditions are shown in figure 5-18 which includes three graphs. The knee moment which was calculated on the basis of the ground reaction forces and the dynamics of the limb segment motions, is an indicator of the muscle activity at the knee. The red graph shows the knee moment for the slow walking condition. The green and blue graphs represent walking with the UT dynamic KAFO in the locked mode and the dynamic mode,

respectively. In the slow walking condition, the graph shows an internal extension moment during the loading response and the mid-swing phases, and the maximum value during these two periods is about 0.4 Nm/kg and 0.1 Nm/kg, respectively. Walking in the locked mode generated a similar knee moment pattern but with less of an internal extension moments (about 0.3 Nm/kg which is 25% less than the healthy walking). During the stance phase, it appeared that the subject again tended to try to flex the knee on the orthotic side. However, the joint was locked and too stiff to be deformed. Walking in the dynamic mode reproduced the same profile over the gait cycle but with higher and stiffer moments (up to 0.5 Nm/kg and 0.3 Nm/kg which are 25% and 200% more than the slow walking, respectively). During the terminal stance phase, high flexion moments (up to 0.2 Nm/kg which is about 150% higher than that in slow walking) were created in the dynamic condition. It appeared that the subject tried to extend the knee joint in order to achieve the switching between the two actuating parts which was only allowed in the full extension position at the knee.

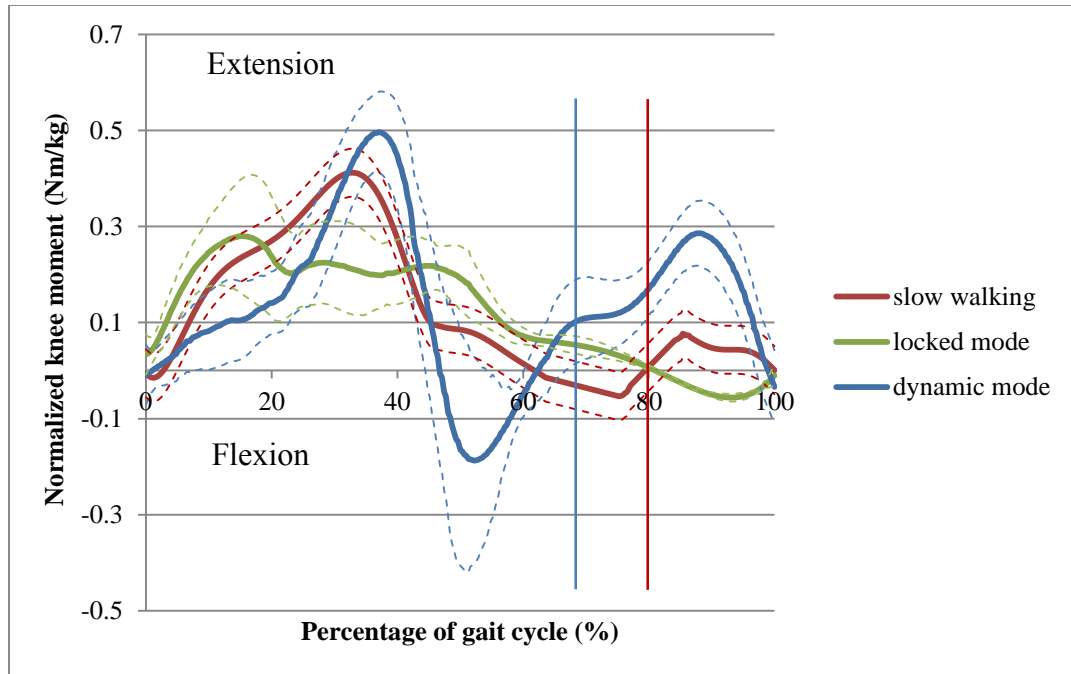


Figure 5-18. Knee Moment over the Entire Gait Cycle with One Standard Deviation in the Three Walking Conditions. The Red and Blue Solid Lines Represent the End of Stance Phase for the Slow Walking and the Dynamic Walking, Respectively.

Knee stiffness profiles

Knee stiffness profiles have been calculated based on the measured knee angle and moment data. The results for the three testing conditions are shown in figures 5-19 and 5-20, which compare the stiffness profiles between the slow walking and the locked mode, and between the slow walking and the dynamic mode, respectively. The red graph shows the slow walking mode. The green and blue graphs represent walking with the UT dynamic KAFO in the locked mode and the dynamic mode, respectively. The stiffness profiles consist of two distinct sections in both slow walking and dynamic walking. One section is stiffer and with less hysteretic behavior, representing the stance phase. The other is softer and with more hysteresis, representing the swing phase. In slow walking, a

0.4 Nm/kg internal extension moment was generated by about 9 degrees of flexion in the stance phase and a 0.1 Nm/kg extension moment was created by about 52 degrees of flexion in the swing phase. In the dynamic walking condition, 0.5 Nm/kg and 0.3 Nm/kg internal extension moments were generated via 6 and 42 degrees of rotation in the stance and swing phases, respectively. In the locked walking mode, knee stiffness was almost linear and the maximum extension moment was around 0.3 Nm/kg, showing a different profile from the other two cases. The results indicate that slow walking and walking in the dynamic mode have close stiffness profiles.

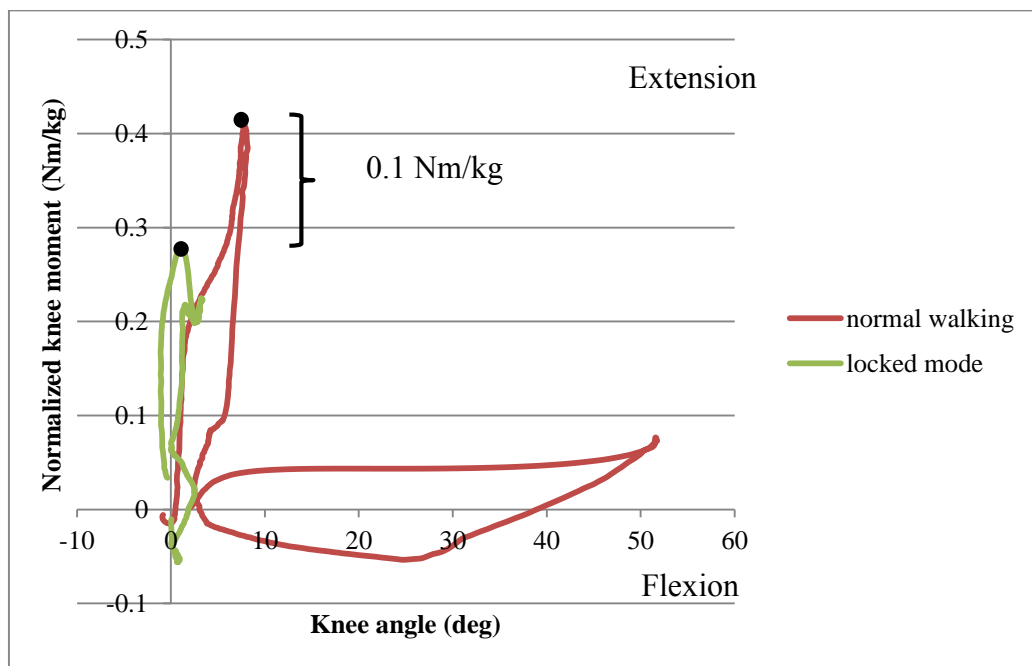


Figure 5-19. Comparison of the Knee Stiffness Profiles (Weight-Normalized Knee Moment vs. Knee Angle Change) in the Slow Walking and the Locked Mode.

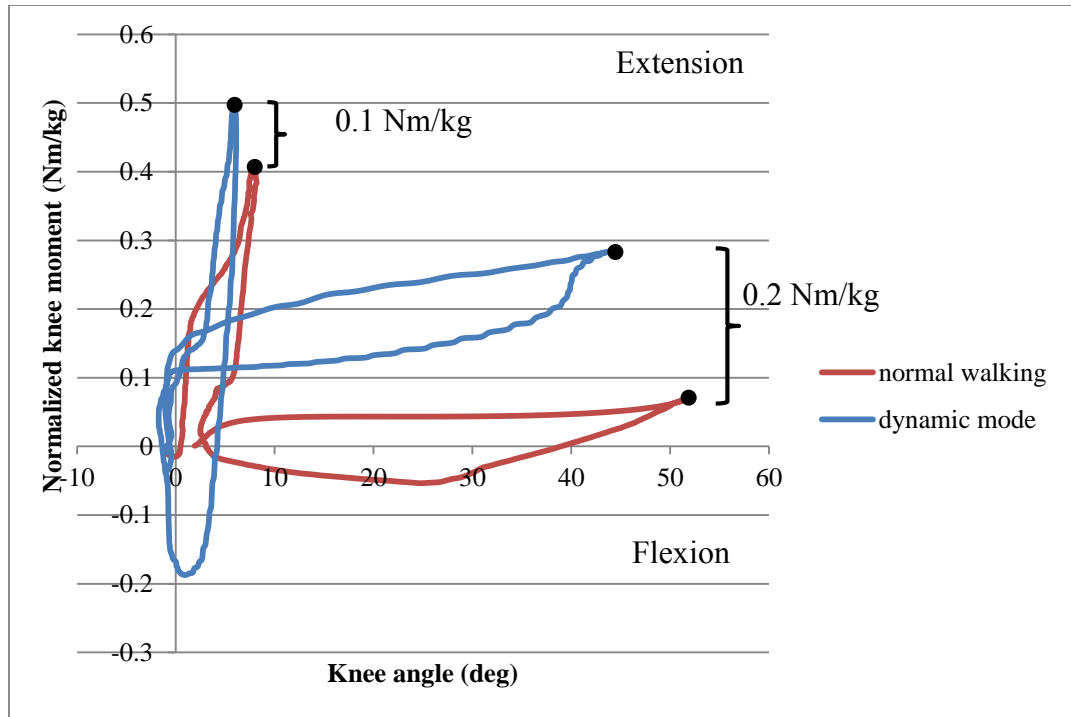


Figure 5-20. Comparison of the Knee Stiffness Profiles (Weight-Normalized Knee Moment vs. Knee Angle Change) in the Slow Walking and the Dynamic Mode.

5.4 Summary

Motion tests were conducted to evaluate the UT dynamic KAFO. Hypotheses had been proposed at the beginning of this chapter and then the experimental procedures that were followed. Testing results were also presented, comparing between the slow walking condition, walking in the locked mode, and walking in the dynamic mode. All of these results will be explained and discussed in the next chapter.

Chapter 6

Discussion

6.1 Discussion of the Spatiotemporal Results

All spatiotemporal parameters in the three walking conditions have been summarized in table 6-1, showing the average values and the associated standard deviations. The subject maintained a constant walking speed (0.2 m/s) throughout the motion tests. This allowed us to compare the testing results between the three conditions and get rid of influences from different walking speeds. After establishing the consistent speed in the dynamic walking condition, the same speed was set as a goal in the other two conditions. This value, 0.2 m/s is considered as very slow walking in normal gait and may have been caused by two main reasons. First, when using the dynamic KAFO, the subject had to extend the knee intentionally before the heel strike and the heel off in order to activate the heel switch successfully between the stance and swing phases. Second, the subject was not very confident in walking with the dynamic KAFO since she didn't have enough training to fully accommodate with the unique gait elicited by the device. It is expected that with longer training a more normal walking pattern could be established. Step length, stride length, and cadence are related to the walking speed and can be used to

determine gait symmetry. In all the three testing conditions, stride length fluctuated slightly around 0.6m and no significant difference was shown between both sides in the same condition or for the same side in different conditions. Such results were consistent with the same walking speed over the tests.

On the orthotic side, walking in the dynamic mode had the longest step length. This is because the subject tried to match the low speed in the slow walking and in the locked mode conditions by reducing the corresponding step length. On the contrary, the step length on the non-orthotic side was much higher in the slow walking condition than in the other two conditions. This was due to the inflexible knee in the locked mode and the switching problem in the dynamic mode, so that the subject needed to maintain stability by shortening the swing phase of the left leg. The slow walking showed good symmetry between the two legs, while walking in the locked mode and the dynamic mode did not. This would appear to be due to the fact that the user had to accommodate to the stiff leg in the locked mode and had to operate the dynamic mode properly, which affected gait symmetry dramatically.

Percentage of stance phase, double limb support, and single limb support are also commonly examined in motion tests of gait to evaluate orthoses performance. In slow walking, the percentage of the stance phase on both legs was around 80% of the gait cycle. When walking in the locked mode and the dynamic mode, the percentage of stance phase on the orthotic side was reduced to around 58% and 65%, respectively. But the percentage of stance phase on the left side was increased to 85% in both cases. The slow walking condition matched the low speed by increasing the stance and decreasing the swing phases. Walking in the locked mode showed the shortest double and single support

periods among the three walking conditions. The double support phase was extended in order to slow the walking speed and strengthen the walking stability. When compared to the locked mode, the results of the dynamic mode were closer to those of the slow walking.

Table 6-1. Average Spatiotemporal Parameters with One Standard Deviation for the Three Testing Conditions. The Right and Left Sides Represent the Orthotic and Sound Legs, Respectively.

	Slow walking (right/ left)		The UT dynamic KAFO in the locked mode (right/ left)		The UT dynamic KAFO in the dynamic mode (right/ left)	
	Step length (m)	0.33 ± 0.01	0.25 ± 0.01	0.35 ± 0.01	0.21 ± 0.01	0.36 ± 0.02
Stride length (m)	0.57 ± 0.02	0.62 ± 0.01	0.55 ± 0.03	0.59 ± 0.02	0.59 ± 0.03	0.65 ± 0.05
Cadence (steps/min)	127.3 ± 8.7	136 ± 5.2	160.2 ± 9.4	101.7 ± 2.1	149.4 ± 9.6	121.5 ± 8.6
Stance phase percentage (%)	79.5 ± 0.7	78.5 ± 1.3	57.4 ± 1.3	84.7 ± 0.5	66.2 ± 1.9	84.3 ± 1.6

Double limb support (%)	26.8 ± 0.6		19.2 ± 3.7		22.0 ± 2.2	
Single limb support on the orthotic side (%)	51.7 ± 1.7		39.0 ± 1.8		44.0 ± 2.2	
Max knee flexion angle in stance (deg)	9.3 ± 0.4	7.1 ± 1.3	2.2 ± 0.3	6.3 ± 0.4	6.1 ± 0.5	8.3 ± 1.0
Max knee flexion angle in swing (deg)	60.6 ± 1.9	58.9 ± 1.8	2.2 ± 0.3	42.3 ± 4.6	41.0 ± 4.3	47.6 ± 2.7

6.2 Discussion of the Kinematic Results

Compared to the stiff walking gait produced by the locked mode, the dynamic mode was able to produce patterns that were closer to normal walking patterns. This KAFO allowed for knee flexion during the entire walking cycle. The stance flexion helped in relieving the abrupt striking and loading of the orthotic leg in the loading response. Allowing knee flexion during the swing phase helped the subject to avoid some of the compensation motions such as hip hiking and leg circumduction. When walking in the dynamic mode, the maximum flexion angles were about 6 and 42 degrees in the

stance and swing phases, respectively, which are 33% and 20% less than the values in slow walking, as shown in figure 5-11 but significantly more than those were seen in the locked mode. This might have occurred because of the following reasons. First of all, the dynamic knee actuator was designed on the basis of the assumption that the user walked at normal speeds. In fact, the walking speed used for the testing was much slower than normal. This may have minimized the degree to which the subject was able to load the actuator to the degree to which it was designed. Also, in order to flex the knee joint, the subject had to overcome the weight of the device and the resistance of the actuator. This also contributed to the reduction of the knee flexion angle. Moreover, due to the subject's inexperience in using the KAFO, her attention may have been focused more on the need to cause the actuator to switch between the stance and swing actuators, thus adversely affecting the knee angle patterns.

The comparison of ankle motion between the three conditions has been illustrated in figure 5-14. When walking in the locked mode, the ankle was maintained in a dorsiflexion position over the whole gait cycle, except during the initial stance phase. Walking in the dynamic mode showed a similar ankle pattern to that of slow walking. However, some differences existed and will be discussed as follows. In the dynamic mode, a maximum of 12 degrees of dorsiflexion occurred in the mid-stance phase (about 50% higher than the slow walking and 25% less than the locked mode) since the subject tended to dorsiflex more at the ankle to reach the fully knee extension for actuator switching before the instant of heel off. Also, the subject avoided foot dragging by dorsiflexing the ankle right after the toe off, therefore about 75% less plantarflexion angle was generated in the dynamic walking condition than in the slow walking condition.

During the terminal swing phase, the gait provided by the dynamic mode showed about 10 degrees of dorsiflexion (100% higher than the healthy walking) before the next heel strike to prepare the knee in full extension so that the stance actuator could be engaged again. The hip angle profiles in the sagittal plane provided a good match between the three testing conditions. Compared to the slow walking condition, less hip flexion was generated in the locked mode and the dynamic mode right before the instant of the heel strike, and more hip extension in the mid-stance phase. Such differences may have occurred because the subject had the stiff leg in the locked mode and must extend more to maintain the locked knee during the stance phase. Also in the dynamic mode, the subject appeared to try to extend the knee before the heel strike and the heel off to switch between the stance and swing phases.

Walking with a locked knee joint requires some compensation motions to advance the leg movement, such as circumduction and hip hiking. The dynamic KAFO improved (lessened) the circumduction motions produced by the locked mode, which can be evaluated by the hip angle patterns in the frontal plane, as shown in figure 5-16. In the locked and dynamic walking, the orthotic leg was kept in an abducted position since it moved laterally to avoid the conflict between the medial sides of the KAFO and the non-orthotic leg. The inflexible knee joint in the locked mode induced larger abduction angles during the swing phase, and using the KAFO in the dynamic mode was able to improve this abnormal behavior. The pelvic obliquity profiles of the three walking conditions provide critical information in studying the hip hiking performance. First, the obliquity angles at the instant of the heel strike on the right leg indicated this issue, which can be observed from the distance between the neutral line and the initial points of the curves in

figure 5-17. At the heel strike of the right leg, about 5 degrees of positive pelvic obliquity in the locked mode and the dynamic mode indicates that the subject had hip hiking just before the right foot contact. Second, in the locked mode, since the orthotic leg was not allowed to flex at the knee joint, the left leg needed to rise up more (about 7 degrees of pelvic obliquity) than in the other two cases when the orthotic leg was supporting the body. Five degrees of negative pelvic obliquity was generated in the slow walking and the dynamic mode during the loading response of the right leg. In addition, compared to the slow walking condition, a large amount of positive pelvic obliquity could be observed in the other two conditions during the left stance period, which indicates severe hip hiking motions on the orthotic leg when it was swinging. This caused the upper body lean to the non-orthotic side in both the locked and dynamic modes.

6.3 Discussion of the Kinetic Results

Weight-normalized knee moment profiles for the three walking conditions have been shown in figure 5-18. The results indicate that using the UT dynamic KAFO in the dynamic mode could produce knee moment profiles that were close to those of the normal knee moment pattern. In the slow walking condition, internal extension moments were generated during the loading response and the early and mid-swing phases to resist the knee flexion motions that were occurring. And internal flexion moments were generated during the rest of the stance and swing phases to control knee extension. In the dynamic walking, the profile followed the same pattern, but higher extension moments occurred at the foot flat (25% more than that of the slow walking) and the end of the mid-

swing phase (200% more than that of the slow walking), causing a stiffer moment pattern. Also large internal flexion moments (300% more than the healthy walking) were shown around the heel off because the subject purposely extended the knee to overcome the weight of the device and to get the full extension position.

Knee stiffness profiles were calculated by combining the knee angle and moment data. Figure 5-19 compares the knee stiffnesses between the three testing conditions, indicating that the dynamic knee actuator was able to reproduce patterns that were closer to normal knee joint behavior. From figure 5-19, the dynamic walking condition generated hysteretic knee stiffness in both the stance and swing phases, which combined the responses of the knee actuator and the biological muscles. The knee actuator showed linear stiffnesses when the actuator was loaded under knee flexion. And the subject's own muscles contributed to the hysteretic area when the actuator was unloaded in extension.

6.4 Summary

All testing results recorded in chapter 5 were discussed in this chapter. The discussion was divided into three sections: the spatiotemporal results, the kinematic results, and the kinetic results. The results indicate that the dynamic KAFO facilitated reproduction of the normal knee behavior and improved the abnormal gait pattern associated with the locked knee KAFO.

Chapter 7

KAFO Industry Overview

7.1 KAFO Market in the US

Patients suffering from post-polio, spinal cord injury (SCI), and multiple sclerosis (MS) are among the major KAFO users. Of these three causes of disability, post-polio patients constitute the biggest KAFO user group and such patients are the most functional users, and are those who typically use those devices all of the time. Post-polio patients often lose muscle strength and control of the lower legs, while retaining good sensory input. SCI and MS patients represent a relatively small portion of KAFO users. They are called part time KAFO users, as they often only use KAFOs for certain activities. Most SCI and MS patients ultimately opt for wheelchairs because they are less trouble and much easier to move around.

There are three types of KAFOs presently available in the market: conventional KAFOs, stance control KAFOs (SCKAFOs), and dynamic KAFOs (C-brace®). Conventional KAFOs are classified into drop lock KAFOs, free hinge KAFOs, bail lock KAFOs, posterior offset joint KAFOs, and etc. Typical stance control KAFOs have already been discussed in section 2.2. What they have in common is that SCKAFOs

block knee motion during the stance phase and allow free knee rotation during the swing phase. C-brace® is the only commercial dynamic KAFOs in the market. All types of KAFOs can be fabricated in steel, aluminum, polypropylene, or carbon fiber based on different situations and user requirements.

In order to better understand the KAFO market in the US, a survey was been conducted among 51 individuals who are KAFO practitioners. They are KAFO users, physicians (such as rehabilitation doctors), physical therapists, orthotists, and orthotic manufacturers all over the country. About 30,000-50,000 KAFOs can be sold per year according to the KAFO manufacturers' investigation. Although conventional KAFOs produce a rigid walking gait pattern, they are the most commonly prescribed among the three types and occupy about 90% of the market. This is because the conventional KAFOs can provide enough support with the least weight and the simplest mechanisms. These devices are so stable that users have good confidence in them. Also, the practitioners have the best understanding of the conventional KAFOs, so that most frequently those are what they introduce to their patients. Another critical reason is, while all types of KAFOs are very expensive, most of the conventional KAFOs can be fully reimbursed by insurance plans. SCKAFOs have been developed and improved in the past twenty years and have much less market share than the conventional ones. For KAFO users and practitioners, some unfamiliar technologies have been introduced by SCKAFOs, and people haven't yet obtained enough hands on experience with these devices to trust them. Also, SCKAFOs require users to have some amount of muscle strength in the lower legs to realize proper operation. This means that SCKAFOs have limited target customers. In addition, these KAFOs typically cost approximately 5 times

more than the conventional devices. And, the C-brace® KAFO costs even more. The costs and insurance coverage for the three KAFO types have been summarized in table 7-1. Although the C-brace® appears to have good functionality and can produce a relatively smooth walking gait pattern, it is not widely accepted in the market due to the unaffordable price. For SCKAFOs and dynamic KAFOs, very few published data is available to evaluate their feasibility and reliability when used by patients. Thus, no clear indication or prescription guidelines can be used in choosing them, making it even harder to find proper user population for those devices. It is critical for the practitioners to have good knowledge of these new products so that they can educate patients with some fundamental attitudes in using SCKAFOs and C-brace®.

Table 7-1. The Costs and Insurance Coverages of the Three KAFO Types.

	Conventional KAFOs	Stance control KAFOs	Dynamic KAFOs (C-brace®)
Cost of devices	\$1,500 – \$ 3,000	About \$ 7,000	About \$ 20,000
Insurance coverage	100%	Maximum 80%	No specific reimbursement code available

From the market survey, KAFOs have been used for a long time to mitigate abnormal walking gait. However, their acceptance and long term use rate is quite low due to two major issues: the limited functionality and the bulkiness of the devices.

Functionality is a critical factor when choosing proper KAFOs, but most KAFOs don't work very well. The conventional KAFOs only have two working modes. They either lock the knee joint completely during standing and walking or always allow free knee motions, requiring specific body compensation to maintain stability. Therefore, these devices provide a less than desirable rigid walking gait pattern or may be unable to produce enough support. Stance control KAFOs lock the knee joint to stabilize the lower limb during the loading response and release knee movements during the swing phase, relieving the stiff walking patterns generated by the conventional devices. However, they have issues of consistency. Locking and unlocking doesn't always occur properly in each step as required. Sometimes SCKAFOs are locked when the patients are not ready or they are still unlocked when patients expect the devices to be locked. Such situations cause patients to fall more easily than when using conventional KAFOs. Also, some degree of muscle strength and joint mobility is necessary to function with SCKAFOs. Moreover, SCKAFOs and C-brace® don't provide any knee extension assistance, which limits their use for people with severe quadriceps weakness.

Presently, most conventional KAFOs, SCKAFOs, and dynamic KAFOs are too heavy and bulky, which is considered a great burden for patients with weak muscles. Usually, a conventional KAFO weighs about 3 lbs. SCKAFOs and C-brace® add at least 2 lbs more on this basis. Patients using them experience fatigue due to their weight, in addition to the rigid walking gait pattern that they produce.

Some additional issues of KAFOs are discussed as follows. Wearing KAFOs are uncomfortable because hard materials used to fabricate the devices contact with the skin directly, causing concentrated pressure and swelling. Adding cushioning inside the devices could relieve these problem to some extent, but this induces other issues such as sweating. Straps are used on KAFOs to fasten the devices and this makes the device very difficult to be put on since most users also have paralysis problems on the upper body. Additionally, most KAFOs need loose clothes to fit over them, and some of them can only be worn outside the pants. Last but not least, high development cost is always a big disadvantage for KAFOs.

7.2 Ecosystem for the KAFO Market

The ecosystem flow for the KAFO market is shown in figure 7-1 and all details will be discussed in this section. Three sub-flows are included in the ecosystem: the process of prescribing KAFOs for patients, the process of licensing new KAFOs in manufacturers, and the process of marketing new KAFOs.

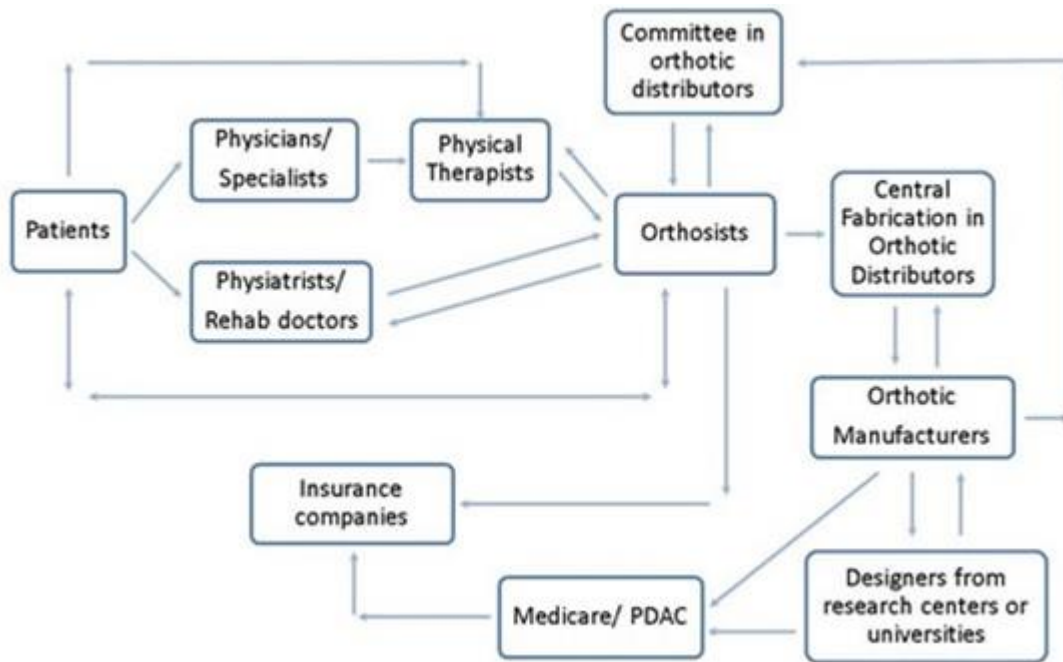


Figure 7-1. The KAFO Ecosystem Flow Chart.

7.2.1 The Process of Prescribing KAFOs for Patients

First of all, physicians prescribe KAFOs for patients, and physical therapists and orthotists provide suggestions and recommendations in this process. Patients go to visit orthotists with detailed prescriptions from physicians. Sometimes the prescriptions include specific KAFO types for the orthotists to follow. But in most cases, the orthotists are those who decide the proper devices for the patients based on some lower limb evaluations. The evaluating tests aim at hip, knee, and ankle joints and main muscles of the lower limb. In general, the weaker these joints and muscles are, the more restrictive the orthoses will be. After getting the evaluation results, the orthotists will send feedback to the doctors, informing them of the patients' conditions and the final decisions that they have made. The final decisions depend on the patients' walking capability and

willingness. Before the specific KAFOs are ordered, the orthotists will explain to the patients the functionality and the corresponding walking patterns provided by the devices and let them decide to accept or reject the plan. Almost all patients will be asked to try the devices on to see whether they can control them correctly, and to determine if these devices do improve their walking motions. The orthotists always suggest the optimal KAFOs for the patients, which they think would provide the most benefits. But, due to the patients' own willingness or the price issues, the patients might not take the orthotists' advice so they have to figure out other solutions for the patients. When settling down the orthoses, some measurements need to be done so that customized devices can be made for the patients.

Meanwhile, claim documents need to be sent to insurance companies. Approvals of reimbursing the KAFOs must be obtained and usually it takes a couple of weeks. Usually, sweeping statements from the doctors are not accepted by the companies. Due to legal issues, particular scripts of KAFOs from the orthosists are requested, which present the evaluation results, list every component of the devices, and describe the decision-making process in a detailed way. The insurance companies will check all submitted materials in order to find the necessity of using the KAFOs. If SCKAFOs or C-brace® are prescribed for patients, the orthotists will have to make clear statements, such as what kind of benefits such devices can provide rather than the conventional KAFOs. There exist high risks of rejection and if this happens, the orthotists can either appeal or choose other options and repeat the whole procedure once again. As soon as the orthotists receive the approvals, they will contact the central fabrication (CF) department in their companies (orthosis distributors). Technicians from the CF department are in charge of

purchasing all components and fabricating the devices. The orthosists will send bills to the patients and the insurance companies when the KAFOs are completed.

The orthosists are responsible for teaching the patients and the physical therapists how to use the KAFOs. They train the patients to walk with the devices in the beginning and educate the physical therapists as well so that they can help the patients later. The physical therapists continuously provide instructions for the patients and their family members, training them to use the devices independently in daily life, such as taking them on/ off and ascending/ descending stairs with them. With the help of the physical therapists, the patients can increase their use time gradually. Also, patients can visit the orthotists and ask for adjustments anytime they have issues with the KAFOs. Usually after 2-3 years, some parts of the KAFOs need to be replaced or furnished because of the attrition. If the devices don't fit the patients anymore or something has changed in their health situations, the patients will be suggested to have new KAFOs.

7.2.2 The Process of Licensing New KAFOs in Manufacturers

The orthotic manufacturers always have their own research and development (R&D) department. They keep in contact with the practitioners over the country to collect new requirements from the market. On the other side, designers from universities and research centers approach the manufacturers and present their new ideas from time to time. In such cases, non-disclosure agreements are usually signed prior to revealing the design information to the manufacturers. This aims to protect the designers so that the manufacturers cannot share or use the ideas without permission and it also paves the way

for further discussion. Then in the first stage representatives from the manufacturers work with the designers to check the possibility of cooperation, such as if similar designs exist, if the ideas are worthy to be invested, and if the new designs can fit the manufacturers' product line. In the second stage, a committee gathers together to evaluate the designs and make final decisions. Usually about 4-5 people from departments of research and development, sales and marketing, and manufacturing consist of this committee, bringing extensive viewpoints from different aspects. They make decisions based on the following factors: how the devices work, how they meet market requirements, if there is a market existed for the new products, what costs and profits the new products can generate, and etc. If the manufacturers decide to license the new products, further discussion will be conducted between the two parties, reaching detailed development plans for the next step. The orthotic manufacturers are responsible for all costs in the cooperating procedure and also provide assistance in patent applications. Some designers come with preliminary concepts and others present mature prototypes so the whole licensing process ranges anywhere from several months to as much as a year or more, depending on various situations.

Generally speaking, there are two cooperating categories of licensing the new KAFO products. The first category is that the manufacturers completely purchase the ideas from the designers. They will take care of the further development, fabrication, sales, and marketing for the new products. In this case, the designers could receive one-time payment and then get a percentage of benefits every time the products are sold. The second one is call royalty category. The designers work as outside workshops for the orthotic manufacturers while the manufacturers sell the devices for them. There is no

one-time payment in this category and the designers receive a percentage of benefits whenever the KAFOs are sold.

In both cases, the licensing process discussed above needs to be conducted completely so that the new products can be included into manufacturers' catalogs. In the second category, the designers have to bear all risks that are involved in manufacturing, ensuring, and keeping the products in inventory. If the designers overestimate the market of their products, they will confront issues such as overwhelming costs. However, the royalty category contains larger potential profits than the first category because the designers are able to take more control during the process. Also, the designers are forced to continuously improve the products and reduce the costs. Sometimes the designers start collaborating with the manufacturers in the first category and later switch to the royalty category to increase profits due to the successful sale of the products.

Two major issues need to be overcome before the new products enter the orthotic market. One is that insurance reimbursement is necessary for all new products. No matter how well the KAFOs can function, the patients are not willing to have them unless the insurance companies could pay the cost because they are not able to afford high prices of the devices. The insurance companies only follow the reimbursement rules set by Medicare and Medicaid. However, applying for new reimbursement codes for novel products is a tough task. In many situations, the manufacturers choose to get approvals of fitting current codes on their new products. The other problem is that in nature it is hard for people to adapt changes. The patients don't want to try the new products if they are used to having the current devices. Also, the orthotists are very resistant to change the new devices according to the KAFO survey. Lots of testing data is requested in order to

get the patients and the practitioners accept the new technologies, proving that they do function much better than those old devices and can provide more benefits.

7.2.3 The Process of Marketing New KAFOs

The next critical process is to release the new products into the orthotic market. The manufacturers have their own engineers and sales and marketing people to reach and train the practitioners. Many trade shows and national and local prosthetic and orthotic meetings are held by American Orthotic and Prosthetic Association (AOPA) and American Academy of Orthotists & Prosthetists (AAOP) all over the US every year. The manufacturers attend these meetings to launch their new products and attract the practitioners' attention. They exhibit new product samples, spread out educational materials (manuals and brochures), and make presentations on these shows. As we presented before, the orthotists are those who play important roles in the KAFO prescription process. Besides the optional trade shows and professional meetings, the orthotists are mandatory to attend continue educations held by American Board Certification (ABC) and Board of Certification (BOC) to maintain their certifications. The orthotists are trained of various orthotic and prosthetic devices on the meetings. Therefore, it is relatively efficient for the manufacturers to take advantage of these educational meetings to show their new devices. Some trade magazines, such as O&P Edge, are very popular in the orthotic market. The manufacturers make advertisements on those magazines and describe the detailed specifications of the new products, widening the potential KAFO market. Moreover, the manufacturers distribute products information

via mails and emails and even make individual visits to their customers. All products are sold with detailed instructions and sometimes the manufacturers hold training workshops to educate their customers about the new devices.

Good after-sale services are crucial in keeping current customers and growing potential customers. Technical assistance is always available via phone, video, and individual conferences, which helps build good relationships with the customers. Also, the manufacturers have to focus on developing new devices and improving current products to better satisfy the customers' needs. It is not easy for the practitioners to accept new products so that continuous researching and verifying these devices on the patients will be very helpful in persuading them. This will increase the products' competitiveness as well since most KAFOs in the market lack of vivo testing data. Spreading out information of the new products to students in the orthotic and prosthetic schools is as important as those regular marketing policies. There are about 15 O&P schools around the United States. Talking to the instructors and the students is like a long term investment because they will be future orthotists to enter this market and can help with spreading the devices.

7.3 Business Model for the UT Dynamic KAFO

A business model was built for the UT dynamic KAFO. There are nine main sections included in this model: value propositions, customer segments, channels, customer relationships, revenue streams, key resources, key partners, key activities, and cost structures. At first, assumptions were made for all the sections. Then, they were

tested and modified in the survey. The final version for the business model canvas is shown in figure 7-2.

The value proposition is the first section and shows the problems and the needs that this device is trying to solve for the customers. Due to the rigid and abnormal walking gait pattern provided by the current KAFOs, customers often choose to forgo their use or only use them for certain activities. The dynamic knee module can be attached on any conventional KAFOs, potentially increasing KAFO acceptance rate and daily using time by reproducing a more normal walking gait. This should also help the orthotic manufacturers to increase their sales. The next section is a customer segment, which represents potential users, buyers, and payers of the dynamic knee module. As was discussed before, KAFOs are prescribed for patients by a group of physicians, physical therapists, and orthotists. So they are considered as the device users in this model. The orthotic manufacturers buy the concept from the designers and would pay for all the costs in the development and licensing of the UT dynamic KAFO. The channels section includes all the relationships that we plan to use when distributing the products to the customers. Through individual visits, publications, and conferences, we can exhibit the UT dynamic KAFO in front of the orthotic manufacturers in the market, obtaining investments and cooperations from them. Then they will reach out to the KAFO users via sales and marketing representatives as long as the products are added into their catalogs. The fourth section is called customer relationships, which interacts with the first three segments. In this model, several ways are proposed to get potential customers. Being active in the trade shows, professional conferences, and mandatory continuing education could attract the customers' attention to our products. Also making advertisements

through the media, planning individual visits, and distributing product information via calls, mails, and emails could be efficient methods with the help of the orthotic manufacturers. After getting the customers, it is pivotal to keep them around by providing thoughtful after-sell services and to encourage them to use our products even more by getting insurance reimbursements, respecting the customers' feedbacks to improve current devices and services, etc. The revenue streams section shows how to make money from selling the products to the customers. Our strategy is to sell the technology directly to the orthotic manufacturers, and then receive a one-time payment from them. After that whenever the products are sold, we can keep getting payments based on the profits.

The key resources section includes all resources that need to make the whole business model work. We need researchers and engineers as intellectual properties to develop the dynamic knee modules, machine shops as partners to fabricate the modules, and specific equipment as physical assets to test them. The key partners section includes all involved partners and suppliers. The dynamic knee module can be developed and tested in the Biomechanics and Assistive Technology Lab and the Dynamic and Smart Systems Lab from the University of Toledo. Material suppliers provide superelastic Nitinol and other materials that are used in fabricating the prototypes in the machine shops. Then, the orthotic manufacturers will license and launch the dynamic knee products, taking care of all the marketing activities and after-sale services. Three key activities are presented in the business model. First is to keep developing and improving the knee module technology. Second is to collaborate with the orthotic manufacturers in licensing and selling the products. And the last is to get feedbacks from the patients and the practitioners in the market, which are used to progress the current technology. It is of

greatest importance to understand that this design exists to satisfy the market. Finally, the cost structure section shows the total expense in research and development, manufacturing, and purchasing materials and testing facilities.

The Business Model Canvas








<p>Key Partners </p> <ul style="list-style-type: none"> - Biomechanics and Assistive Technology Lab - Dynamic and Smart Systems Lab - Orthotic manufacturers (Becker, Filluar, and etc.) - Machine shops - Material suppliers (Fort Wayne, McMaster, and etc.) 	<p>Key Activities </p> <ul style="list-style-type: none"> - Dynamic knee actuator development - Cooperating with orthotic manufacturers - Getting feedback from the market 	<p>Value Proposition </p> <ul style="list-style-type: none"> - Increase the acceptance rate of KAFO and daily using time by providing normal walking gaits; - Sell more products; 	<p>Customer Relationships </p> <ul style="list-style-type: none"> - Get: trade shows and etc. - Keep: after-sell service and etc. - Grow: reimbursement and etc. 	<p>Customer Segments </p> <ul style="list-style-type: none"> - User: Physicians, orthosists, and patients; - Buyer and payer: Orthotic Manufacturers (Fillauer, Becker, and etc.)
<p>Cost Structure </p> <ul style="list-style-type: none"> - Research and development - Manufacturing - Materials and accessories purchasing - Facilities to test the dynamic knee actuator 		<p>Revenue Streams </p> <ul style="list-style-type: none"> - One-time payment - Payment whenever products are sold 		

Figure 7-2. The Business Model Canvas for the Dynamic Knee Joint Module.

7.4 Directions for Future Research in the KAFO Area

Based on the above discussion of the current KAFO market, some future directions in KAFO development are recommended as follows.

1) Make the KAFOs to be user-friendly, improving the current mechanisms and overall structures in order to let users put them on/ off efficiently.

2) Reduce the weight and the volume of the KAFOs. Meanwhile, these devices should be able to endure high enough loads.

3) Eliminate the noises of the devices by improving the switching mechanisms integrated inside the KAFOs.

4) Make the KAFOs be more stable and reliable. Using SCKAFOs causes patients to fall more easily than with the conventional KAFOs since they are not able to function properly as required.

5) Further refine the specifications for the current KAFOs. Most products are not efficiently prescribed because the related motion tests on subjects and clear specifications are lacking.

6) Develop novel KAFOs that can accommodate various walking conditions, such as different walking speeds, uneven grounds, and climbing upstairs/ downstairs/ ramps.

7) Also, educate the practitioners more so that they are familiar with the new technologies and can gain hands-on experience to help users get better rehabilitation.

7.5 Summary

A KAFO survey has been conducted among various KAFO users and practitioners throughout the US. All results were concluded in this chapter, providing an overview of the current KAFO market in the US. A complete business model for the UT dynamic KAFO was then built based on this survey, which can be used in future business activities related to this product. Finally, general directions for further KAFO research were proposed.

Chapter 8

Conclusions and Future Work

As discussed in the previous chapter, the UT dynamic KAFO is able to reproduce closer to normal knee motions and improve the behavior at the ankle and hip joints as well, compared to conventional KAFOs with a locked knee. However, one advantage of this device has not been evaluated in this study. The dynamic actuator is supposed to assist knee extension during the entire gait cycle. Two EMG sensors were used in the motion tests to detect quadriceps muscle activities. However, the EMG signals didn't provide enough information to determine the difference between the slow walking and walking in the dynamic mode. Therefore, the extension assistance of the actuator cannot be verified since the test subject has no quadriceps deficiency and may still rely on her own knee extensors. Further motion tests need to be conducted by involving more subjects, especially individuals with weak quadriceps.

The dynamic knee actuator has several limitations that need to be improved in the future work. First, the current device was designed for someone weighing no more than 60 kg. It might not be able to provide enough support for those who exceed this weight. The internal actuating module of the dynamic actuator should be custom made for different users to better meet specific requirements. Second, the stance and swing

actuators can only be engaged and disengaged at the full extension position. Users have to pay close attention to their walking gait, extending their knee before the heel strike and the heel off to switch properly between the two actuating parts. Improving the control algorithm can eliminate this disruption of the gait pattern. Third, this dynamic knee actuator has the potential of matching the nonlinear stiffness pattern of normal walking by involving the superelastic Nitinol rods in the design. Later, the system should be modified to have stiffness with more hysteresis in the stance phase and with much more in the swing phase, reproducing more normal knee performance. And last, the volume and weight of the dynamic knee joint need to be further reduced.

In this study, only one subject was involved in the motion tests. The sample size is far from adequate and provides limited information in assessing the UT dynamic KAFO. Future studies are planned to improve the design and increase the number of subjects, both healthy people and individuals with quadriceps weakness, collecting more data to evaluate the functionality and reliability of the device on various users. The long-term goal of this research is to determine whether the UT dynamic KAFO is an effective alternative to current KAFOs and can be launched to the KAFO market.

References

1. Lovell, W.W., et al., *Lovell and Winter's Pediatric Orthopaedics*. 2006: Lippincott Williams & Wilkins. 131-156.
2. DeLisa, J.A., B.M. Gans, and N.E. Walsh, *Physical Medicine and Rehabilitation: Principles and Practice*. 2005: Lippincott Williams & Wilkins. 155-166.
3. Inman, V.T., H.J. Ralston, and F. Todd, *Human walking*. 1981: Williams & Wilkins.
4. Lafortune, M., et al., *Three-dimensional kinematics of the human knee during walking*. Journal of biomechanics, 1992. **25**(4): p. 347-357.
5. MacKinnon, C.D. and D.A. Winter, *Control of whole body balance in the frontal plane during human walking*. Journal of biomechanics, 1993. **26**(6): p. 633-644.
6. Mummolo, C., L. Mangialardi, and J.H. Kim, *Quantifying dynamic characteristics of human walking for comprehensive gait cycle*. J Biomech Eng, 2013. **135**(9): p. 91006.
7. *Gait cycle*. Available from: http://www.physio-pedia.com/Gait_Cycle.
8. Poppe, R., *Vision-based human motion analysis: An overview*. Comput. Vis. Image Underst., 2007. **108**(1-2): p. 4-18.
9. Pasparakis, D.a.D., N., *Normal walking Principles, basic concepts, terminology 3-dimensional clinical gait analysis*. EEXOT, 2009. **60**(4): p. 183-194.
10. Jordan, K., J.H. Challis, and K.M. Newell, *Walking speed influences on gait cycle*

variability. *Gait & Posture*, 2007. **26**(1): p. 128-134.

11. Collins, S.H., *Dynamic Walking Principles Applied to Human Gait.*, in *Mechanical Engineering*. 2008, The University of Michigan. p. 107.

12. Zajac, F.E., R.R. Neptune, and S.A. Kautz, *Biomechanics and muscle coordination of human walking: Part I: Introduction to concepts, power transfer, dynamics and simulations*. *Gait & posture*, 2002. **16**(3): p. 215-232.

13. Zajac, F.E., R.R. Neptune, and S.A. Kautz, *Biomechanics and muscle coordination of human walking: part II: lessons from dynamical simulations and clinical implications*. *Gait & posture*, 2003. **17**(1): p. 1-17.

14. Popovic, M., A. Hofmann, and H. Herr. *Angular momentum regulation during human walking: biomechanics and control*. in *Robotics and Automation, 2004. Proceedings. ICRA'04. 2004 IEEE International Conference on*. 2004. IEEE.

15. Winter, D.A., *Biomechanics and Motor Control of Human Movement*. 2009: Wiley.

16. Tian, F., M. S. Hefzy, and M. Elahinia, *State of the Art Review of Knee–Ankle–Foot Orthoses*. *Annals of Biomedical Engineering*, 2015. **43**(2): p. 427-441.

17. Tian, F., M. S. Hefzy, and M. Elahinia, *A Dynamic Knee-Ankle-Foot Orthosis With Superelastic Actuators*, in *ASME 2013 Conference on Smart Materials, Adaptive Structures and Intelligent Systems*. 2013, ASME: Snowbird, Utah, USA. p. V002T06A005.

18. *Muscle weakness causes*. Available from: http://www.rightdiagnosis.com/symptoms/quadriceps_muscle_weakness/causes.htm.

19. Cullell, A., et al., *Biologically based design of an actuator system for a knee–*

- ankle-foot orthosis*. Mechanism and Machine Theory, 2009. **44**(4): p. 860-872.
20. Bernhardt, K.A., T.H. Oh, and K.R. Kaufman, *Gait patterns of patients with inclusion body myositis*. Gait Posture, 2011. **33**(3): p. 442-6.
21. Schetky, L.M., *Shape - Memory Alloys*. Kirk-Othmer Encyclopedia of Chemical Technology, 1982.
22. Honma, T., *Shape memory alloys*. Kogyo Zairyo,(Tokyo, Japan), 1985: p. 53-57.
23. Funakubo, H. and J. Kennedy, *Shape memory alloys*. Gordon and Breach, xii+ 275, 15 x 22 cm, Illustrated, 1987.
24. Tadaki, T., K. Otsuka, and K. Shimizu, *Shape memory alloys*. Annual Review of Materials Science, 1988. **18**(1): p. 25-45.
25. Hodgson, D.E., W. Ming, and R.J. Biermann, *Shape memory alloys*. ASM International, Metals Handbook, Tenth Edition., 1990. **2**: p. 897-902.
26. Sachdeva, R.C., S. Miyazaki, and F. Farzin-Nia, *Shape memory alloy*. 1991, Google Patents.
27. Lagoudas, D.C., *Shape Memory Alloys: Modeling and Engineering Applications*. 2008: Springer.
28. *Three different crystalline structures of Nitinol alloys*. Available from: http://nptel.ac.in/courses/112104040/lecture34/34_2.htm.
29. *Forward and reverse phase transformation processes*. Available from: <http://smart.tamu.edu/overview/smaintro/simple/definition.html>.
30. *Nitinol alloys with shape memory effects*. Available from: <http://smart.tamu.edu/overview/smaintro/detailed/detailed.html>.
31. Hu, J., *Investigation on the Cyclic Response of Superelastic Shape Memory Alloy*

(SMA) Slit Damper Devices Simulated by Quasi-Static Finite Element (FE) Analyses. Materials, 2014. 7(2): p. 1122.

32. Stirling, L., et al., *Applicability of Shape Memory Alloy Wire for an Active, Soft Orthotic.* Journal of Materials Engineering and Performance, 2011. 20(4-5): p. 658-662.

33. Elahinia, B.M.a.M., *Modeling Variable Stiffness SMA Wires to Achieve Dynamic Ankle Stiffness for Developing Active Ankle Foot Orthosis,* in *ASME 2010 Conference on Smart Materials, Adaptive Structures and Intelligent Systems.* 2010, ASME: Philadelphia, Pennsylvania, USA.

34. Bhadane, M., *Variable Stiffness Actuation for an Ankle Foot Orthosis Using Shape Memory Alloys,* in *Mechanical Engineering.* 2012, the University of Toledo. p. 190.

35. Bhadane, M., M. Elahinia, M. Armstrong C., and Hefzy, M., *A variable stiffness ankle foot orthosis based on SMA wires,* in *Biomedical Engineering Society Annual Meeting.* 2010: Austin, Texas, USA.

36. Deberg, L., et al., *An SMA passive ankle foot orthosis: Design, modeling, and experimental evaluation.* Smart Materials Research, 2014: p. 1-11.

37. Deberg, L., *A fast actuator using shape memory alloys for an ankle foot orthosis,* in *the Ecole Supérieure des Sciences.* 2012, the University of Toledo and the Technologies de l'Ingénieur de Nancy. p. 100.

38. Andani, M.T., *Constitutive Modeling of Superelastic Shape Memory Alloys Considering Rate Dependent Non-Mises Tension-torsion Behavior,* in *Mechanical Engineering.* 2013, The University of Toledo.

39. Mataee, M.G., M.T. Andani, and M. Elahinia, *Adaptive ankle-foot orthoses based*

on superelasticity of shape memory alloys. Journal of Intelligent Material Systems and Structures, 2014.

40. Taheri Andani, M. and M. Elahinia, *Modeling and Simulation of SMA Medical Devices Undergoing complex Thermo-mechanical Loadings*. Journal of Materials Engineering and Performance, 2014. **23**(7): p. 2574-2583.

41. Pittaccio, S., et al., *Applications of Shape Memory Alloys for Neurology and Neuromuscular Rehabilitation*. Journal of Functional Biomaterials, 2015. **6**(2): p. 328-344.

42. Viscuso, S.P.a.S., ed. *Shape Memory Actuators for Medical Rehabilitation and Neuroscience, Smart Actuation and Sensing Systems - Recent Advances and Future Challenges*. 2012.

43. Schofield, J.S., *Knee ankle foot orthosis*. 2013, Google Patents.

44. *Drop lock KAFO*. Available from: <http://www.scheckandsiress.com/documents/kafo-jm.pdf>.

45. Braddom, R.L., *Physical Medicine and Rehabilitation*. 2010: Elsevier Health Sciences.

46. W, B.C.M.L.V., V.W. Lin, and C.M. Bono, *Spinal Cord Medicine: Principles and Practice*. 2014: Demos Medical Publishing, LLC.

47. Radcliffe, C.W., *Four-bar linkage prosthetic knee mechanisms: Kinematics, alignment and prescription criteria*. Prosthetics and Orthotics International, 1994. **18**(3): p. 159-173.

48. *Ratchet lock joint KAFO*. Available from: <http://www.beckerortho.com/Catalog/CentralFabCatalog.pdf>.

49. Miller, F. and E. Browne, *Cerebral Palsy*. 2005: Springer.
50. *Stance control KAFOs*.
51. Suga, T., et al., *Newly designed computer controlled knee-ankle-foot orthosis (Intelligent Orthosis)*. Prosthetics and Orthotics International, 1998. **22**(3): p. 230-239.
52. Bakker, J.P.J., et al., *The effects of knee-ankle-foot orthoses in the treatment of Duchenne muscular dystrophy: review of the literature*. Clinical Rehabilitation, 2000. **14**(4): p. 343-359.
53. Zissimopoulos, A., S. Fatone, and S.A. Gard, *Biomechanical and energetic effects of a stance-control orthotic knee joint*. J Rehabil Res Dev, 2007. **44**(4): p. 503-13.
54. Rafiaei, M., et al., *The gait and energy efficiency of stance control knee-ankle-foot orthoses: A literature review*. Prosthetics and Orthotics International, 2015.
55. Yakimovich, T., E.D. Lemaire, and J. Kofman, *Engineering design review of stance-control knee-ankle-foot orthoses*. J Rehabil Res Dev, 2009. **46**(2): p. 257-67.
56. McMillan, A.G., K. Kendrick, and J. W. Michael, *Preliminary Evidence for Effectiveness of a Stance Control Orthosis*. JPO: Journal of Prosthetics and Orthotics, 2004. **16**: p. 6-13.
57. Hebert, J.S. and A.B. Liggins, *Gait Evaluation of an Automatic Stance-Control Knee Orthosis in a Patient With Postpoliomyelitis*. Archives of Physical Medicine and Rehabilitation, 2005. **86**(8): p. 1676-1680.
58. Yakimovich, T., J. Kofman, and E.D. Lemaire, *Design and evaluation of a stance-control knee-ankle-foot orthosis knee joint*. IEEE Trans Neural Syst Rehabil Eng, 2006. **14**(3): p. 361-9.
59. Yakimovich, T., E.D. Lemaire, and J. Kofman, *Preliminary kinematic evaluation*

- of a new stance-control knee-ankle-foot orthosis*. Clin Biomech (Bristol, Avon), 2006. **21**(10): p. 1081-9.
60. Yakimovich, T., E.D. Lemaire, and J. Kofman. *Gait Evaluation of a New Electromechanical Stance-Control Knee-Ankle-Foot Orthosis*. in *Engineering in Medicine and Biology Society, 2006. EMBS '06. 28th Annual International Conference of the IEEE*. 2006.
61. Yakimovich, T., E. Lemaire, and J. Kofman, *Articulating joint*. 2008, Google Patents.
62. Terris Yakimovich, J.K., Edward Lemaire, *Design, Construction and Evaluation of an Electromechanical Stance-Control Knee-Ankle-Foot Orthosis*, in *Proceedings of the 2005 IEEE Engineering in Medicine and Biology 27th Annual Conference*. 2005: Shanghai, China.
63. Raftopoulos, D.D., L. Poulos, and C. W. Armstrong, *Knee-ankle-foot orthotic with a hydraulic twist*. SOMA, 1988: p. 49-53.
64. Bernhardt, K.A., S.E. Irby, and K.R. Kaufman, *Consumer opinions of a stance control knee orthosis*. Prosthet Orthot Int, 2006. **30**(3): p. 246-56.
65. Irby, S.E., K.A. Bernhardt, and K.R. Kaufman, *Gait of stance control orthosis users: the dynamic knee brace system*. Prosthet Orthot Int, 2005. **29**(3): p. 269-82.
66. Irby, S.E., et al., *Automatic control design for a dynamic knee-brace system*. IEEE Trans Rehabil Eng, 1999. **7**(2): p. 135-9.
67. Irby, S.E., et al., *Optimization and application of a wrap-spring clutch to a dynamic knee-ankle-foot orthosis*. IEEE Trans Rehabil Eng, 1999. **7**(2): p. 130-4.
68. Kaufman, K.R., S. E. Irby, J. W. Mathewson, and D. H. Sutherland, *Energy-*

http://professionals.ottobockus.com/cps/rde/xbcr/ob_us_en/646D642-EN-02-1207w.pdf.

78. *C-brace Practitioner IFU*. Available from:

http://professionals.ottobockus.com/cps/rde/xbcr/ob_us_en/CBrace_Practitioner_IFU_647G631.pdf.

79. *C-brace clinical reference guide*. Available from:

http://professionals.ottobockus.com/cps/rde/xbcr/ob_us_en/13022564_3_C-Brace_Clinical_Reference_Guide.pdf.

80. *C-brace brochure*. Available from:

http://professionals.ottobockus.com/cps/rde/xbcr/ob_us_en/11082209.4_C-Brace_Brochure.pdf.

81. Schmalz, T., et al., *A functional comparison of conventional knee–ankle–foot orthoses and a microprocessor-controlled leg orthosis system based on biomechanical parameters*. Prosthetics and Orthotics International, 2014.

82. Hwang, S., et al., *Biomechanical effect of electromechanical knee-ankle-foot-orthosis on knee joint control in patients with poliomyelitis*. Med Biol Eng Comput, 2008. **46**(6): p. 541-9.

83. *OttoBock Brochure*. Available from:

http://professionals.ottobockus.com/cps/rde/xbcr/ob_us_en/12032294.1_KAFO_FamilyBro_v3.pdf.

84. *Stance phase control KAFOs*.

85. Andani, M.T., A. Alipour, and M. Elahinia, *Coupled rate-dependent superelastic behavior of shape memory alloy bars induced by combined axial-torsional loading: a semi-analytic modeling*. Journal of Intelligent Material Systems and Structures, 2013.

24(16): p. 1995-2007.

86. Mirzaeifar, R., et al., *Coupled thermo-mechanical analysis of shape memory alloy circular bars in pure torsion*. International Journal of Non-Linear Mechanics, 2012.

47(3): p. 118-128.

87. Taheri Andani, M., et al., *Modifying the torque–angle behavior of rotary shape memory alloy actuators through axial loading: A semi-analytical study of combined tension- torsion behavior*. Journal of Intelligent Material Systems and Structures, 2013.

88. Tian, F., M. Elahinia, and M. S. Hefzy, *Storing and Releasing Energy with Superelastic NiTi in a Knee-Ankle-Foot Orthosis*, in *Proceedings of the 2015 Midwest ASB Regional Meeting*. 2015: The University of Akron, Akron, Ohio, USA.

89. Tian, F., M. S. Hefzy, and M. Elahinia, *Development of a Dynamic Knee Actuator for a KAFO Using Superelastic Alloys*, in *ASME 2014 International Mechanical Engineering Congress and Exposition*. 2014, ASME: Montreal, Quebec, Canada. p. V003T03A065.

90. Tian, F., M. Elahinia, and M. S. Hefzy, *Design and Evaluation of a Knee Actuator for a Dynamic Knee-Ankle-Foot Orthosis*, in *ASME 2014 Conference on Smart Materials, Adaptive Structures and Intelligent Systems*. 2014, ASME: Newport, Rhode Island, USA. p. V002T06A013.

91. Tian, F., M. Elahinia, and M. S. Hefzy, *Development of a knee actuator for a dynamic knee-ankle-foot orthosis*, in *Proceedings of the 2014 Midwest ASB Regional Meeting*. 2014: The University of Akron, Akron, Ohio, USA. p. 52.

92. Levitas, V.I. and I.B. Ozsoy, *Micromechanical modeling of stress-induced phase transformations. Part 1. Thermodynamics and kinetics of coupled interface propagation*

- and reorientation*. International Journal of Plasticity, 2009. **25**(2): p. 239-280.
93. Levitas, V.I. and E. Stein, *Simple micromechanical model of thermoelastic martensitic transformations*. Mechanics Research Communications, 1997. **24**(3): p. 309-318.
94. LExcellent, C., et al., *Characterization, thermomechanical behaviour and micromechanical-based constitutive model of shape-memory Cu · Zn · Al single crystals*. Acta Materialia, 1996. **44**(9): p. 3773-3780.
95. Olier, P., et al., *Effects of Impurities Content (Oxygen, Carbon, Nitrogen) on Microstructure and Phase Transformation Temperatures of Near Equiatomic TiNi Shape Memory Alloys*. J. Phys. IV France, 1997. **07**(C5): p. C5-143-C5-148.
96. Frenzel, J., et al., *Influence of Ni on martensitic phase transformations in NiTi shape memory alloys*. Acta Materialia, 2010. **58**(9): p. 3444-3458.
97. Brinson, L.C., A. Bekker, and S. Hwang, *Deformation of Shape Memory Alloys Due to Thermo-Induced Transformation*. Journal of Intelligent Material Systems and Structures, 1996. **7**(1): p. 97-107.
98. Brinson, L.C., *One-Dimensional Constitutive Behavior of Shape Memory Alloys: Thermomechanical Derivation with Non-Constant Material Functions and Redefined Martensite Internal Variable*. Journal of Intelligent Material Systems and Structures, 1993. **4**(2): p. 229-242.
99. Tanaka, K. and S. Nagaki, *A thermomechanical description of materials with internal variables in the process of phase transitions*. Ingenieur-Archiv, 1982. **51**(5): p. 287-299.
100. Liang, C. and C.A. Rogers, *One-Dimensional Thermomechanical Constitutive*

Relations for Shape Memory Materials. Journal of Intelligent Material Systems and Structures, 1990. **1**(2): p. 207-234.

101. Qidwai, M.A. and D.C. Lagoudas, *Numerical implementation of a shape memory alloy thermomechanical constitutive model using return mapping algorithms*. International Journal for Numerical Methods in Engineering, 2000. **47**(6): p. 1123-1168.

102. Mehrabi, R., M. Kadkhodaei, and M. Elahinia, *Constitutive modeling of tension-torsion coupling and tension-compression asymmetry in NiTi shape memory alloys*. Smart Materials and Structures, 2014. **23**(7): p. 075021.

103. Mehrabi, R., et al., *Microplane modeling of shape memory alloy tubes under tension, torsion, and proportional tension–torsion loading*. Journal of Intelligent Material Systems and Structures, 2014.

104. *Internal loops in superelastic shape memory alloy wires under torsion – Experiments and simulations/predictions*. International Journal of Solids and Structures, 2014. **51**(25-26): p. 4554.

105. Bar-Cohen, Y., *High Temperature Materials and Mechanisms*. 2014: Taylor & Francis.

106. Mehrabi, R., et al., *Anisotropic behavior of superelastic NiTi shape memory alloys; an experimental investigation and constitutive modeling*. Mechanics of Materials, 2014. **77**(0): p. 110-124.

107. Mehrabi, R., et al., *Investigation of influences of operational parameters on chatter vibration of cold rolling machines using finite element method*. STEEL RESEARCH INTERNATIONAL, 2008: p. 467-474.

108. Reza, M., K. Mahmoud, and E. Mohammad, *Constitutive modeling of tension-*

torsion coupling and tension-compression asymmetry in NiTi shape memory alloys. Smart Materials and Structures, 2014. **23**(7): p. 075021.

109. Taheri Andani, M., W. Anderson, and M. Elahinia, *Design, modeling and experimental evaluation of a minimally invasive cage for spinal fusion surgery utilizing superelastic Nitinol hinges*. Journal of Intelligent Material Systems and Structures, 2014.

110. Che-Chang, Y., et al. *Real-time gait cycle parameters recognition using a wearable motion detector*. in *System Science and Engineering (ICSSE), 2011 International Conference on*. 2011.

111. *Relevant biomechanics of the knee for knee replacement*. Available from: <http://aboutjoints.com/physicianinfo/topics/biomechanicknee/biomechanics.htm>.

112. Andani, M.T., et al., *Metals for bone implants. Part 1. Powder metallurgy and implant rendering*. Acta Biomaterialia, 2014. **10**(10): p. 4058-4070.

113. Andani, M.T., et al. *An Investigation of Effective Process Parameters on Phase Transformation Temperature of Nitinol Manufactured by Selective Laser Melting*. in *ASME 2014 Conference on Smart Materials, Adaptive Structures and Intelligent Systems*. 2014. American Society of Mechanical Engineers.

114. Elahinia, M., et al. *Site-specific Material Properties And The Additive Manufacturing Of Nitinol Musculoskeletal Implants*. in *TISSUE ENGINEERING PART A*. 2014. MARY ANN LIEBERT, INC 140 HUGUENOT STREET, 3RD FL, NEW ROCHELLE, NY 10801 USA.

115. Rahmanian, R., et al. *Modeling and Validation of Additively Manufactured Porous Nitinol Implants*. in *ASME 2014 Conference on Smart Materials, Adaptive Structures and Intelligent Systems*. 2014. American Society of Mechanical Engineers.

116. Shirani, M., et al. *A Modified Microplane Model Using Transformation Surfaces to Consider Loading History on Phase Transition in Shape Memory Alloys*. in *ASME 2014 Conference on Smart Materials, Adaptive Structures and Intelligent Systems*. 2014. American Society of Mechanical Engineers.
117. Walker, J., et al. *Additive Manufacturing of Nitinol Shape Memory Alloys to Overcome Challenges in Conventional Nitinol Fabrication*. in *ASME 2014 International Mechanical Engineering Congress and Exposition*. 2014. American Society of Mechanical Engineers.
118. Elahinia, M., et al. *Mitigating Implant Failure Through Design and Manufacturing of Nitinol Fixation Hardware*. in *TISSUE ENGINEERING PART A*. 2015. MARY ANN LIEBERT, INC 140 HUGUENOT STREET, 3RD FL, NEW ROCHELLE, NY 10801 USA.
119. Helen Hayes marker set. Available from: http://www.lifemodeler.com/LM_Manual/A_motion.shtml.
120. Kerrigan, D.C., et al., *Hip hiking and circumduction: quantitative definitions*. *Am J Phys Med Rehabil*, 2000. **79**(3): p. 247-52.
121. Gard, S.A. and D.S. Childress, *The effect of pelvic list on the vertical displacement of the trunk during normal walking*. *Gait & Posture*, 1997. **5**(3): p. 233-238.
122. Michaud, S.B., S.A. Gard, and D.S. Childress, *A preliminary investigation of pelvic obliquity patterns during gait in persons with transtibial and transfemoral amputation*. *J Rehabil Res Dev*, 2000. **37**(1): p. 1-10.